GUIDELINES FOR STRUCTURAL HEALTH MONITORING SYSTEMS ON TALL BUILDINGS AND A CASE STUDY

A THESIS SUBMITTED TO
THE GRADUATE SCHOOL OF NATURAL AND APPLIED SCIENCES
OF
MIDDLE EAST TECHNICAL UNIVERSITY

BY

OĞUZHAN GÜMÜŞ

IN PARTIAL FULFILLMENT OF THE REQUIREMENTS
FOR
THE DEGREE OF MASTER OF SCIENCE
IN
CIVIL ENGINEERING

FEBRUARY 2021

Approval of the thesis:

GUIDELINES FOR STRUCTURAL HEALTH MONITORING SYSTEMS ON TALL BUILDINGS AND A CASE STUDY

submitted by **OĞUZHAN GÜMÜŞ** in partial fulfillment of the requirements for the degree of **Master of Science in Civil Engineering, Middle East Technical University** by,

Prof. Dr. Halil Kalıpçılar
Dean, Graduate School of **Natural and Applied Sciences** _____

Prof. Dr. Ahmet Türer
Head of the Department, **Civil Engineering** _____

Assoc. Prof. Dr. Ozan Cem Çelik
Supervisor, **Civil Engineering, METU** _____

Examining Committee Members:

Prof. Dr. Hakkı Polat Gülkan
Civil Engineering, Başkent University _____

Assoc. Prof. Dr. Ozan Cem Çelik
Civil Engineering, METU _____

Prof. Dr. Yalın Arıcı
Civil Engineering, METU _____

Prof. Dr. Ayşegül Askan Gündoğan
Civil Engineering, METU _____

Prof. Dr. Özgür Kurç
Civil Engineering, METU _____

Date: 15.02.2021

I hereby declare that all information in this document has been obtained and presented in accordance with academic rules and ethical conduct. I also declare that, as required by these rules and conduct, I have fully cited and referenced all material and results that are not original to this work.

Name, Last name: Oğuzhan Gümüş

Signature:

ABSTRACT

GUIDELINES FOR STRUCTURAL HEALTH MONITORING SYSTEMS ON TALL BUILDINGS AND A CASE STUDY

Gümüş, Oğuzhan
Master of Science, Civil Engineering
Supervisor: Assoc. Prof. Dr. Ozan Cem Çelik

February 2021, 139 pages

The new Turkish Building Earthquake Code requires real-time monitoring of the structural response of buildings of Earthquake Design Class 1 and 2 that are taller than 105 m. Structural health monitoring (SHM) systems on tall buildings have to comply with the SHM Guidelines by the Disaster and Emergency Management Presidency of Turkey, developed as part of two research projects that were undertaken at METU and Bogazici University. Two tall buildings in Izmir and Istanbul, respectively, were instrumented as case studies for the SHM systems on tall buildings per the new Code. This thesis presents the development of the SHM Guidelines and the instrumentation of a 216 m tall office building in Izmir, whose structural system consists of reinforced concrete (RC) core shear walls, RC moment-resisting frames with circular composite columns, and buckling-restrained braces at two mechanical floors. Structural response of the building is currently monitored in real time by a dense network of 27 channels of accelerometers. Structural system dynamic properties of the building for the first four translational modes in both East-West and North-South directions and the first four torsional modes were identified from the ambient vibration records. Structural responses of the building recorded

during the earthquakes in 2019 with moment magnitudes M_w 3.9–6.0 and epicenters 15–283 km away from the building were analyzed. A finite element structural model of the building was developed. Natural vibration frequencies and vibration mode shapes from the finite element model agreed well with those from the system identification of the building.

Keywords: Ambient Vibration, Dynamic Properties, Earthquake Response, Structural Health Monitoring, System Identification

ÖZ

YÜKSEK BİNALARDA KURULACAK YAPI SAĞLIĞI İZLEME SİSTEMİ STANDARDININ BELİRLENMESİ VE ÖRNEK UYGULAMASI

Gümüş, Oğuzhan
Yüksek Lisans, İnşaat Mühendisliği
Tez Yöneticisi: Doç. Dr. Ozan Cem Çelik

Şubat 2021, 139 sayfa

Yürürlüğe giren Türkiye Bina Deprem Yönetmeliği, Deprem Tasarım Sınıfı 1 ve 2 olan 105 m'den yüksek binalarda yapı tepkilerinin gerçek zamanlı olarak izlenmesini zorunlu hale getirmiştir. Yüksek binalarda kurulacak yapı sağlığı izleme (YSİ) sistemleri, ODTÜ ve Boğaziçi Üniversitesi'nde yürütülen iki araştırma projesi kapsamında hazırlanan Türkiye Afet ve Acil Durum Yönetim Başkanlığı'nın yayımladığı YSİ Yönergesi'ne uygun olmalıdır. Bu projeler kapsamında sırasıyla İzmir ve İstanbul'da iki yüksek binaya örnek uygulama olarak YSİ sistemleri kurulmuştur. Bu tez, YSİ Yönergesi'nin hazırlanmasını ve İzmir'de 216 m yüksekliğindeki bir ofis binasına YSİ sistemi kurulmasını sunmaktadır. Binanın yapısal sistemi, çekirdekte betonarme perdeler, dairesel kompozit kolonları olan moment aktaran çerçeveler ve iki mekanik katta bulunan burkulması önlenmiş çelik çaprazlardan oluşmaktadır. Binanın yapısal tepkisi ivmeölçerlerden oluşan 27 kanallı kapsamlı bir YSİ sistemi ile gerçek zamanlı olarak izlenmektedir. Binanın Doğu-Batı ve Kuzey-Güney eksenleri doğrultularındaki ilk dört öteleme modları ve binanın ilk dört burulma modlarına ait yapısal sistem dinamik özellikleri çevresel titreşim kayıtlarından tespit edilmiştir. Binanın 2019 yılında meydana gelen moment büyüklükleri M_w 3.9–6.0 ve binaya uzaklıkları 15–283 km olan depremler sırasında

alınan tepki kayıtları analiz edilmiştir. Binanın sonlu eleman yapısal modeli oluşturulmuştur. Sonlu eleman modelinden elde edilen doğal titreşim frekansları ve titreşim mod şekilleri binanın sistem tanılamasından tespit edilenlerle uyuşmaktadır.

Anahtar Kelimeler: Çevresel Titreşim, Deprem Tepkisi, Dinamik Özellikler, Sistem Tanılaması, Yapı Sağlığı İzleme

To my family,

ACKNOWLEDGMENTS

The author wishes to express his deepest gratitude to his supervisor Dr. Ozan Cem Çelik for his guidance, advice, criticism, encouragement and insight throughout the research.

This study is funded by the Disaster and Emergency Management Presidency of Turkey under grant UDAP- G-17-04. This support is gratefully acknowledged.

The author thanks Mistral Izmir Management for authorizing the deployment of the SHM system, Ozan Çağlar İnaç for coordinating all these efforts, and Süleyman Tunç and Mustafa Hatipoğlu for setting up the SHM system.

The author thanks his friends and colleagues: Yavuz Semerdöken, Yunus Işıkli, Erhan Budak, Yaşar Çepni, Esat Çandır and Gökhan Coşkun for their support, constant encouragement and devoting of precious times.

The author would like to present his deepest thanks and heartfelt love to his parents, brothers and sister, who have been with him all the time to spur his spirits.

Finally, the author would like to thank everybody who was important to the successful realization of this thesis, as well as express apologies that he could not mention all participants one by one.

TABLE OF CONTENTS

LIST OF TABLES

TABLES

LIST OF FIGURES

FIGURES

CHAPTER 1

INTRODUCTION

1.1 Background

In recent years, tall building construction has rapidly increased in major cities in the world due to the exponential increase in urban population (rural to urban migration), land acquisition costs (insufficient construction sites), global competition, urban regeneration, and the insufficient space for transportation and infrastructure. In seismic regions, tall buildings should be monitored in real time to quickly assess their safety and minimize downtime following earthquake events. There were 147 completed buildings taller than 100 m as of the end of the year in 2019 in Turkey: 98 in Istanbul, 36 in Ankara, 10 in Izmir, two in Konya and one in Mersin (The Council on Tall Buildings and Urban Habitat, 2020). Five tall buildings in Istanbul have been permanently instrumented (Cakti and Safak, 2014; Kaynardag and Soyoz, 2014). Structural health monitoring (SHM) systems on these buildings were installed in the absence of any specific guidelines in Turkey due to lack of regulation in this matter which only changed very recently. The new Turkish Building Earthquake Code (Disaster and Emergency Management Presidency of Turkey, 2018) now requires real-time monitoring of the structural response of buildings that are taller than 105 m and of Earthquake Design Class 1 and 2 (i.e., design earthquake spectral acceleration parameter at short periods, $S_{DS} \geq 0.50$). In order to develop guidelines for the SHM systems that will be installed on these tall buildings, the Disaster and Emergency Management Presidency of Turkey has funded two concurrent research projects, which were undertaken at Middle East Technical University and Bogazici University. Within the scope of these projects, two tall buildings in Izmir (Gumus and Celik, 2019) and Istanbul (Aytulun and Soyoz, 2019), respectively, were instrumented as case studies for SHM systems on tall buildings per the new Code.

This study focuses on the development of SHM Guidelines for Tall Buildings in Turkey, the instrumentation of the case study building in Izmir, the interpretation of its ambient and earthquake vibration records, and the development of a finite element structural model to verify the results.

1.2 Objectives and Scope

The main goals of this study are listed below:

1. Review the literature on building response monitoring and examine the existing SHM guidelines for buildings and the strong motion instrumentation examples of buildings.
2. Instrument a tall building to set an example for the SHM systems on tall buildings per the new Turkish Building Earthquake Code.
3. Identify the structural system dynamic properties of the building from its ambient vibration records.
4. Develop a finite element structural model of the building to compute its natural vibration frequencies and mode shapes, and compare with those identified from ambient vibration records.
5. Present the recorded structural responses of the building during multiple earthquakes in 2019.
6. Develop guidelines for SHM systems on similar tall buildings in Turkey.

1.3 Thesis Outline

This chapter has presented the background and the objectives and scope of this study.

Chapter 2 reviews the previous research on structural response monitoring, examines the existing SHM guidelines and presents the strong-motion instrumentation examples, for buildings in particular.

Chapter 3 presents the structural system of the case study building, a 216 m tall office building in Izmir and its instrumentation scheme.

Chapter 4 presents the signal processing of the ambient vibration records of the building and its system identification by algorithms that use Fourier transforms and band-pass filters.

Chapter 5 presents the structural response records during earthquakes in 2019 with moment magnitudes M_w 3.9–6.0 and epicenters 15–283 km away from the building.

Chapter 6 explains the finite element structural modeling of the building, presents the eigenvalue analysis performed to determine its natural vibration frequencies and mode shapes, and compares them with the system identification results.

Chapter 7 presents the guidelines developed for the SHM systems on tall buildings in Turkey.

Finally, Chapter 8 presents a summary of the research, conclusions drawn from this study and future needs in the structural response monitoring of buildings.

CHAPTER 2

LITERATURE REVIEW

2.1 Structural Response Monitoring

Monitoring structural response provides invaluable information for understanding the behavior of structures under dynamic excitations, developing the building codes, improving the modeling of structural systems and assessing the condition of structures following severe earthquakes. Data recorded from SHM systems are basically used to identify the structural system dynamic properties (natural vibration frequencies, damping ratios and vibration mode shapes). These properties can be determined from laboratory tests, computer simulations and the natural laboratory of the earth (Celebi, 2002). For the latter approach, forced vibration testing (Celik et al., 2015), ambient vibration testing (Skolnik et al., 2006) and seismic monitoring (Celebi and Safak, 1991) studies can be carried out on existing structures. Substantial equipment, labor and time are required to produce the sinusoidal excitation in forced vibration tests (Celebi et al., 1987), whereas such an artificial excitation is not required in ambient vibration tests (Ivanovic and Trifunac, 1995). Hence, ambient vibration tests are generally preferred. The ultimate objective is monitoring the dynamic response of buildings during earthquakes (Jennings and Housner, 1971; Foutch et al., 1975).

The U.S. Coast and Geodetic Survey (USCGS) started implementing ambient vibration tests to capture the fundamental periods of buildings in the 1930s (Carder, 1936). The first strong-motion accelerometer was deployed on the Hollywood Storage Building following the 1933 M_w 6.3 Long Beach, California earthquake (Trifunac and Todorovska, 2001).

During the 1971 M_w 6.6 San Fernando earthquake, earthquake-induced vibrations of a large number of buildings were recorded for the first time thanks to the 1965 Los Angeles City Building Code. This Code had required three triaxial accelerometers (one in the basement, one at the mid-height and one on the roof) to be deployed in buildings taller than six stories in the city. Building responses during this destructive earthquake were recorded by more than 175 accelerometers deployed at various levels of multi-story buildings in and near the Los Angeles area. The absence of free-field strong motion records was the most remarkable deficiency of the SHM network of the Los Angeles area (Hudson, 1971; Foutch et al., 1975).

In the U.S., the seismic instrumentation of structures has been accomplished by state, federal and private institution programs. One of the most important state programs is the California Strong Motion Instrumentation Program (CSMIP), which was established by the California Department of Conservation Division of Mines and Geology following the 1971 San Fernando earthquake. More than 170 buildings were instrumented in California until 2001 within the scope of the CSMIP (Erdik et al., 2001; Johnson et al., 2001). Federal programs are mainly nationwide instrumentation programs managed by the U.S. Geological Survey (USGS). One of these programs is the National Strong Motion Program (NSMP), which was established in 1929 (Committee for the Future of the US National Strong-Motion Program, 1997). The USGS instrumented more than 160 buildings in the earthquake-prone areas of the U.S. and Puerto Rico until 2001 within the scope of the NSMP (Committee for the Future of the US National Strong-Motion Program, 1997; Johnson et al., 2001). The Advanced National Seismic System (ANSS) is another instrumentation program authorized by the USGS. It was launched in 2000 to monitor and report the earthquake responses of structures from national, regional and urban networks (ANSS Technical Integration Committee, 2002). The ANSS program was initially funded to install 3000 accelerometers to monitor various buildings within a decade (Johnson et al., 2001). Instrumentation programs developed by the International Business Machines and the University of Southern

California are two well-known instrumentation programs of private institutions (Celebi et al., 1987).

The distribution of the SHM instruments throughout the building has an important role in collecting the necessary information about the structural response of the building under dynamic and ambient loads (Shakal et al., 1998) and in verifying the adequacy of the mathematical models of the structural systems (Celebi et al., 1987). Accordingly, the required information about the structural response dictates the minimum number of channels used in SHM systems. Initially, the 1976 Uniform Building Code (UBC) recommended that typical buildings be instrumented with three triaxial accelerometers: one in the basement, one at the mid-height and one on the roof (International Conference of Building Officials, 1976). However, the analysis of the recorded vibrations indicated that the 1976 UBC instrumentation scheme was insufficient. For example, the rocking motion of the building foundation could not be calculated, which is essential for identifying the contribution of the soil-structure interaction (SSI) effects to the total building response (Trifunac and Todorovska, 2001). The mathematical model of the building could not be validated due to the lack of information about the torsional modes (Celebi et al., 1987). Hence, in the late 1970s, a new instrumentation scheme, which consisted of uniaxial accelerometers and a central recording system, was introduced. This scheme provided flexibility in deploying the accelerometers and permitted collecting the required information about the structural response of various buildings (Trifunac and Todorovska, 2001). It is generally assumed that floors in buildings show rigid diaphragm action. In which case, two translational components and one rotational component of motion are required to define the motion of the floor in the horizontal plane. Therefore, at least three horizontal uniaxial accelerometers are required as shown in Figure 2.1a. In total, 12 uniaxial accelerometers are required to identify the first four translational modes along both axes and the first four torsional modes of the building (Rojahn and Matthiesen, 1977). If rocking responses of the building are also of concern in addition to the horizontal base motion, then at least six additional uniaxial accelerometers at the base of the building, three in the horizontal direction

and three in the vertical direction, are required as shown in Figure 2.1b (Rojahn and Matthiesen, 1977; Celebi et al., 1987). In case of a flexible floor, uniaxial accelerometers are placed at the edge of each rigid sub-segment of the floor (Celebi et al., 1987). Figure 2.2 shows an example instrumentation plan for a flexible floor. Special instrumentation arrays are needed to collect additional information about the building responses. The following information can be collected depending on the layout of the accelerometers throughout the building:

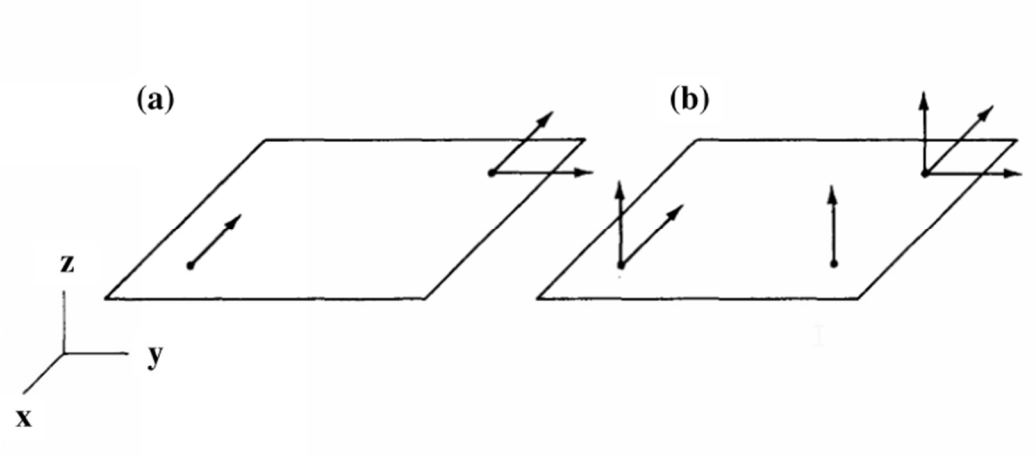

Figure 2.1 Typical instrumentation plan for a rigid floor: (a) horizontal motion, (b) horizontal and vertical motion (Celebi et al., 1987).

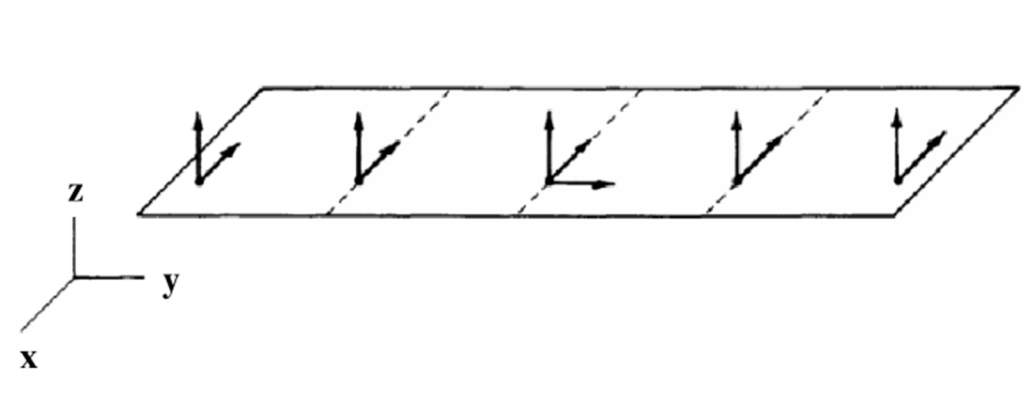

Figure 2.2 Instrumentation plan for a flexible floor that is rigid along and around the y-axis only (Celebi et al., 1987).

- Both translational and torsional floor responses are recorded by placing three horizontal accelerometers on a floor (two parallel along one axis of the building and a third along the perpendicular axis; Celebi, 2002). Torsional responses are calculated as the differences between the recorded translational responses by two parallel accelerometers divided by the distance between them.
- Rocking responses are calculated similarly from the records of at least three vertical accelerometers at the basement level of the building (Celebi et al., 1987).
- Interstory drifts are calculated from the records of horizontal accelerometers on two consecutive floors (Skolnik et al., 2008).
- Wave propagation and damage detection studies are possible when consecutive floor responses are recorded (Garevski, 2013).
- The rigid diaphragm assumption is validated by placing a third parallel accelerometer on the floor center (Celebi, 2002).
- SSI analysis is possible when free-field and downhole instrumentation arrays exist at the building site. Characteristics of the underlying soil layers and seismic wave amplification in the soil strata can also be determined by these arrays (Celebi et al., 1987; Garevski, 2013).
- The performance of base-isolated buildings and the effectiveness of their isolators are monitored by placing triaxial accelerometers at the top and bottom of the isolators (Garevski, 2013).

During the workshop by the Consortium of Organizations for Strong-Motion Observation Systems (COSMOS), six instrumentation schemes shown in Figure 2.3 were proposed by Huang and Shakal (2001). Scheme 1 includes two triaxial accelerometers, one at the building base and one at the free field. This scheme provides the input ground motion for the building and the strong ground motion

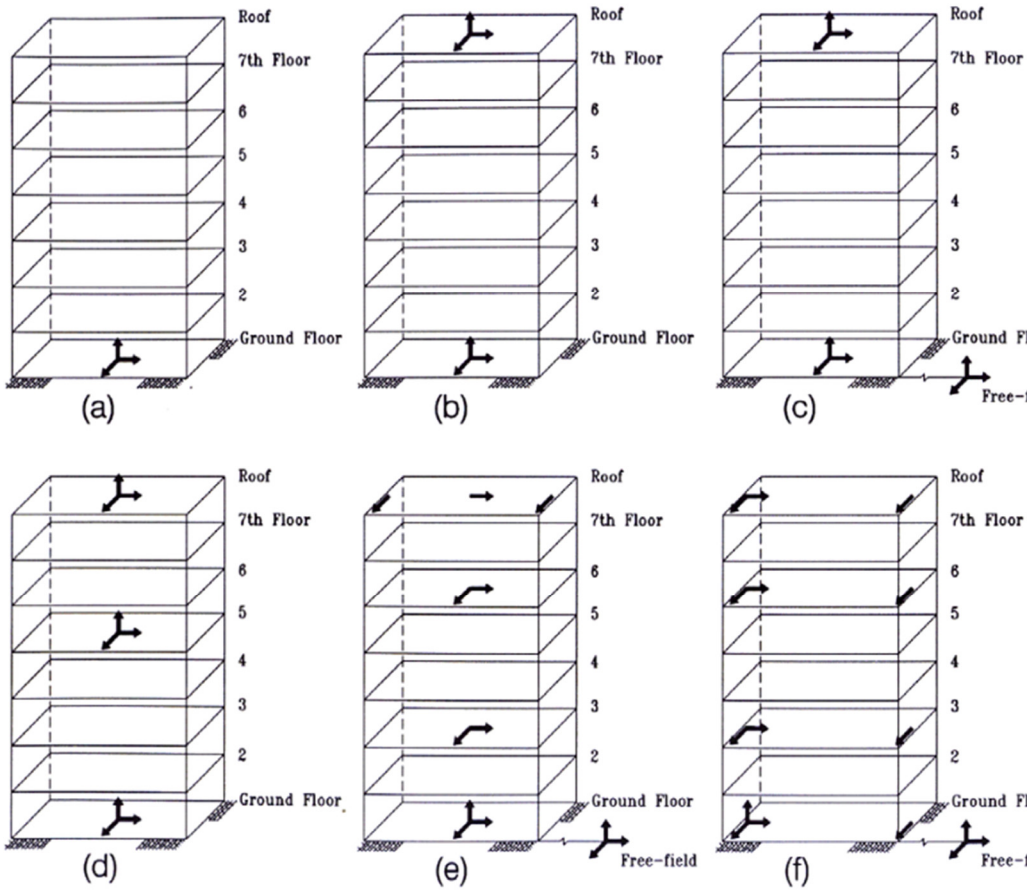

Figure 2.3 Instrumentation schemes proposed by the CSMIP: (a) Scheme 1, (b) Scheme 2, (c) Scheme 3, (d) Scheme 4, (e) Scheme 5 and (f) Scheme 6 (Johnson et al., 2001).

at the site. Scheme 2 includes two triaxial accelerometers, one at the building base and one on the roof. This scheme provides the input ground motion, the roof response, and the natural vibration frequencies and damping ratios for the first few translational modes of the building. However, it does not provide torsional responses, rocking responses, vibration mode shapes or SSI responses. Scheme 3 is the same as Scheme 2 except an additional triaxial accelerometer at the free field. This scheme also provides the strong ground motion at the site. Scheme 4 is the scheme recommended by the 1997 UBC (International Conference of Building Officials, 1997), which is the same scheme as in the 1977 version. This scheme provides the same information as Scheme 2 and in addition the vibration mode shapes for the first

two translational modes of the building. However, it lacks a free-field station. Scheme 5 is a multi-level instrumentation scheme with 13 channels of accelerometers: three uniaxial accelerometers on the roof; four uniaxial accelerometers on two intermediate floors (two accelerometers on each); and two triaxial accelerometers, one at the building base and one at the free field. This scheme also provides the translational responses of two intermediate floors and the torsional response of the roof when compared to Scheme 3. Scheme 6 is another multi-level instrumentation scheme, with 16 channels of accelerometers. This scheme also provides the torsional responses of two intermediate floors and the building base. If required, vertical accelerometers can be placed at the basement to evaluate the rocking responses of the building. In general, Schemes 5 and 6 are used for the instrumentation of buildings by the CSMIP (Johnson et al., 2001).

The following priorities should be considered in instrumenting buildings (Celebi et al., 1987):

1. Firstly, one set of accelerometers should be placed at the basement level to monitor the response of the building base during an earthquake event.
2. The second set should be placed on the roof level due to non-zero amplitudes for all vibration modes at this level.
3. The subsequent sets should be placed at levels where there are dynamic response modification features (e.g., bucking-restrained braces (BRBs), mass tuned dampers), structural discontinuities, and sudden changes in floor mass, floor stiffness or geometry.
4. Finally, the remaining sets should be placed at levels where vibration mode shape amplitudes are expected to reach their maximum values.
5. If free-field stations are not available in the vicinity of the building, a triaxial accelerometer should be placed at the free field. Vertical accelerometers should be placed at the building base when rocking responses are significant.

2.2 Existing Standards on Strong-Motion Instrumentation of Buildings

In the last decades, the number of instrumented structures has dramatically increased worldwide. Guidelines for SHM systems are required for building owners and practicing engineers to benefit to the maximum extent from the information that the SHM systems offer (Zhou et al., 2013). SHM guidelines, standards and reports for different types of structures, mainly buildings and bridges, released by different regional, national and international administrations are reviewed below.

In the U.S., there are a number of SHM guidelines prepared by government agencies and private organizations. The 1976 UBC recommendations can be accepted as the first guidelines on the instrumentation of buildings. Placing three triaxial accelerometers (one at the basement, one at the mid-height and one on the roof) were enforced for buildings over ten stories — six stories if the total floor area is greater than 5600 m^2 — in seismic zones 3 and 4 for monitoring purposes (International Conference of Building Officials, 1976). This instrumentation scheme did not provide adequate information to analyze the structural response of buildings. In between 1976 and 1997, many other reports that refer to the 1976 UBC recommendations were published. In 1997, the USGS prepared the Seismic Instrumentation of Federal Buildings (Celebi and Nishenko, 1997) to provide more extensive information about the seismic instrumentation of buildings. This document was a preliminary report not endorsed by the U.S. government. The target buildings were only the federal buildings in seismic zones 3 and 4 because no authorization was required for installing SHM systems on these buildings. There were different instrumentation schemes for different objectives such as monitoring the whole structural response (translational, torsional and rocking responses), identifying the flexible diaphragm response and determining the response of a base-isolated building. It also included a free-field instrumentation scheme for analyzing the SSI responses. This report was revised in 1998 and 2000, and its final version was published in 2002 (Celebi et al., 1998; Celebi, 2000, 2002b). The latest version included information about data retrieval and processing in addition to the required

instrumentation schemes, and a case study, the seismic instrumentation of Pacific Park Plaza in Emeryville, California. ANSS Technical Integration Committee (2002) published another guidelines, which was not endorsed by the U.S. government, that described the methodology and implementation of the integrated ANSS network. Data archival and analysis were also covered in this document. It was later updated to provide detailed information about the installation of SHM systems for implementing strong ground motion monitoring (ANSS Structural Instrumentation Guideline Committee, 2005). On the bridge front, a research group from Drexel University Intelligent Infrastructure Institute prepared SHM guidelines for bridges, which was reported to the Federal Highway Administration Research and Development of the U.S. Department of Transportation (Aktan et al., 2002). SHM, condition assessment and operational management of bridges in the U.S. were covered in this document. There are also other SHM guidelines that were published as parts of available codes; for example, an attachment to the 2013 San Francisco Building Code (2014), a section in seismic provisions for tall buildings in Los Angeles, California (Los Angeles Tall Buildings Structural Design Council, 2017) and an appendix in performance-based seismic design guidelines for tall buildings (Pacific Earthquake Engineering Center, 2017).

In Canada, the Canadian Network of Centers of Excellence on Intelligent Sensing for Innovative Structures (ISIS Canada) published a document presenting SHM guidelines as a series of design manuals in 2001 (ISIS Canada, 2001). This document was for SHM systems on civil engineering structures, particularly on bridges. It includes SHM system requirements, static and dynamic field-testing methodologies, periodic monitoring methodology and several case studies.

In the European Union, the Federal Institute of Materials Research and Testing prepared a document presenting SHM guidelines as a part of the final report of Structural Assessment, Monitoring and Control (SAMCO; Rucker et al., 2006). It includes SHM system requirements, monitoring procedures, static and dynamic field tests, numerical analysis procedures, damage identification methods and several case studies.

In the United Kingdom, the SHM of dams has been mandatory since the collapse of a 30 m embankment dam that caused the death of 254 people near Sheffield in 1864. The most recent version of the legislation is the Reservoir Act of 1975 (Brownjohn, 2007).

In Russia, the SHM of buildings is mandatory and the SHM systems should comply with the standard entitled Buildings and Constructions, Rules of Inspection and Monitoring of the Technical Condition (Russian GOST R 53778-2010; The State Unitary Enterprise of the City of Moscow, 2010). It includes SHM procedures, testing methods and structural condition assessment by SHM systems.

In China, there are a number of SHM standards for different types of structures:

1. SHM System Technical Specification for the Tianjin Grand Bridge, which was developed by the Tianjin Municipality in 2011 (Wang et al., 2011).
2. Design Standard for SHM Systems, which was developed for bridges and high-rise buildings by the China Association for Engineering Construction Standardization in 2012 (Li et al., 2012).
3. Technical Code for Construction Process Analyzing and Monitoring of Building Engineering (Mao et al., 2013) and Technical Code for Monitoring of Building and Bridge Structures (Ministry of Housing and Urban-Rural Development of PRC, 2014), which were published by the China Ministry of Housing and Urban-Rural Development in 2013 and 2014, respectively.
4. The new Chinese SHM code, which was developed for SHM systems on highway bridges (Moreu et al., 2018).

In Germany, official guidelines for SHM systems on bridges and other structures were developed in 2012 (Osterreichische and Forschungsgellschaf, 2012; Yang et al., 2017).

In Philippines, the Guidelines and Implementing Rules on Earthquake Recording Instrumentation for Buildings was published by the Department of Public Works and Highway of the Philippines (2015).

Moreover, the International Federation for Structural Concrete released a report entitled Monitoring and Safety Evaluation of Existing Concrete Structures to monitor and evaluate concrete bridges worldwide (Bergmeister et al., 2003).

2.3 Examples of Strong-Motion Instrumentation of Buildings

SHM applications on different buildings in earthquake-prone regions are presented below. There are several SHM arrays for buildings in the U.S. completed within the scope of NSMP (USGS, 2020).

2.3.1 Federal Government Building

An ambient vibration test of the 72 m tall Federal Government Building was performed in 1964 within the scope of a trial program of the USCGS (Crawford and Ward, 1964). It is a 19-story building in Ottawa, Canada, with a rectangular footprint of 43 m by 27 m. Its structural system consists of steel columns and composite core shear walls. Ambient vibration records from seven uniaxial accelerometers deployed on different floors at different locations in multiple sets (Figure 2.4) were used in its system identification. The first three translational modes along its both short and long axes and the first three torsional modes were identified. The fundamental vibration period of the building was 1.28 s along the short axis. Modal damping ratios were not reported.

2.3.2 Transamerica Building

The structural response of the Transamerica Building was recorded during the 1989 M_w 6.9 Loma Prieta earthquake (Celebi and Safak, 1991; Safak and Celebi, 1991). The building is a 257 m tall (including its 64 m spire) 49-story vertically-tapered steel building in San Francisco, California, which was completed in 1972. It has a square footprint with 53 m sides. Its structural system consists of a very rigid box

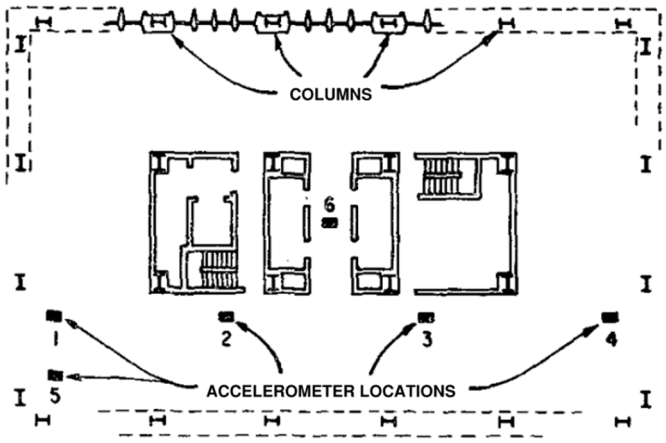

(a)

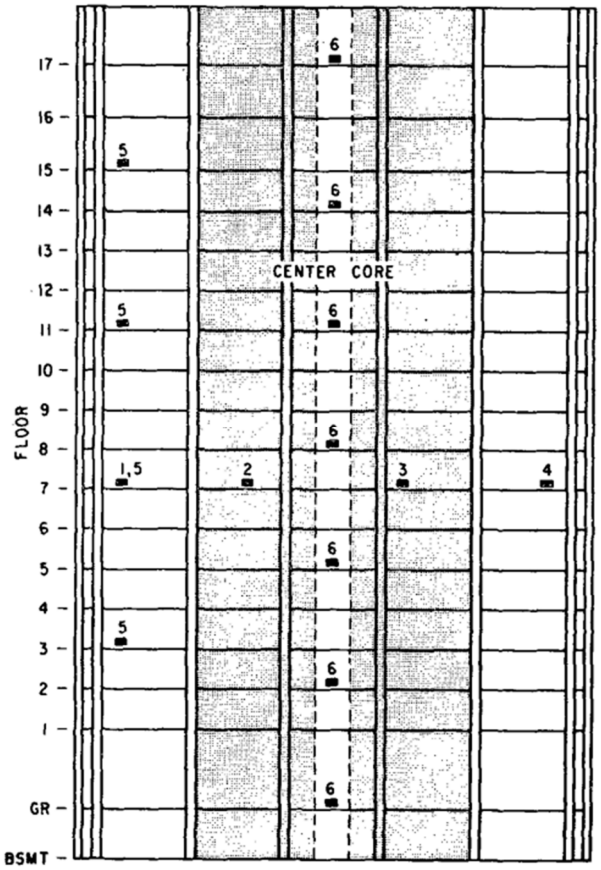

(b)

Figure 2.4 Instrumentation scheme of the Federal Government Building: (a) typical floor plan, (b) elevation (Crawford and Ward, 1964).

shear wall at the basement, a tubular space truss system between second- and fifth-floor levels and a moment-resisting frame with an inward slope of 1:11 above the fifth-floor level. The building has a 2.7 m thick mat foundation without piles. It was instrumented by 13 uniaxial accelerometers and three triaxial accelerometers deployed at six different levels of the building (Figure 2.5). There is no free-field accelerometer around the building. The maximum horizontal and vertical accelerations in the basement were 0.12 g and 0.07 g, respectively, whereas the maximum horizontal acceleration at the 49th floor was 0.31 g in the North-South (N-S) direction. The fundamental natural vibration periods were 3.6 s (0.28 Hz) in both

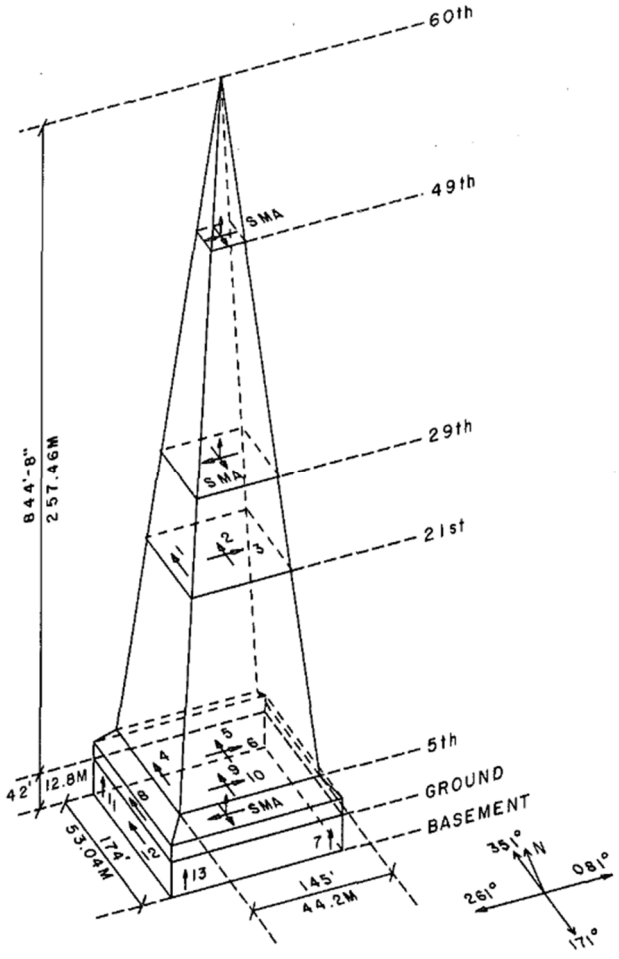

Figure 2.5 Instrumentation scheme of the Transamerica Building (Celebi and Safak, 1991).

N-S and East-West (E-W) directions. Associated damping ratios were 5% and 2%, respectively. The torsional response of the building was measured by accelerometers at the lower floor levels and stated as negligible compared to the translational response. The rocking periods of the building were 0.56 s (1.8 Hz) in the E-W direction and 0.50 s (2.0 Hz) in the N-S direction. The revised instrumentation scheme for recording the torsional responses of upper floor levels is given in Figure 2.6 (Dunand et al., 2004).

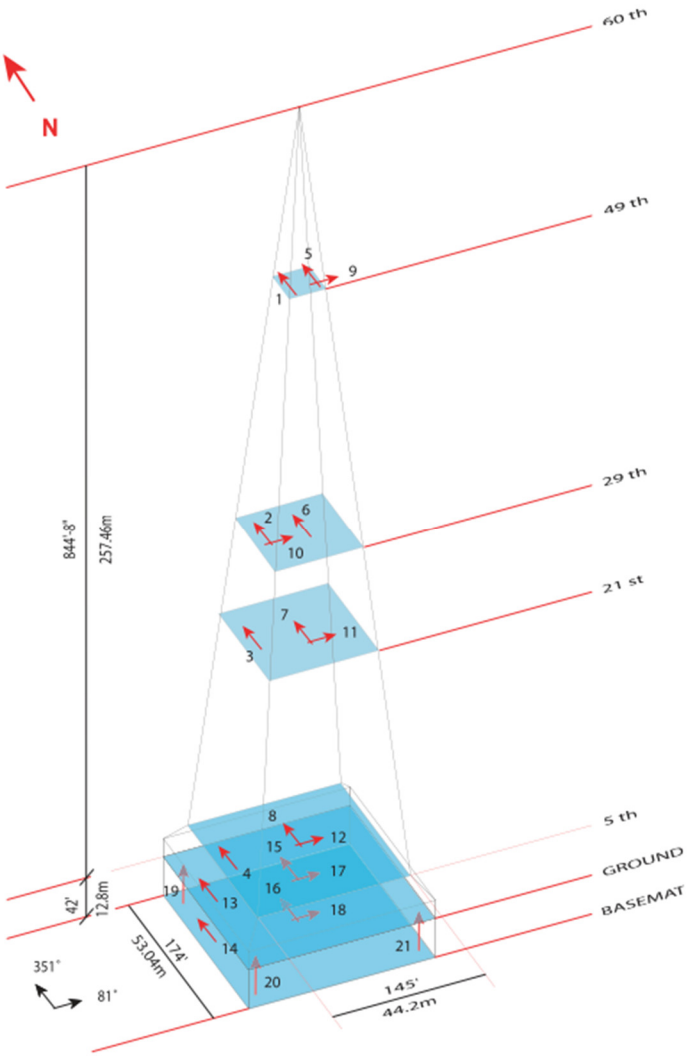

Figure 2.6 Revised instrumentation scheme of the Transamerica Building (Dunand et al., 2004).

2.3.3 Van Nuys Seven-Story Hotel (VN7SH)

The structural response of the VN7SH was recorded during the 1994 M_w 6.7 Northridge earthquake and two series of ambient vibration tests were performed on the building after the Northridge earthquake and its aftershocks (Trifunac et al., 1999; Ivanovic et al., 2000). The building is a seven-story reinforced concrete (RC) hotel building in Los Angeles, California that was constructed in 1966. Its structural system consists of RC perimeter column-deep beam moment-resisting frames and interior RC columns supporting the flat slab (Figure 2.7). The hotel building has a symmetrical rectangular footprint with 18.9 m by 45.7 m sides. The first test was performed to identify the structural system dynamic properties of the damaged building. The purpose of the second test was to record free-field ground motions and to identify the dynamic properties with accelerometers at additional floor levels after the 1994 M_w 5.2 Northridge aftershock event. Ambient vibrations were recorded for three minutes using six accelerometers installed at different locations in multiple setups during the first test. The natural vibration frequencies for the first four modes along both E-W and N-S directions and associated mode shapes were identified. The fundamental natural frequencies were 1.0 Hz and 1.4 Hz in the E-W and N-S directions, respectively. It was concluded that the exterior frames in the E-W direction were damaged extensively and the building was later tagged as unsafe.

2.3.4 One Wall Centre Tower

A series of ambient vibration tests were performed on the One Wall Centre Tower in Vancouver, Canada (Ventura et al., 2002). The building is a slender 48-story RC building (Figure 2.8a) with two concrete water tanks on the roof. The building has an oval-shaped footprint, 48.8 m along the E-W direction and 23.4 m along the N-S direction. Its main structural system consists of an RC core wall, deep outrigger beams at the 5th, 21st and 31st floors, and outrigger columns around the perimeter of the building. Ambient vibrations were recorded in seven setups by 16 channels of

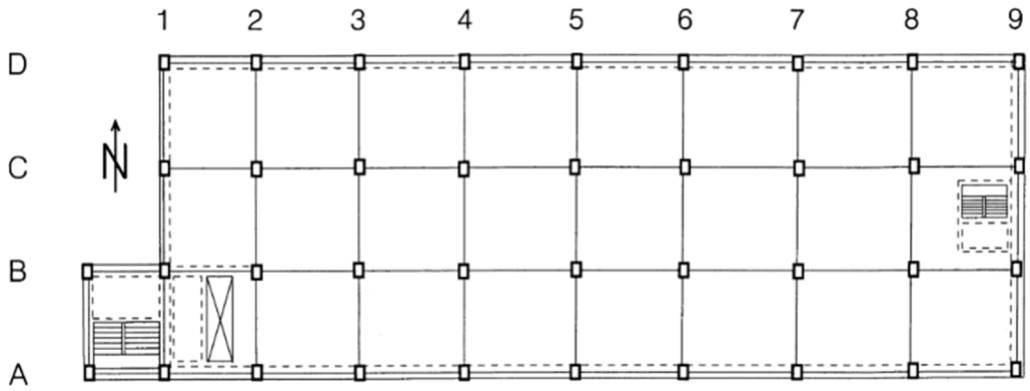

(a)

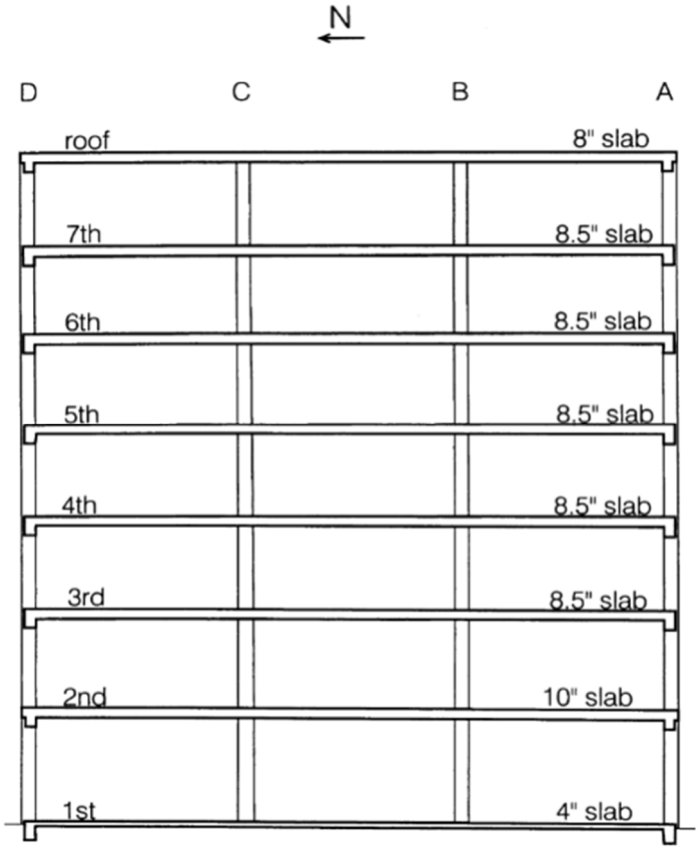

(b)

Figure 2.7 (a) Typical structural plan and (b) elevation view (1 in. = 25.4 mm) of the VN7SH (Ivanovic et al., 2000).

accelerometers. Two accelerometers in the N-S direction and one accelerometer in the E-W direction were deployed close to the building core walls on each floor (Figure 2.8b). Two accelerometers on the 45th floor were used as reference accelerometers. Structural system dynamic properties were identified for three N-S and two E-W translational modes, and three torsional modes. The finite element model (FEM) of the building was updated based on the identified structural system dynamic properties.

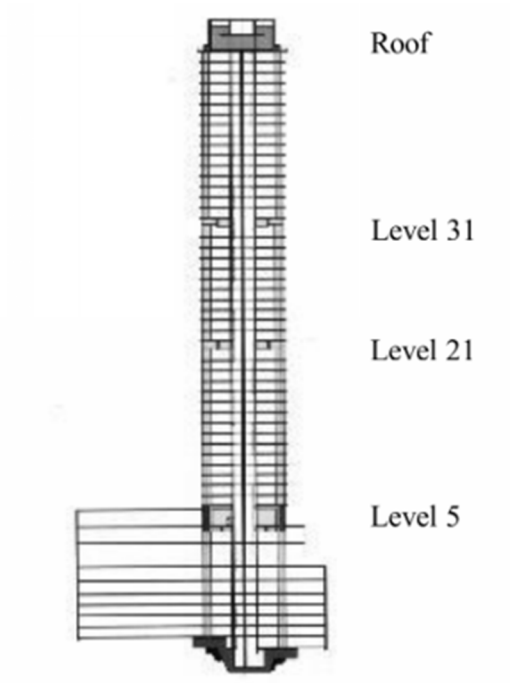

(a)

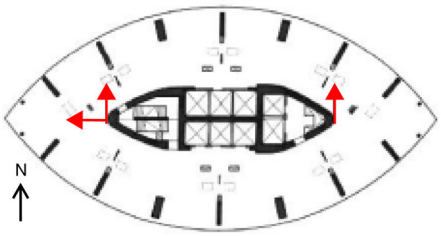

(b)

Figure 2.8 (a) Elevation view and (b) typical instrumentation scheme of the One Wall Centre Tower (Ventura et al., 2002).

2.3.5 Millikan Library

The Millikan Library in Pasadena, California has been monitored since the completion of its construction in 1967 (Clinton et al., 2006). The building is a nine-story RC building with a rectangular footprint, 22.9 m side along the E-W direction and 21.0 m side along the N-S direction. The lateral force resisting system is mainly composed of 30.5 cm thick RC shear walls at the inner core in the E-W direction and along the East and West sides in the N-S direction (Figure 2.9). The 22.5 cm thick RC slabs are supported by deep beams. The foundation system consists of a 1.2 m thick 9.75 m square central pad and a series of stepped transfer beams between the East and West side shear walls and the central pad. The first instrumentation system in 1968 included a triaxial accelerometer on the roof and another at the basement. A 10-channel array (at the basement, 6th floor and on the roof) was added in 1979. The USGS and California Institute of Technology upgraded this system by replacing the existing instrumentation with a dense array of 36 channels of accelerometers (minimum three horizontal on each floor and three vertical at the basement) as shown

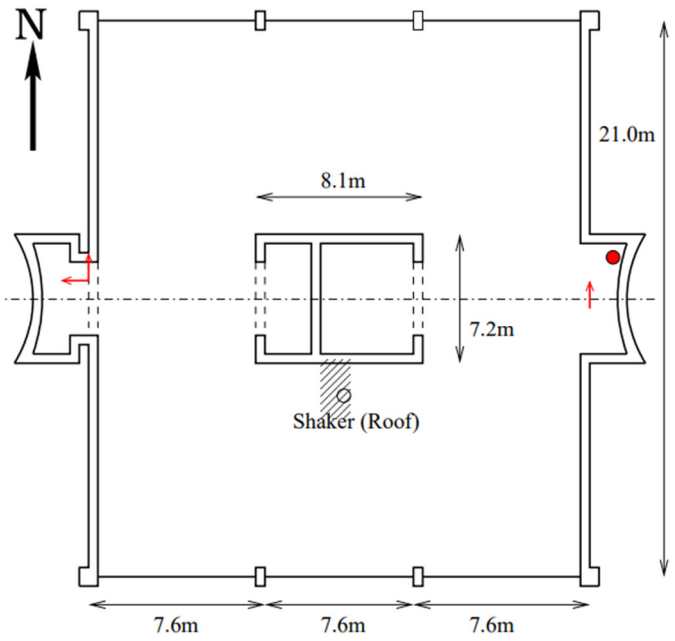

Figure 2.9 Typical floor plan of the Millikan Library (Clinton et al., 2006).

in Figure 2.10. In 2001, a triaxial accelerometer was installed on the 9th floor. The building is among the most extensively instrumented building in the world and has been the subject matter of many studies. For example, Ghahari et al. (2016) studied the changes in the fundamental frequencies due to applied forces during its forced vibration tests, weather conditions such as temperature changes, rain and wind events, minor and strong ground motions. The fundamental natural frequencies of the building identified from its forced vibration tests in 1967 were 1.45 Hz and 1.90 Hz for E-W and N-S directions, respectively. According to the system identification results of all historical data — forced vibration, ambient vibration and strong ground motion records — the fundamental natural frequencies have permanently decreased by 22% in the E-W direction and 12% in the N-S direction during its 36 years of life. These permanent reductions were largely caused by the 1971 M_w 6.6 San Fernando and the 1987 M_w 6.1 Whittier Narrows earthquakes. The changes in the natural frequencies due to weather conditions were not permanent. Strong winds without rainfall decreased all the natural frequencies. Heavy rain and higher temperature increased all the natural frequencies.

2.3.6 One Rincon Hill Tower

Ambient vibrations of the One Rincon Hill Tower in San Francisco, California were recorded (Celebi et al., 2013). The building is a slender 64-story RC building with BRBs and tuned liquid sloshing dampers (TSDs). It has a rectangular footprint, 34.4 m by 41.8 m sides. Its main structural system consists of a perforated tubular RC core wall, concrete perimeter columns, concrete outrigger columns in the E-W direction and steel BRBs at two separate floors (Figure 2.11). The building was instrumented by a dense array of 72 channels of accelerometers (Figure 2.12) within the scope of the CSMIP by the USGS. The natural frequencies for the first five translational modes in both E-W and N-S directions, and the first five torsional modes were identified. The fundamental natural frequencies were 0.28 Hz and 0.30

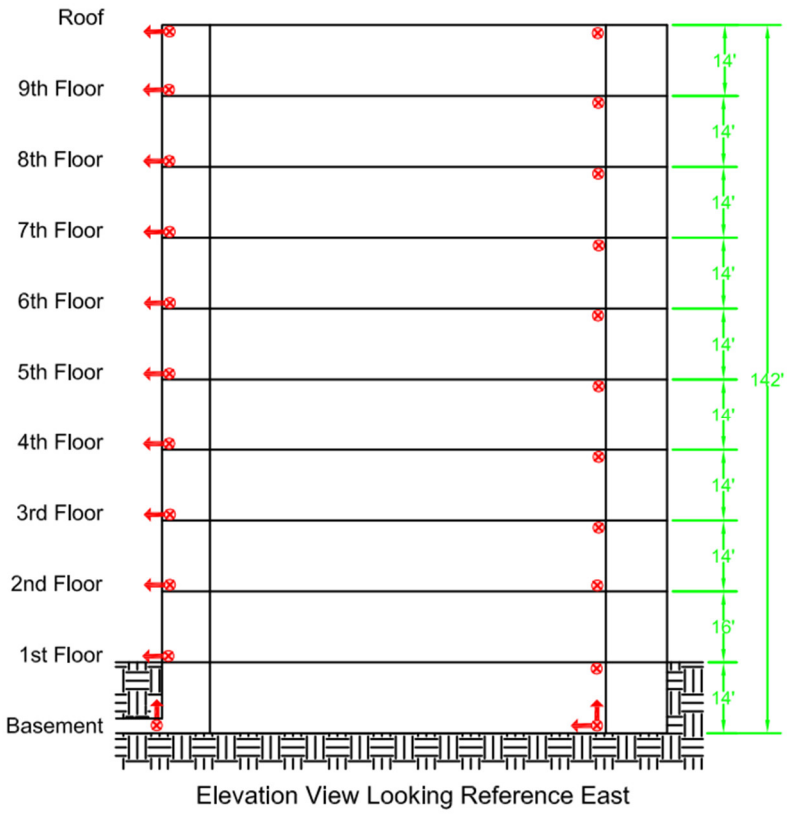

(a)

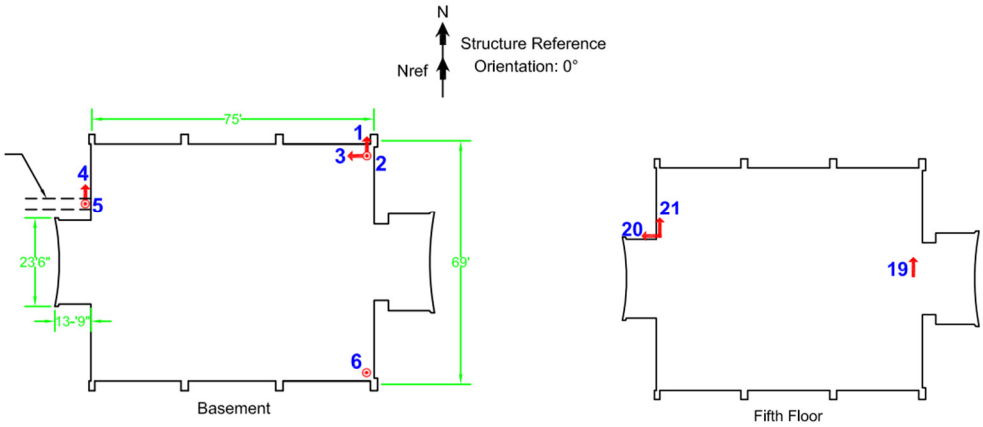

(b) (c)

Figure 2.10 Instrumentation scheme of the Millikan Library: (a) elevation, (b) basement and (c) typical floors.

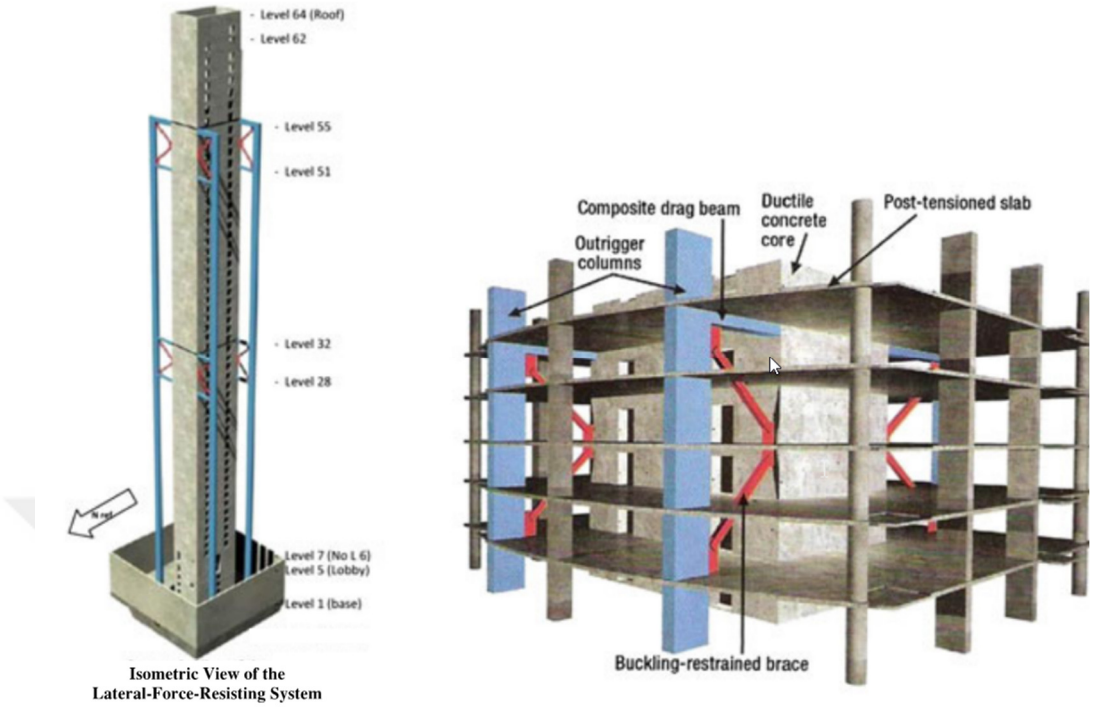

Figure 2.11. Isometric view of the structural system of One Rincon Hill Tower (Celebi et al., 2013).

Hz in the E-W and N-S directions, respectively, and 0.70 Hz for the torsion. The first modal damping ratio was less than 1%. The identified mode shapes indicated negligible contribution of steel BRBs and TSDs to the building response at low-amplitude levels.

2.4 Summary

In this chapter, the essential points and historical development of structural response monitoring were presented, which was followed by a review of existing standards for SHM systems on buildings and bridges. Finally, some important examples of strong motion instrumentation on buildings were presented summarizing their dimensions, structural systems, instrumentation schemes and system identification results.

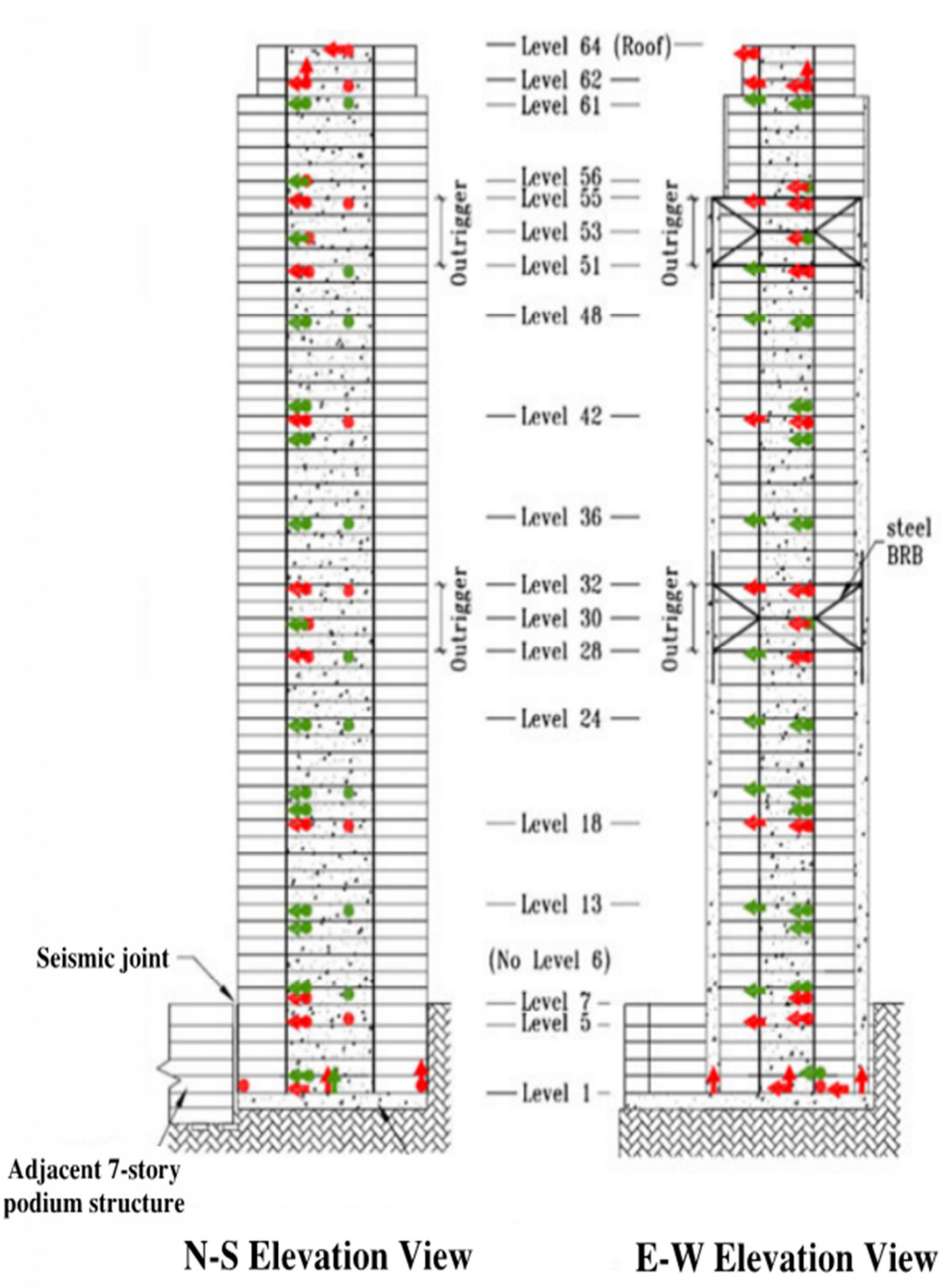

(a)

Figure 2.12 Instrumentation scheme of the One Rincon Hill Tower: (a) elevation and (b) typical floors (Celebi et al., 2013).

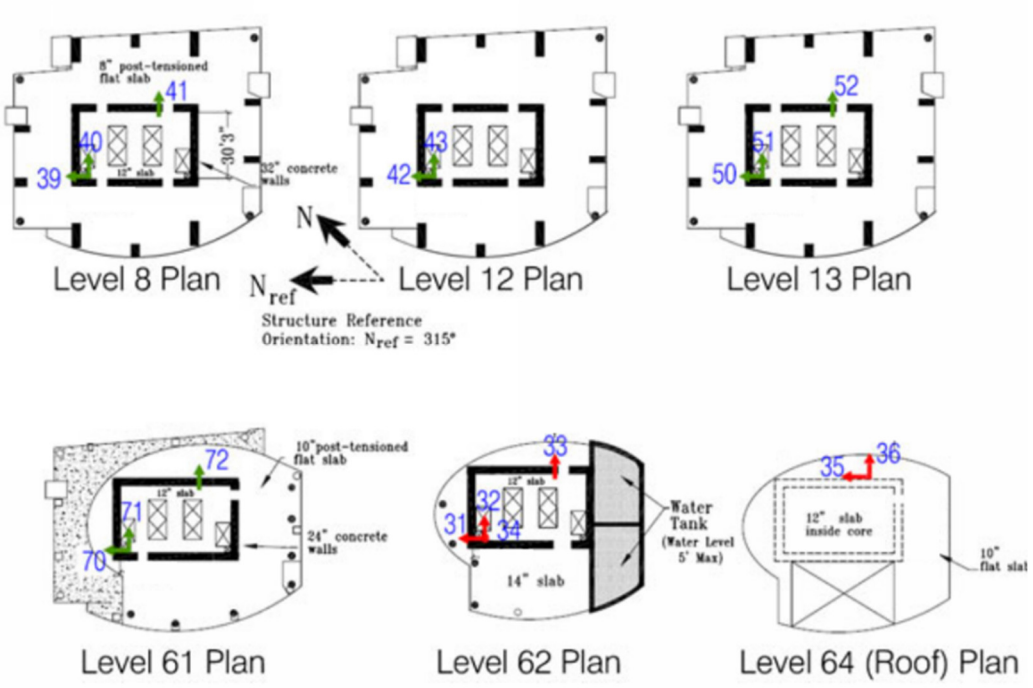

(b)

Figure 2.12 Continued.

CHAPTER 3

CASE STUDY: MISTRAL IZMIR OFFICE TOWER

3.1 Building Description

3.1.1 General

Mistral Izmir Office Tower (Figure 3.1) is a 48-story 216 m tall composite building with BRBs in Konak, Izmir (38.4480° N, 27.1794° E), which was opened in

Figure 3.1 View of the building from the east side.

December 2017. At present, it is the tallest building in Izmir. The typical floor-to-floor height is 4.0 m, whereas the heights of the podium floors, the first two floors above grade, are 5.5 m and 6.1 m, and two basement floors are 3.4 m and 3.0 m, respectively. The building has a right trapezoidal footprint with 52.9 m and 39.4 m long parallel sides along the N-S direction and a 40.8 m long perpendicular side along the E-W direction (Figure 3.2). The tower has a square footprint with 26.6 m sides (see Figure 3.3a for the 10th floor plan). E-W floor dimension reduces by 0.95 m from the West side at each floor above floor 45 (Figure 3.3b). The building facade consists of sloping glass panels that are connected to the overhang slabs of the tower.

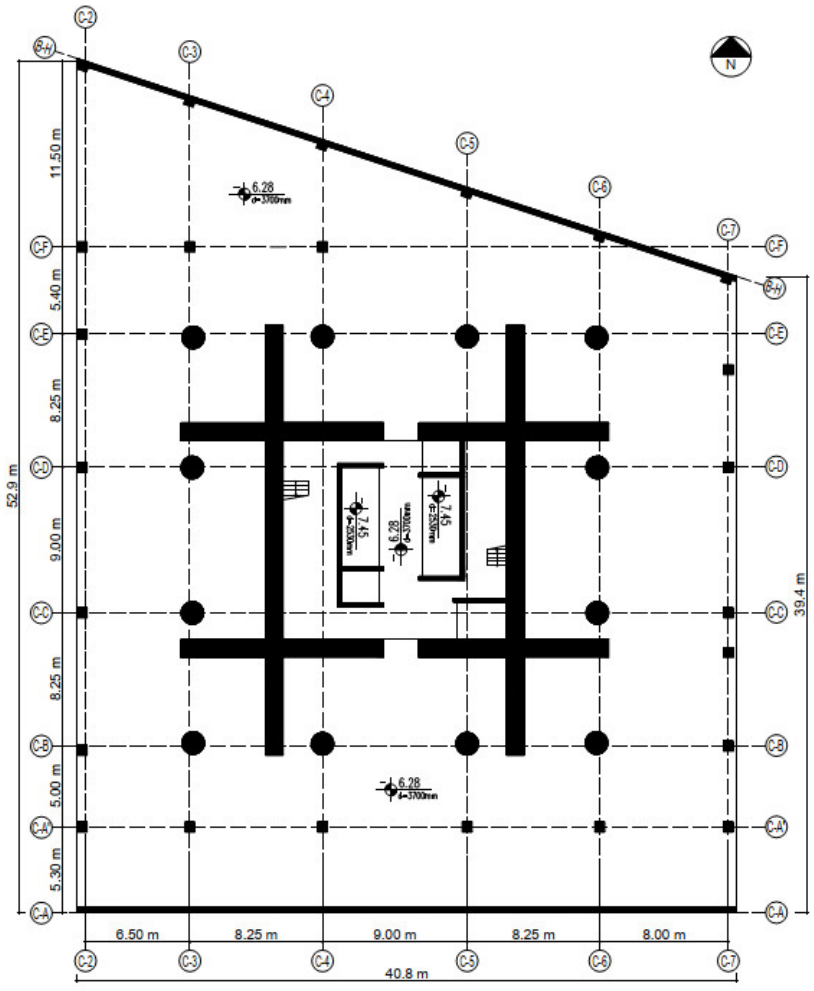

Figure 3.2 Footprint of the building.

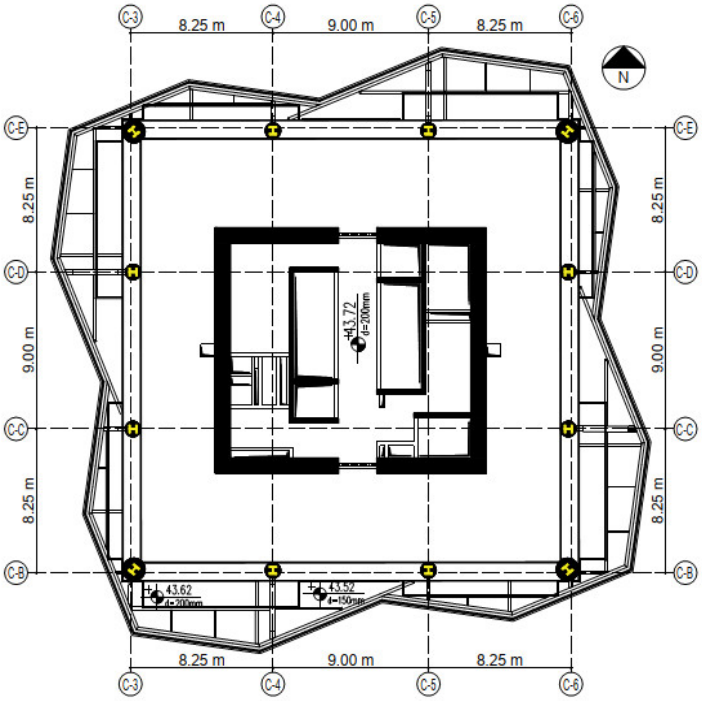

(a)

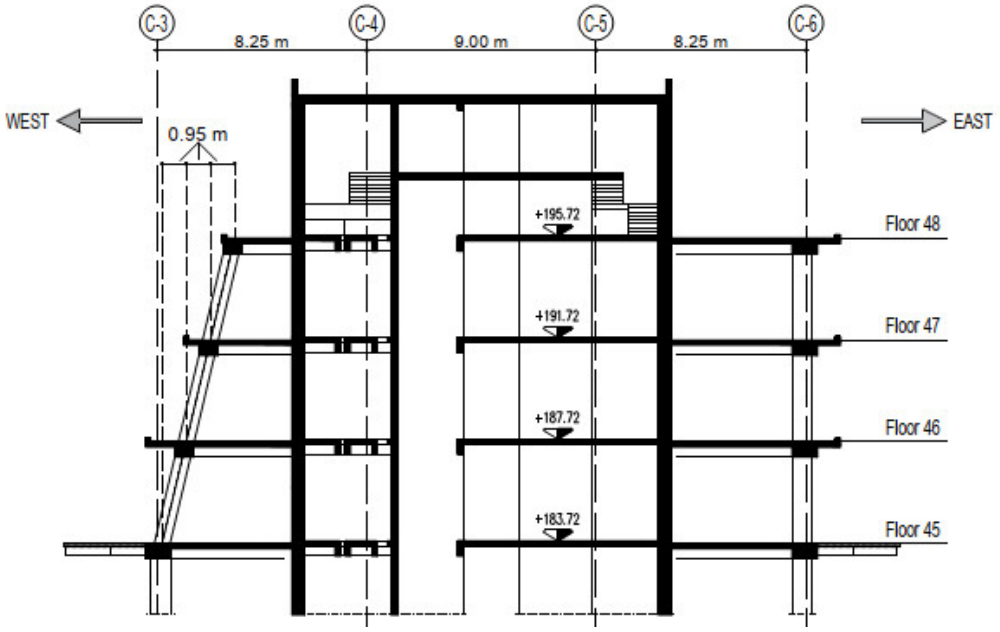

(b)

Figure 3.3 (a) 10th floor plan and (b) elevation of the building between floors 45–47.

3.1.2 Structural system

The structural system of the tower consists of two U-shaped RC core shear walls with steel coupling beams, RC moment-resisting perimeter frames with circular composite columns, and BRBs at two mechanical floors. Core shear wall thickness varies from 1.10 m at the basement to 0.50 m at the top (Table 3.1), whereas the elevator and duct shaft walls are 0.25 m thick throughout the height of the tower. Wall-to-floor area ratio is typically 5% for the tower. HEM/HEB 800 steel sections are used for the coupling beams except for the 1.10 m × 0.80 m RC coupling beams at basement 1 and ground floor. Composite columns with encased W 360 steel sections (Figure 3.4) are 1.40 m in diameter at the basement; the diameter is reduced at the upper stories to 0.80 m at the top (Table 3.2). 0.6 m × 0.6 m square RC columns exist between the basement and floor 2, which support the podium floors. Inclined RC columns on the West side of floors 45–47 are 0.6 m in diameter (Figure 3.3b). RC beams of the tower perimeter frames are 0.60 m deep with varying widths from 1.40 m to 0.75 m except the 1.10 m deep, 1.20 m wide beams at floor 2 (Table 3.3). BRB-outrigger systems link the four corner columns to the nearest corners of the

Table 3.1 Thickness of core shear walls.

Floor	Core Shear Wall Thickness (m)
30–48	0.50
22–28	0.65
21	0.75
9–20	0.90
1–8	1.10
B2–G	1.10

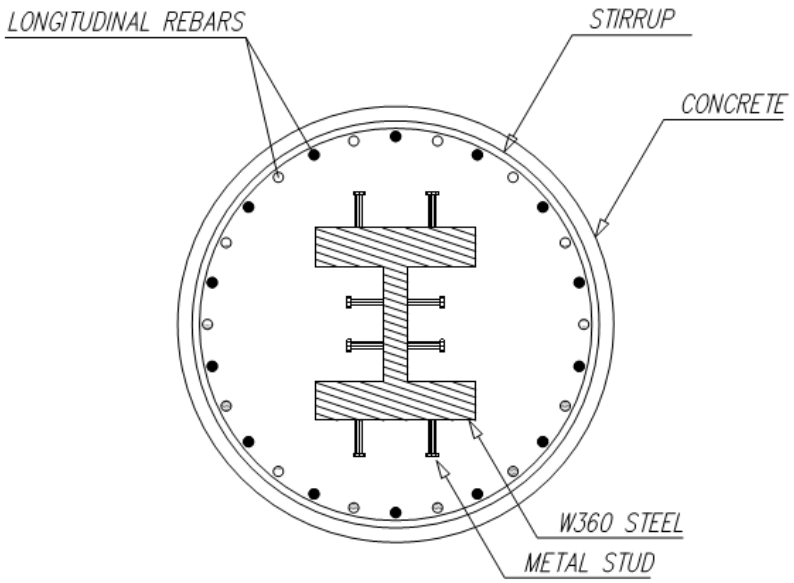

Figure 3.4 Typical composite column section.

core shear walls at floors 19 and 39 (Figure 3.5). Core shear walls are composite with encased concentric X-braced steel frames at floors 18–20 and 38–40 (Figure 3.6), and flat plates are 0.30 m thick with steel framing at floors 19–20 and 39–40 (Figure 3.7). Flat plates at other floors are 0.20 m thick except those outside the core at basement 1 and ground floor, which are 0.40 m thick. Podium slabs at floors 1–2 are 0.15 m thick waffle slabs. Overhangs around the tower perimeter are 0.15–0.20 m thick metal deck composite slabs supported on steel framing with IPE 300, IPE 360 and IPE 400 sections.

3.1.3 Foundation and soil properties

The building has a 3.7 m thick mat foundation on 0.80 m × 2.80 m barrette piles (Figure 3.8). Soil group is D and local site class is Z4 according to the Turkish Earthquake Code (Ministry of Public Works and Settlement, 2007) classification.

Table 3.2 Composite column cross sections.

Floor	Corner Columns		Edge Columns	
	Diameter (m)	Steel section	Diameter (m)	Steel section
45–47	0.8	W 360 × 262	0.8	W 360 × 196
42–44	0.8	W 360 × 421 & 262	0.8	W 360 × 196
41	0.8	W 360×421	0.8	W 360 × 196
38–40	1.2	W 360×421	0.8	W 360 × 196
36–37	1.2	W 360×421	0.8	W 360 × 216
33–35	1.2	W 360×463	0.8	W 360 × 216
30–32	1.2	W 360×509	0.8	W 360 × 216
27–29	1.2	W 360×551	0.8	W 360 × 216
24–26	1.2	W 360×592	0.8	W 360 × 262
23	1.2	W 360×634	0.8	W 360 × 262
21–22	1.2	W 360×634	0.8	W 360 × 314
19–20	1.3	W 360×634	0.8	W 360 × 347
17–18	1.3	W 360×634	0.8	W 360 × 382
15–16	1.3	W 360×677	0.9	W 360 × 421
14	1.3	W 360×677	0.9	W 360 × 509
11–13	1.3	W 360×744	0.9	W 360 × 551
9–10	1.3	W 360×818	0.9	W 360 × 634
8	1.3	W 360×818	0.9	W 360 × 677
7	1.3	W 360×900	0.9	W 360 × 677
5–6	1.3	W 360×900	0.9	W 360 × 818
3–4	1.3	W 360×990	0.9	W 360 × 900
2	1.3	W 360×990	1.2	W 360 × 900
G–1	1.3	W 360×1086	1.2	W 360 × 900
B2–B1	1.4	W 360×818	1.4	W 360 × 818

Table 3.3 RC beam cross sections.

Floor	Primary beams (cm)	Secondary beams (cm)
Top	None	20/60, 25/60
46–48	75/60, 100/60	20/60, 25/60, 60/60
20–45	100/60	20/60, 25/60
4–19	105/60	20/60, 25/60
3	120/60	20/60, 25/60
2	120/110	20/60, 25/60, 30/60, 60/60, 80/60, 90/60, 60/110
1	120/60	20/60, 25/60, 30/60, 60/60, 80/60, 90/60
G	140/60	20/60, 25/60, 60/60
B1	1400/600	20/60, 25/60, 60/60, 30/117.5

Figure 3.5 BRB-outrigger system.

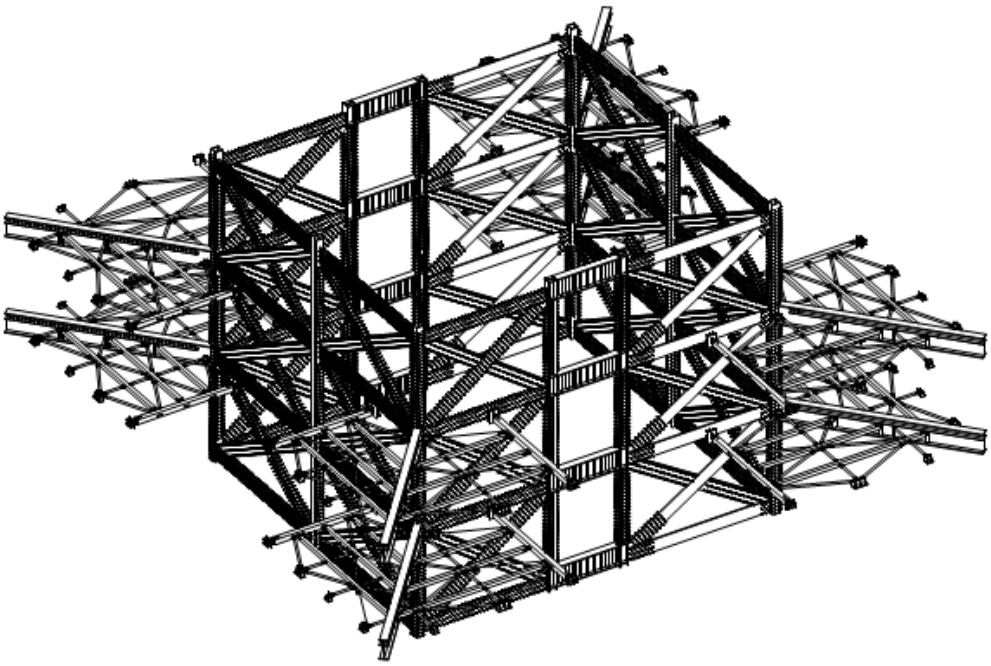

(a)

(b)

Figure 3.6 (a) Isometric and (b) construction view of the concentric X-braced steel frames.

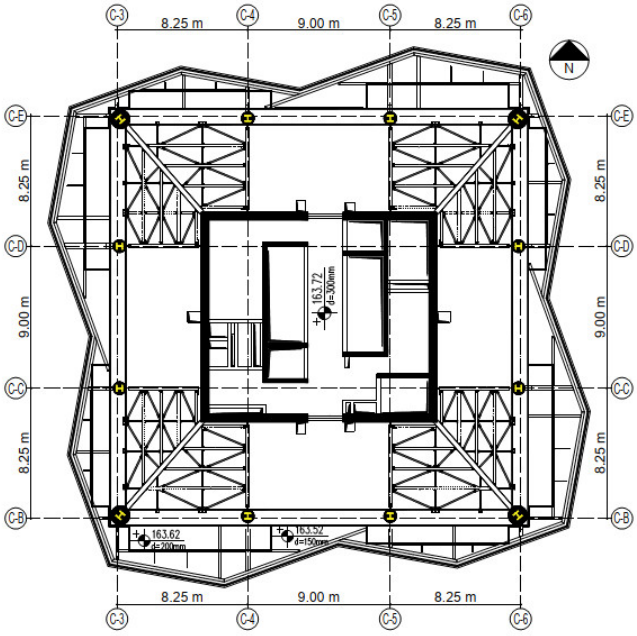

Figure 3.7 Typical plans of floors 19 and 39.

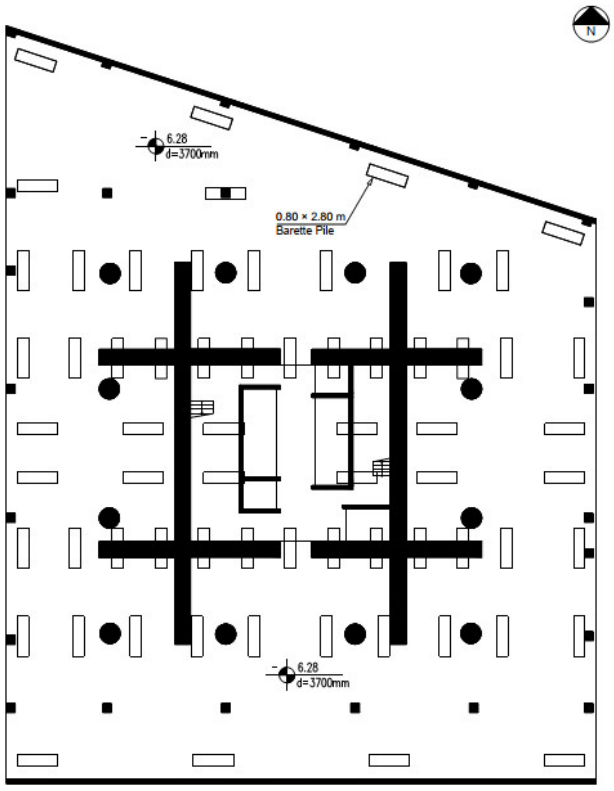

Figure 3.8 Foundation plan of the building.

3.1.4 Material properties

Concrete grades are C50 for the building, C40 for the foundation and C30 for the overhang slabs, whereas steel grades are S420 for the reinforcing steel, S460 for the composite columns and coupling beams, S355 for the built-up steel plates and S275 for the overhang beams.

3.2 Instrumentation Scheme

3.2.1 Selection criteria for SHM application

The 2019 Turkish Building Earthquake Code makes it mandatory to install an SHM system on buildings of Earthquake Design Class 1, 1a, 2 and 2a ($S_{DS} \geq 0.50$) with a height from ground level (H_N) greater than 105 m. The location of Mistral Izmir Office Tower is marked on the seismic hazard map of Turkey shown in Figure 3.9, which depicts the hazard in terms of spectral acceleration at short periods with 10% probability of exceedance in 50 years. The mapped and design spectral acceleration

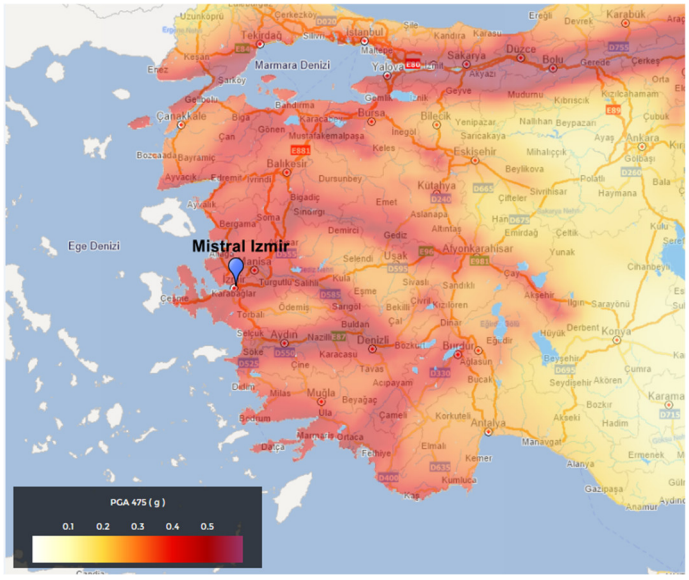

Figure 3.9 Location of the building on the seismic hazard map of Turkey.

parameters at short periods are S_S = 1.12 and S_{DS} = 1.18, respectively. Hence, the Earthquake Design Class is 1 for the building. Mistral Izmir Office Tower with H_N = 201 m is to be equipped with an SHM system according to the new Turkish Building Earthquake Code.

3.2.2 Overview

The structural response of the building has been monitored in real time since January 27, 2019 by a dense network of 27 channels of accelerometers deployed throughout the building. The SHM system on the building consists of 24 uniaxial accelerometers and one triaxial accelerometer (all 24-bit force balance type with a bandwidth of DC to 200 Hz), eight three-channel digital recorders (24-bit), one time-synchronization unit (i.e., network time protocol (NTP) server), one GPS antenna and one laptop computer (Figure 3.10).

3.2.3 Accelerometer locations and orientations

Accelerometers were placed on seven different floors, including four mechanical floors located every 10 floors starting from floor 9, as shown in Figure 3.11. Two uniaxial accelerometers parallel in the N-S direction and one in the E-W direction were placed on each ceiling of floors 47, 39, 29, 19, 9 and basement 1 (18 uniaxial accelerometers in total) within the building core. Floor 47 was additionally instrumented by three uniaxial accelerometers in the vertical direction at three corners of the ceiling. Finally, basement 2 was instrumented by one triaxial accelerometer at one corner, two uniaxial accelerometers, one horizontal and one vertical, at another corner, and one uniaxial accelerometer in the vertical direction at a third corner on the floor. Figures 3.12–3.18 show the accelerometer locations on the floor plans. This layout of the accelerometers enables recording the translational and torsional responses of the building base, ground (G) level, building top and four intermediate floors, and the rocking responses of the building.

(a)

(b)

(c)

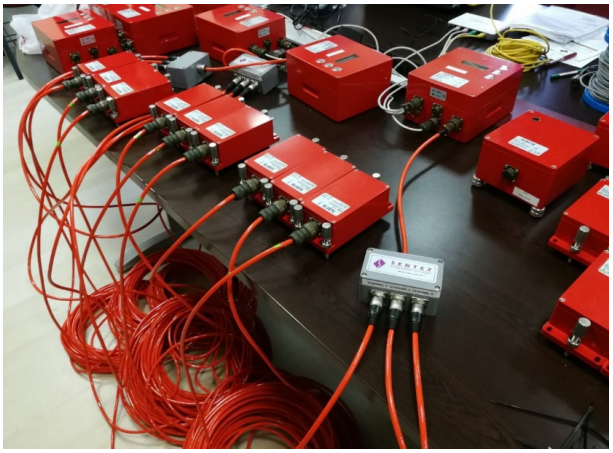

(d)

(e)

(f)

Figure 3.10 (a) Horizontal and vertical accelerometers on the ceiling of floor 47, (b) triaxial accelerometer on basement 2, (c) three-channel digital recorder, (d) general view of the components of the instrumentation system prior to the installation, (e) NTP server and (f) GPS antenna.

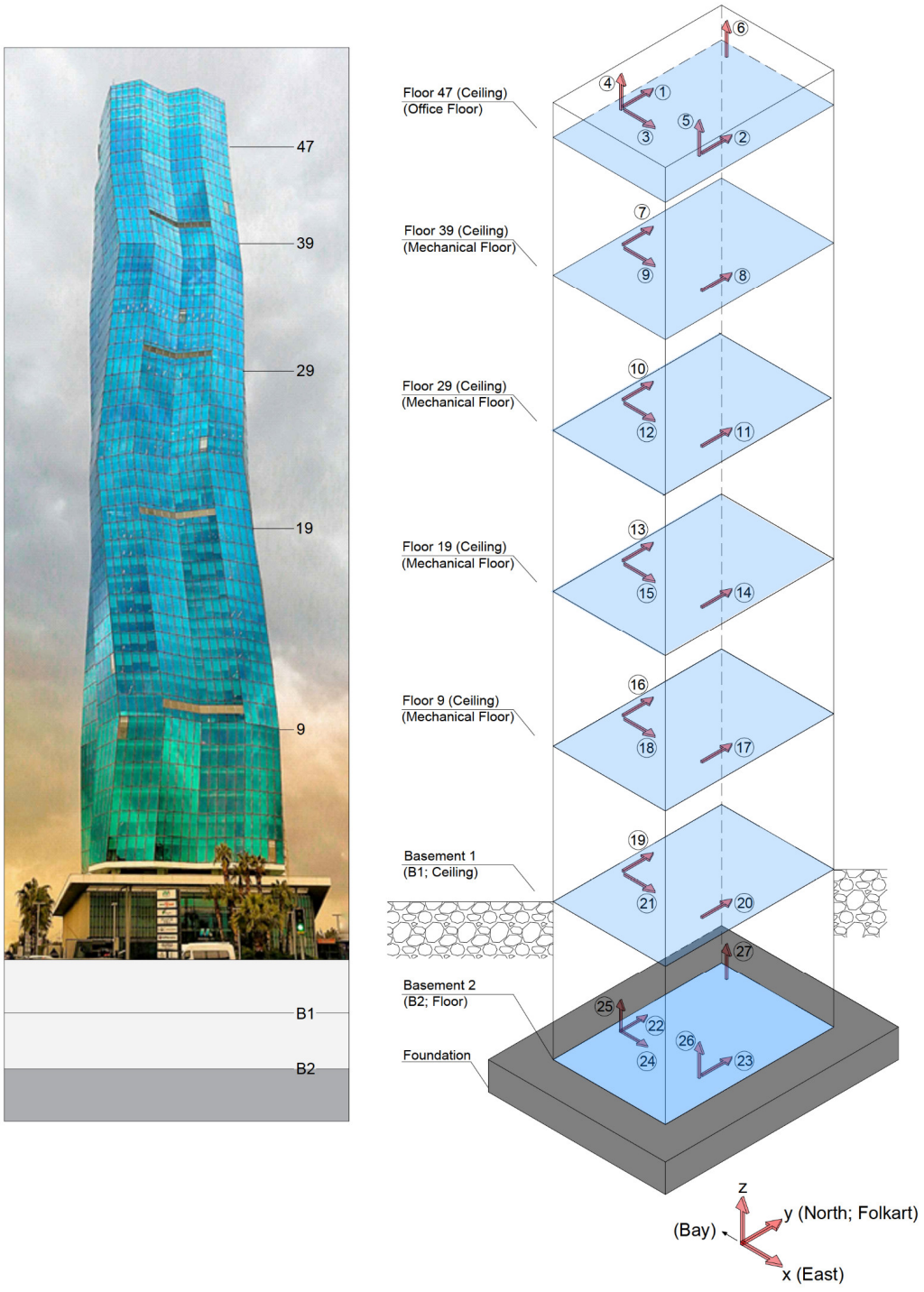

Figure 3.11 Instrumentation scheme of the Mistral Izmir Office Tower.

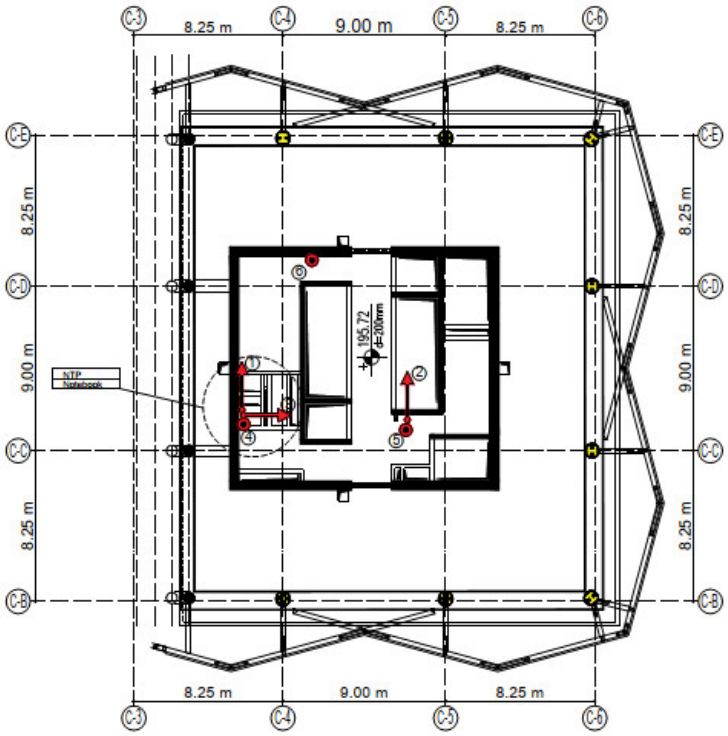

Figure 3.12 Locations and orientations of accelerometers at floor 48.

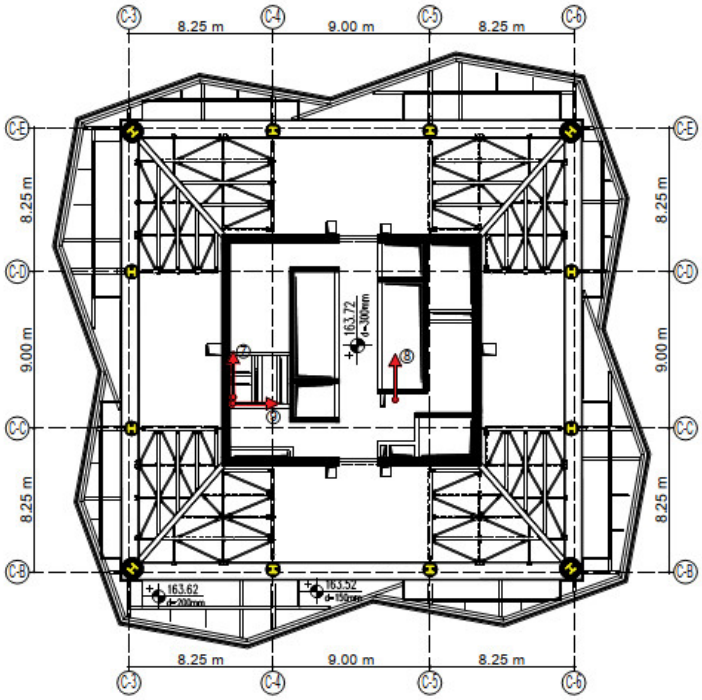

Figure 3.13 Locations and orientations of accelerometers at floor 40.

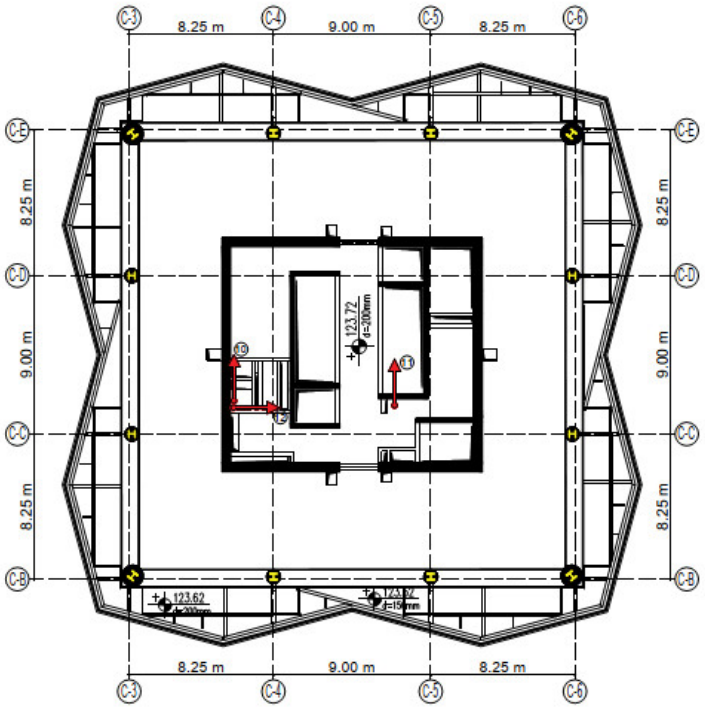

Figure 3.14 Locations and orientations of accelerometers at floor 30.

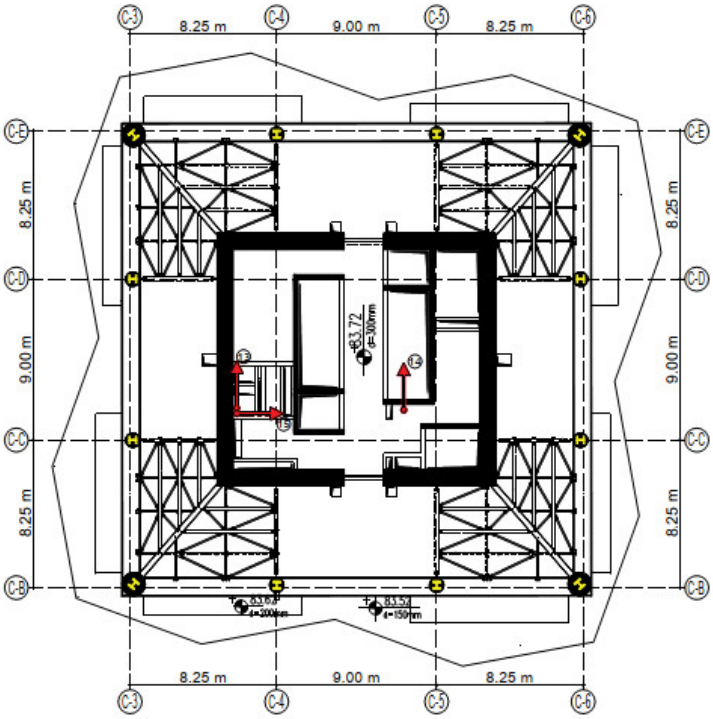

Figure 3.15 Locations and orientations of accelerometers at floor 20.

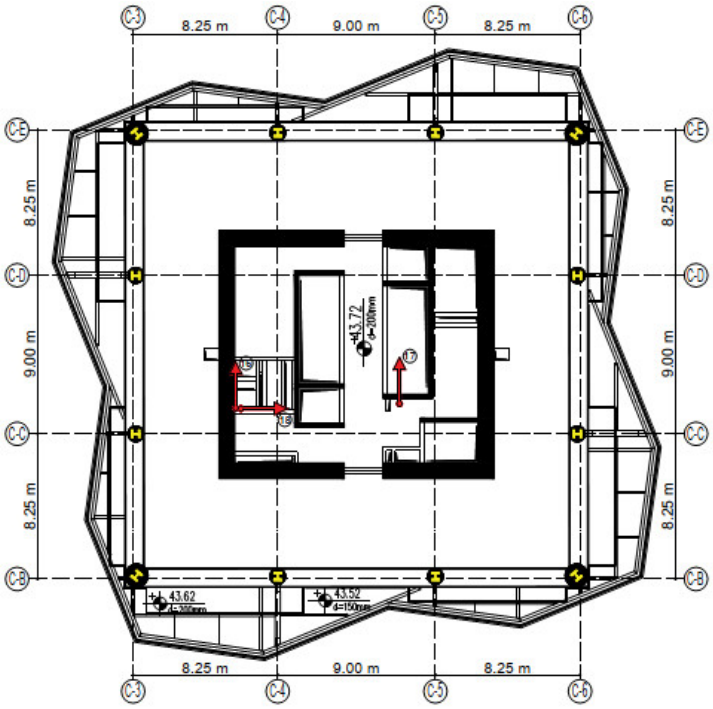

Figure 3.16 Locations and orientations of accelerometers at floor 10.

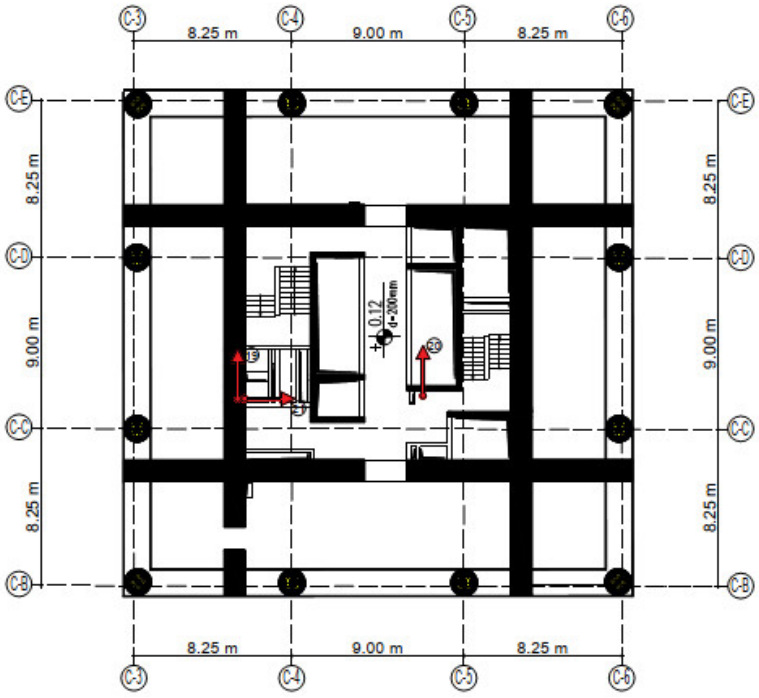

Figure 3.17 Locations and orientations of accelerometers at the ground floor.

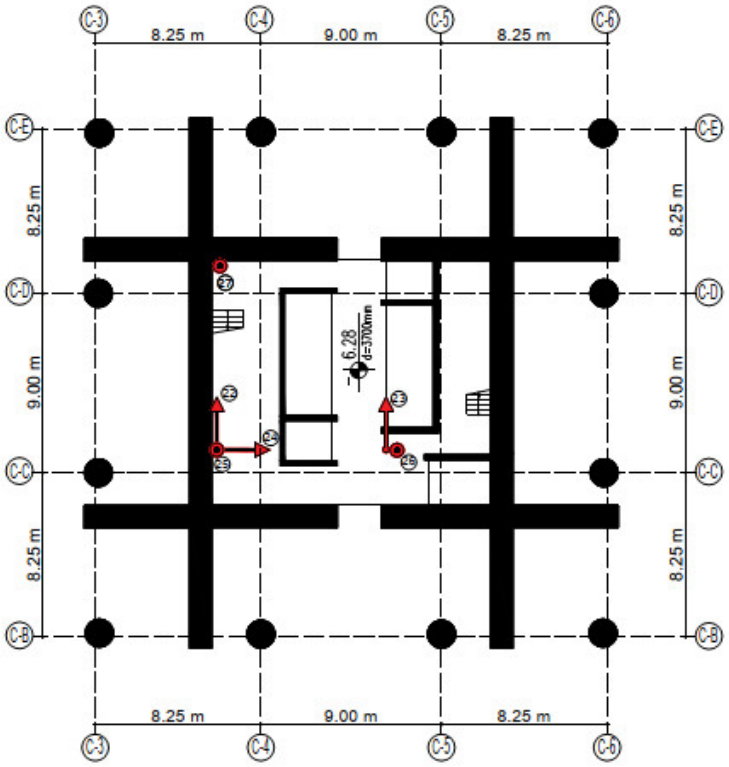

Figure 3.18 Locations and orientations of accelerometers at basement 2.

3.2.4 Streaming of the vibration data

Accelerometers on the instrumented floors were connected to three-channel digital recorders on the same floors. All these recorders stream the structural vibration data to a laptop computer on floor 47 through a local area network that was set up in the building. Hence, only local area network cables were needed in between the floors. Data cables were used for the accelerometer-digital recorder connections only within the floors. The NTP server on floor 47 synchronizes digital recorder times from GPS satellites via the GPS antenna mounted on the roof (Figure 3.19). The SHM system on the building (see Figure 3.20 for the installation plan) records the structural vibration data continuously at 100 samples per second from each channel, yielding a frequency range up to 50 Hz according to the Nyquist frequency criterion. Free

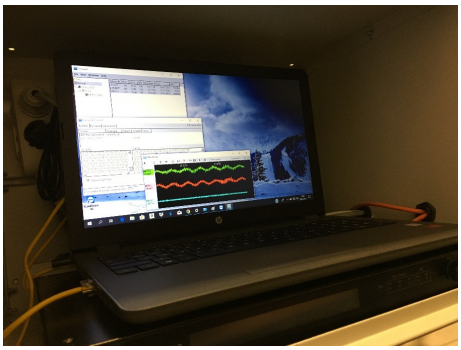

(a)

(b)

Figure 3.19 (a) Laptop for data streaming and NTP server (under the laptop) and (b) GPS antenna on the roof.

field vibration data are recorded by seven strong motion stations (#3513, 3514, 3518, 3519, 3520, 3522, 3530) in the vicinity of the building run by the Disaster and Emergency Management Presidency of Turkey (Figure 3.21).

3.3 Summary

In this chapter, the case study building, Mistral Izmir Office Tower, was described in detail including its structural system, foundation, soil and material properties. Then, the layout of the SHM system on the building was presented together with the stream parameters of the vibration data.

Figure 3.20 Installation plan of SHM system on the building.

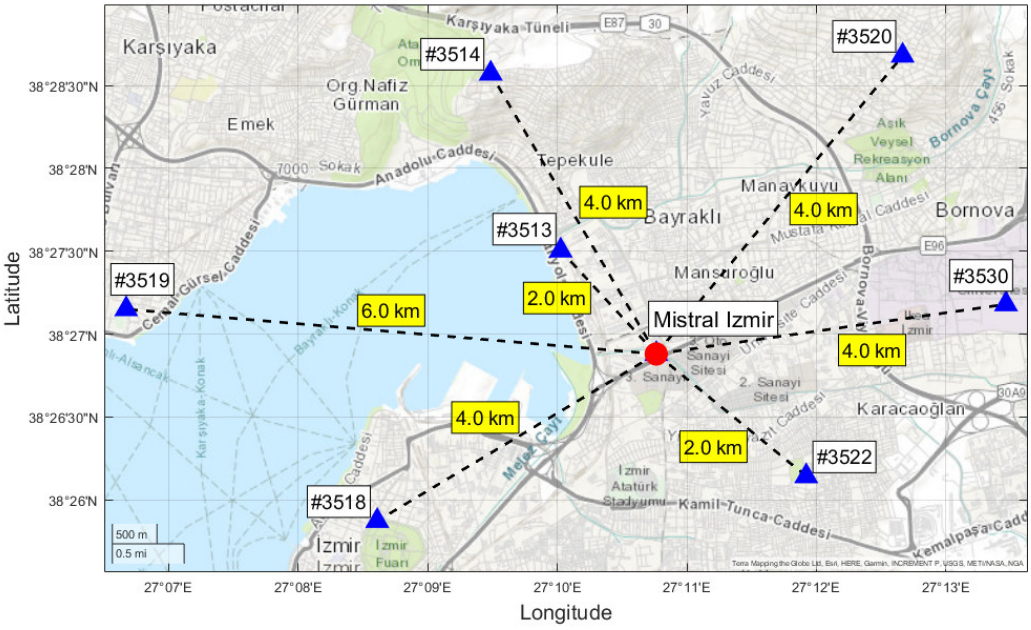

Figure 3.21 AFAD strong motion stations in the vicinity of the building.

CHAPTER 4

SIGNAL PROCESSING AND SYSTEM IDENTIFICATION

4.1 Data Retrieval and Initial Signal Processing

Mistral Izmir Office Tower has been monitored in real time since January 27, 2019. The SHM system stores the structural vibration data to a laptop computer in the building and transfers the data to a desktop computer at METU using the Scream software (Guralp Systems Limited, 2018). Signal processing of the recorded vibration data was performed using the MATLAB software (The MathWorks Inc, 2019) as described below.

The first step of the signal processing is the conversion of the raw data in counts to acceleration in g. For this conversion, all raw data were multiplied by the calibration coefficients provided for each accelerometer and digital recorder channel combination. Then, floor accelerations — A_x (E-W translational), A_y (N-S translational) and A_θ (torsional) — were computed at the floor geometric center based on the rigid floor diaphragm assumption using the transformation

$$\begin{bmatrix} A_x \\ A_y \\ A_\theta \end{bmatrix} = \begin{bmatrix} 0 & 1 & x_1 - x_c \\ 0 & 1 & x_2 - x_c \\ 1 & 0 & y_c - y_3 \end{bmatrix}^{-1} \begin{bmatrix} A_1 \\ A_2 \\ A_3 \end{bmatrix} \tag{4.1}$$

where A_1, A_2 and A_3 are the accelerations recorded by accelerometers #1 and #2 in the N-S direction and accelerometer #3 in the E-W direction, respectively, x_1 and x_2 are the x coordinates of the locations of accelerometers #1 and #2, y_3 is the y coordinate of the location of accelerometer #3, and x_c and y_c are the x and y coordinates of the floor geometric center (cf. Figure 4.1).

The next step is to calculate the floor velocities and displacements using numerical integration. The by-product of numerical integration, drift (very low-frequency

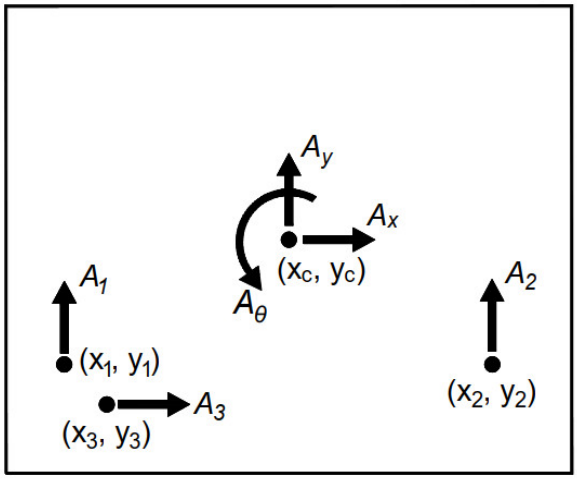

Figure 4.1 Points of recorded and computed accelerations on a floor.

content) and the noise (high-frequency content) present in the data were eliminated using a band-pass filter with appropriate cut-off frequencies. The algorithm of this step is summarized below:

1. Remove the DC offset in the data by subtracting the mean of the data from itself ("detrend" function in MATLAB).
2. Apply a fourth-order Butterworth band-pass filter with cut-off frequencies 0.1 Hz and 40 Hz.
3. Integrate the filtered floor accelerations once using the trapezoidal rule ("cumtrapz" function in MATLAB) to calculate the floor velocities.
4. Integrate the calculated velocities once after applying the first two steps to calculate the floor displacements.

Figure 4.2 shows ambient floor accelerations, velocities and displacements — x (E-W translational), y (N-S translational) and θ (torsional) — computed at the floor geometric center from 02.02.2019 00:00:00 GMT records. Each record is 60 minutes long. These ambient vibration records are used in the following section to illustrate the identification of the structural system dynamic properties — natural vibration frequencies, vibration mode shapes and modal damping capacities — of the building.

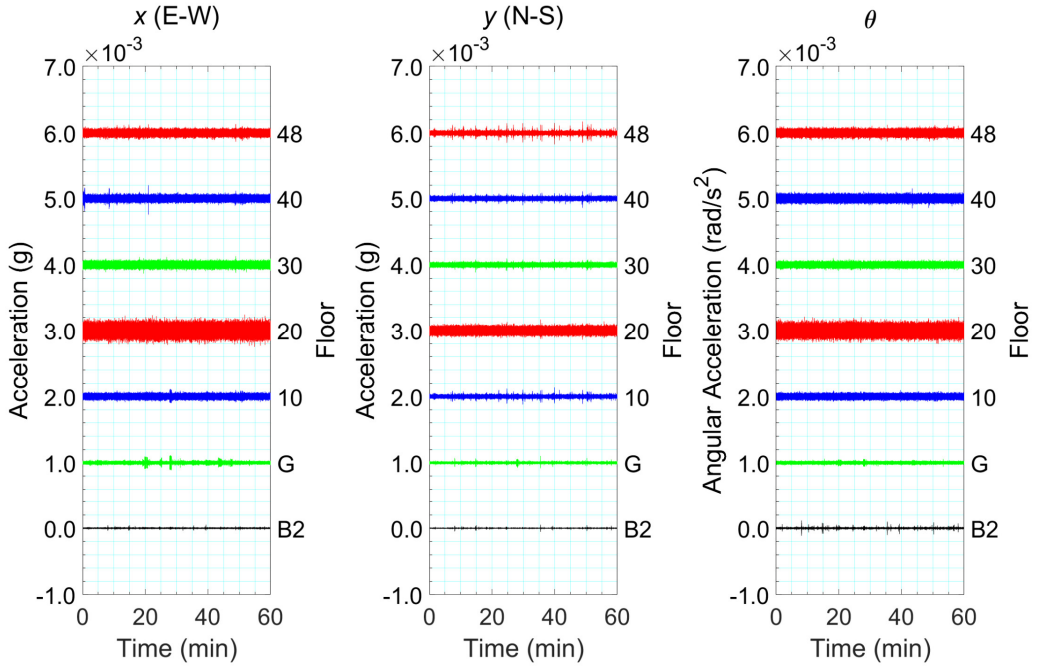

(a)

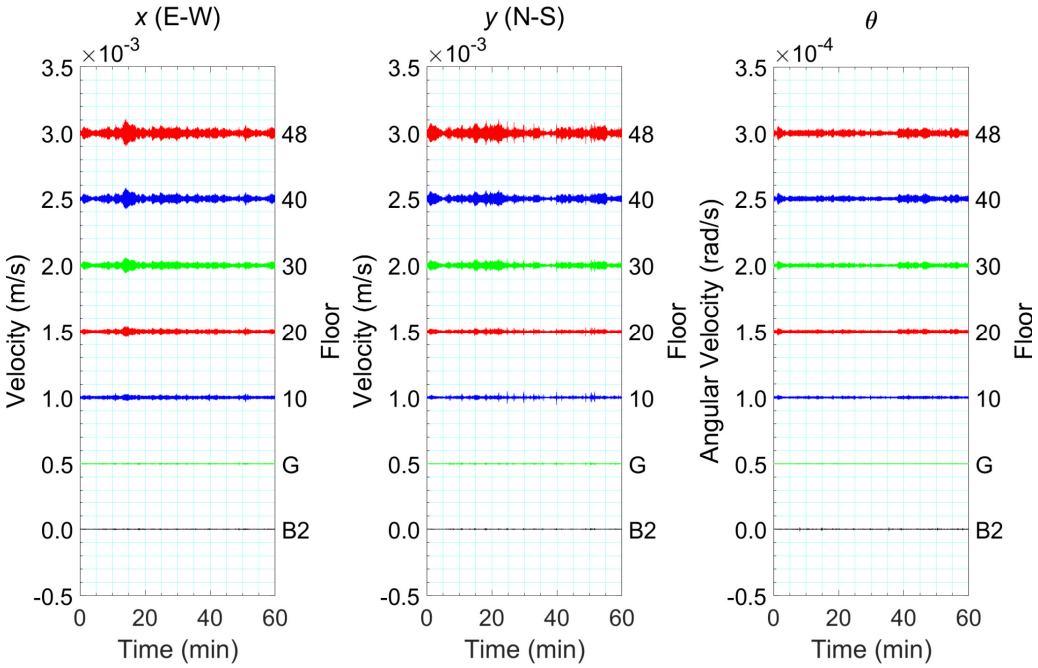

(b)

Figure 4.2 Ambient floor (a) acceleration, (b) velocity and (c) displacement time histories: 02.02.2019 00:00:00 GMT.

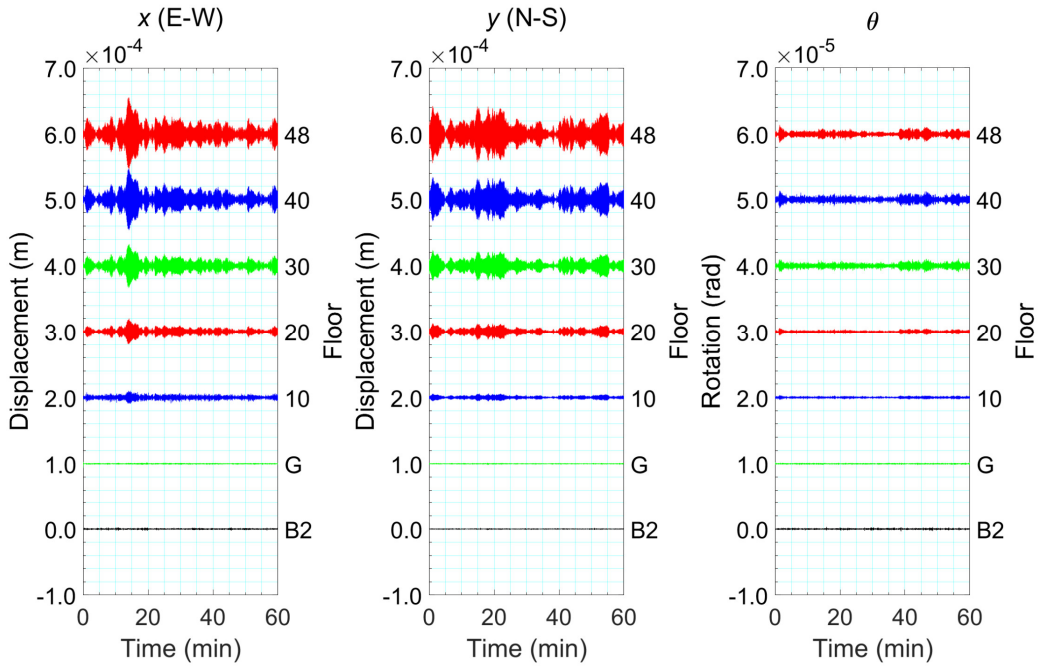

(c)

Figure 4.2 Continued.

4.2 System Identification Using Ambient Vibration Records

Algorithms that use only Fourier transforms and band-pass filters can be used in identifying the dynamic characteristics of buildings (Safak and Cakti, 2014).

4.2.1 Natural Vibration Frequencies

The discrete-time vibration data can be expressed in frequency domain using the fast Fourier transform (FFT). Figure 4.3 shows the Fourier amplitude spectra of the 48th floor ambient accelerations. The frequencies at which the Fourier amplitude spectra attain their peak values correspond to modal vibration frequencies of the building. To facilitate the peak picking process, the mean Fourier amplitude spectra (Petrovic et al., 2018) were calculated. The algorithm of this smoothing method is summarized below:

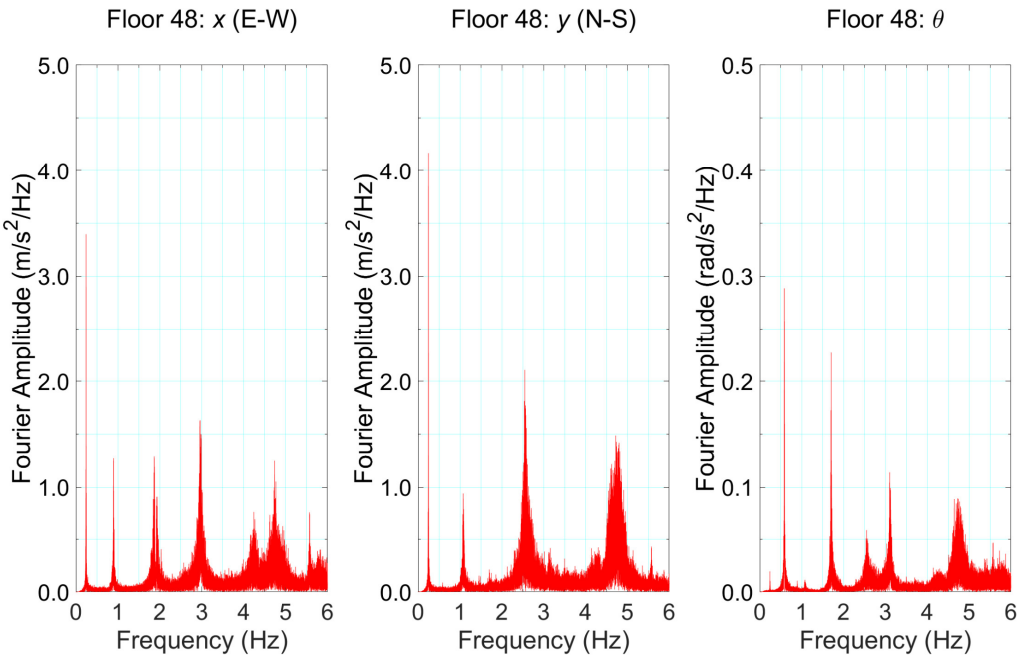

Figure 4.3 Fourier amplitude spectra of the 48th floor ambient accelerations.

1. Divide the recorded discrete-time data into sub-segments using an overlapping moving window. In this study, a moving window of 120 s with 50% overlapping were used.
2. Apply a Hanning window ("Hann" function in MATLAB) to each moving window to eliminate possible aliasing problems.
3. Calculate the FFT of each moving window ("fft" function in MATLAB).
4. Calculate the mean of these FFTs ("mean" function in MATLAB).

Figure 4.4 shows the mean Fourier amplitude spectra of ambient accelerations of all instrumented floors. The dominant peaks in the 0.1–6.0 Hz frequency range were detected from the 48th floor accelerations as shown in Figure 4.5. The identified natural vibration frequencies of the building for the first four translational modes in both E-W and N-S directions and the first four torsional modes are listed in Table 4.1. The natural vibration periods of the building are also listed in Table 4.2.

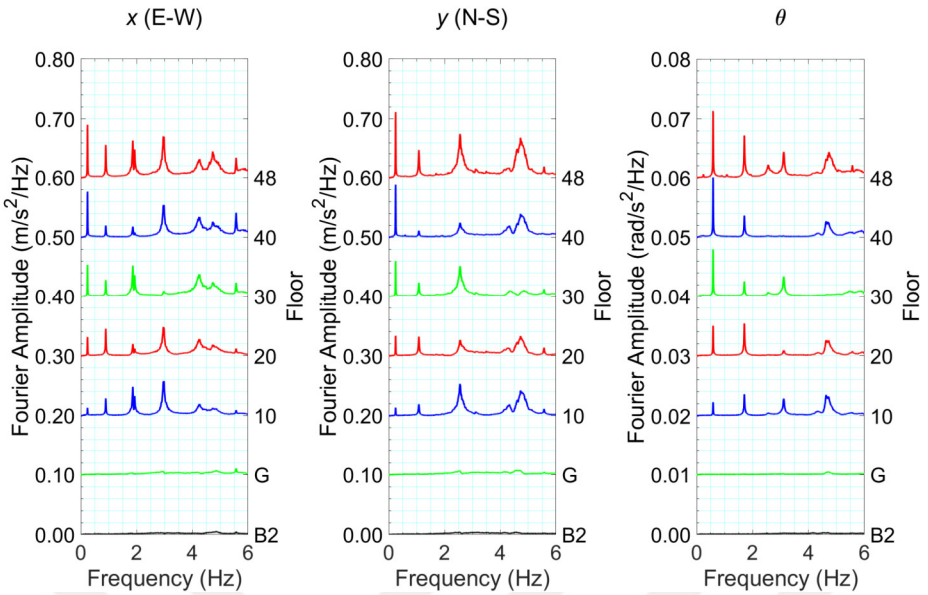

Figure 4.4 Mean Fourier amplitude spectra of all instrumented floor accelerations.

4.2.2 Vibration Mode Shapes

Vibration mode shapes can be determined from modal displacements of instrumented floors if recording times of all data are synchronized (Safak and Cakti, 2014). First, floor displacements were calculated as outlined in Section 4.1. Then, these displacements were narrow band-pass filtered around each identified natural vibration frequency to determine the modal displacements. The filter bandwidth was three times the frequency resolution, $3 \times 1/(N \cdot \Delta t)$ where N is the number of data points and Δt is the time increment. Maximum modal displacements were calculated for the top instrumented floor (floor 48). Then, modal displacements of all other instrumented floors were calculated at the same time that maximum displacement was attained at the top instrumented floor. Finally, these displacements were plotted. Figures 4.6–4.8 present the vibration mode shapes for the first four translational modes in the E-W and N-S directions and the first four torsional modes. The mode shapes associated with closely spaced frequencies look coupled due to the algorithm used but in fact they are not (see finite element modeling in Chapter 6).

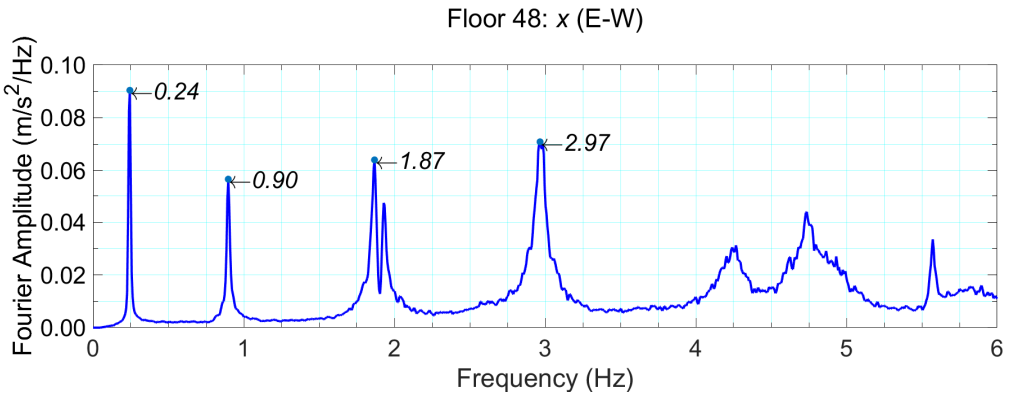

(a)

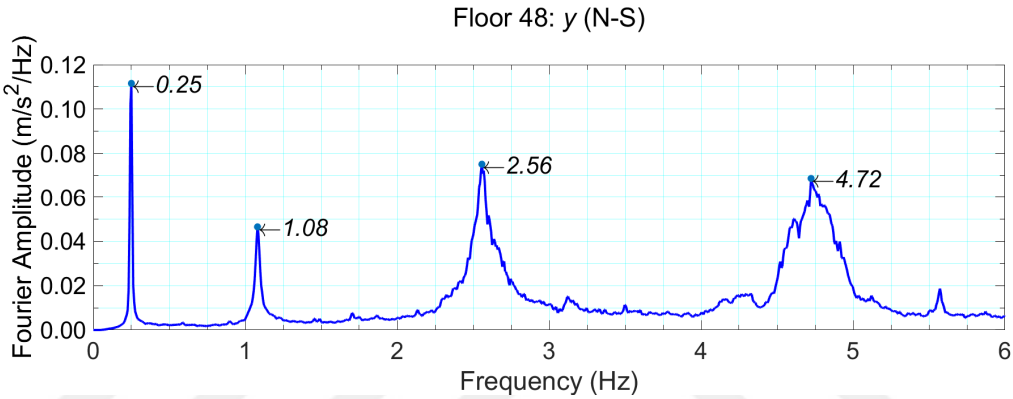

(b)

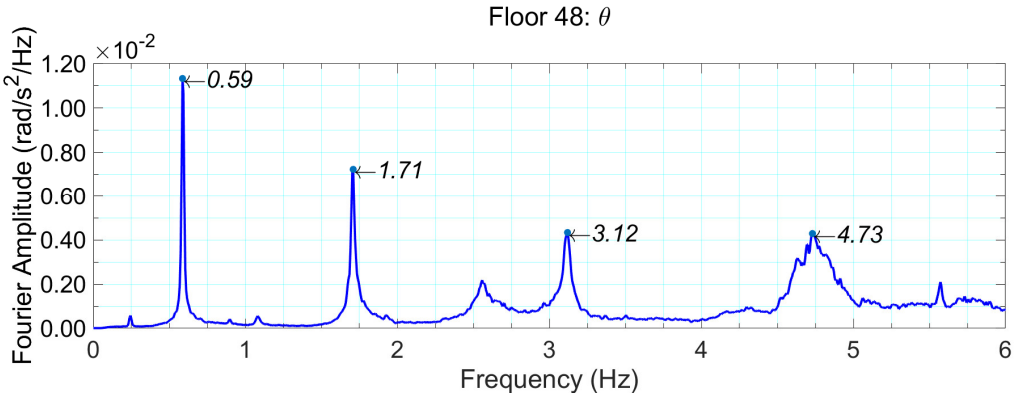

(c)

Figure 4.5 Mean Fourier amplitude spectra of the 48th floor accelerations: (a) E-W, (b) N-S and (c) torsional.

Table 4.1 Natural vibration frequencies (Hz): 02.02.2019 00:00:00 GMT.

Mode	x (E-W)	y (N-S)	θ
1	0.24	0.25	0.59
2	0.90	1.08	1.71
3	1.87	2.56	3.12
4	2.97	4.72	4.73

Table 4.2 Natural vibration periods (s): 02.02.2019 00:00:00 GMT.

Mode	x (E-W)	y (N-S)	θ
1	4.17	4.00	1.71
2	1.11	0.93	0.59
3	0.54	0.39	0.32
4	0.34	0.21	0.21

4.2.3 Modal Damping Capacities

The damping ratio is a critical dynamic property for the design of structures subjected to dynamic loading. Damping values are highly uncertain and no theoretical formula exists for their calculation. Hence, empirical equations derived from full-scale dynamic tests are used to estimate the damping ratios of engineering structures. There are various methods defined in time and frequency domains (Zhang et al., 2004; Kareem and Tamura, 2013; Casiano, 2016) to identify the damping ratios from forced vibration tests, ambient vibration tests and recorded earthquake responses. In this study, damping ratios were identified from ambient vibration records (this chapter) and earthquake response records (Chapter 5). The half-power

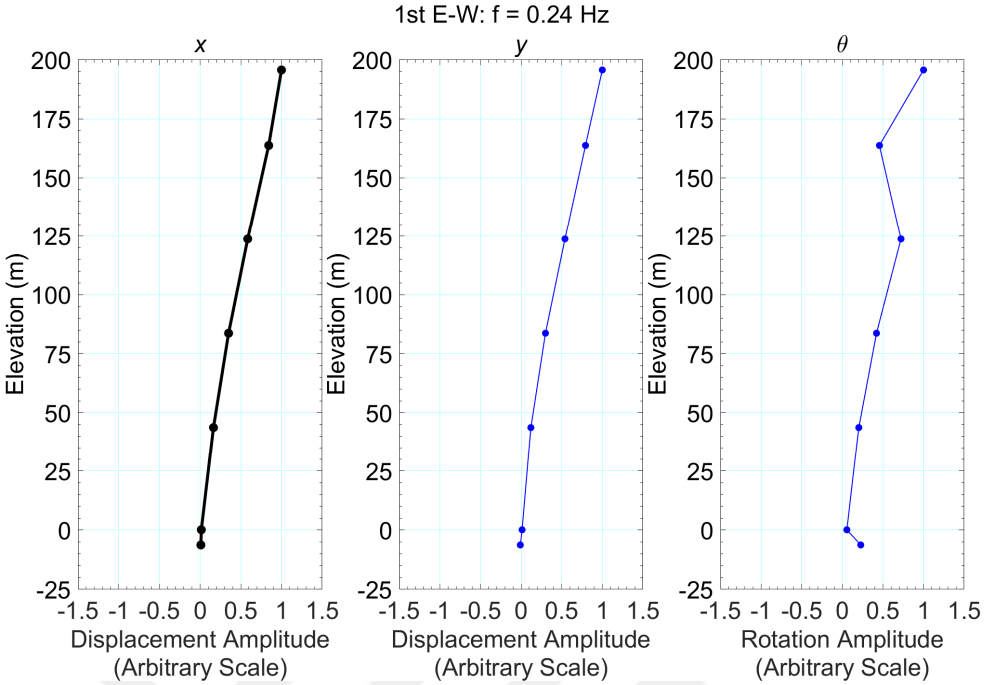

(a)

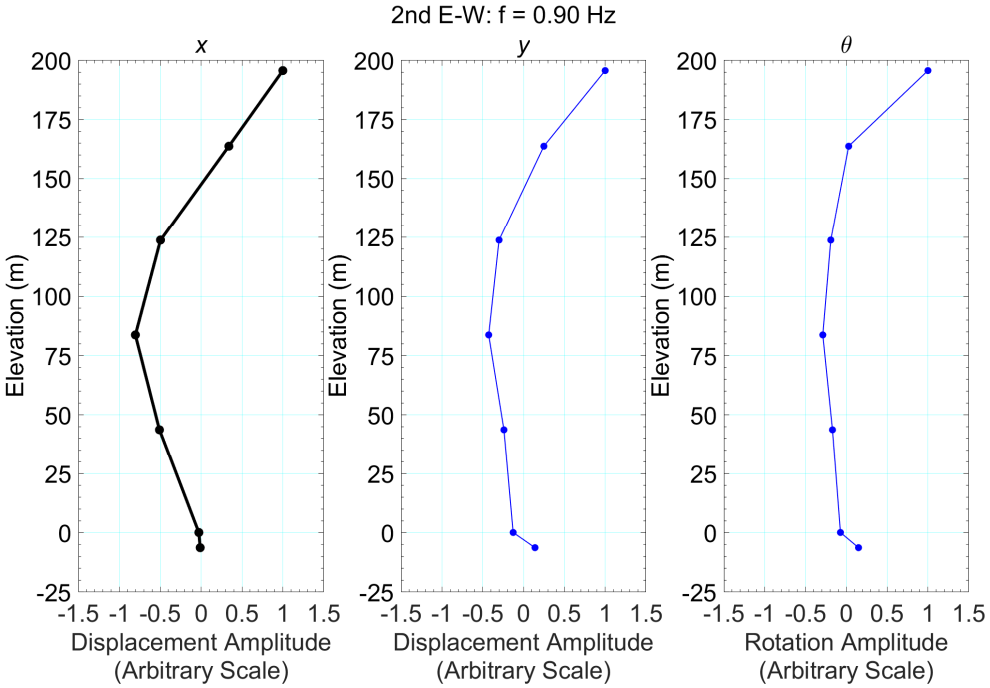

(b)

Figure 4.6 E-W translational vibration mode shapes: (a) 1st mode, (b) 2nd mode, (c) 3rd mode and (d) 4th mode.

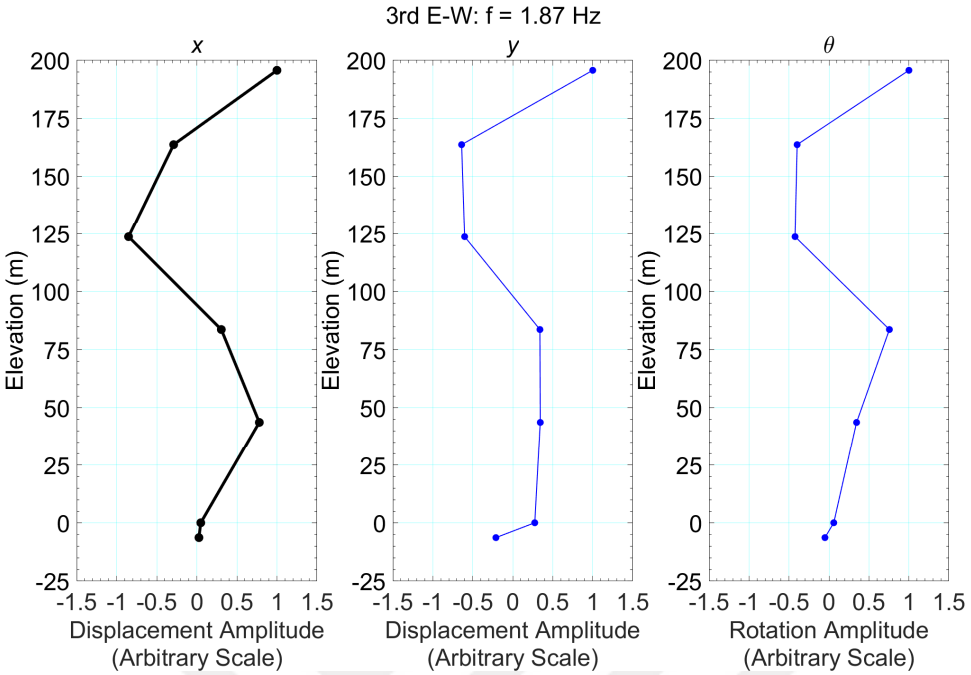

(c)

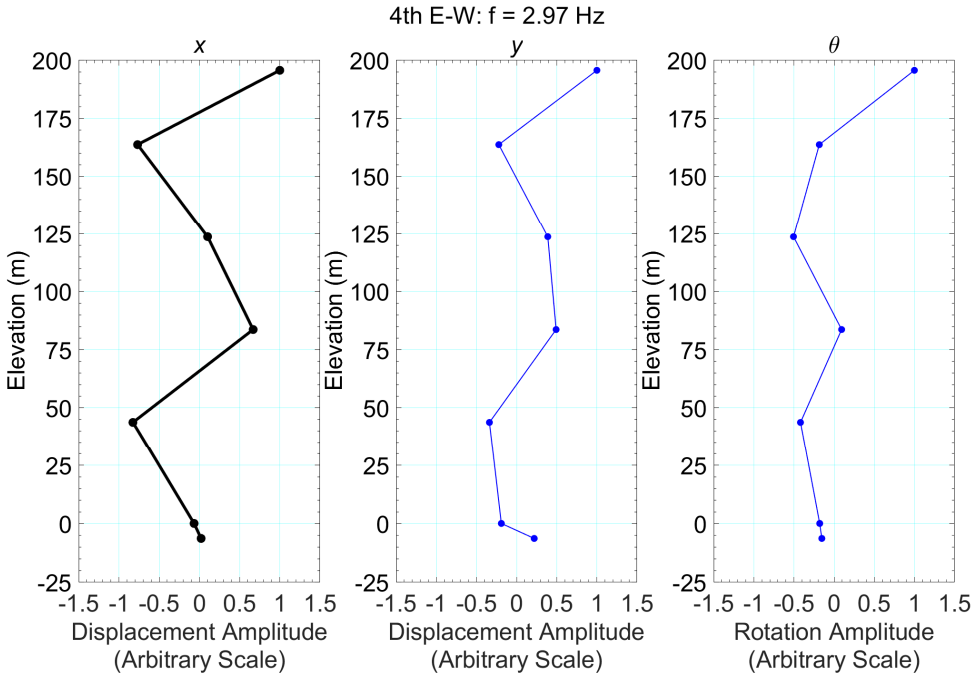

(d)

Figure 4.6 Continued.

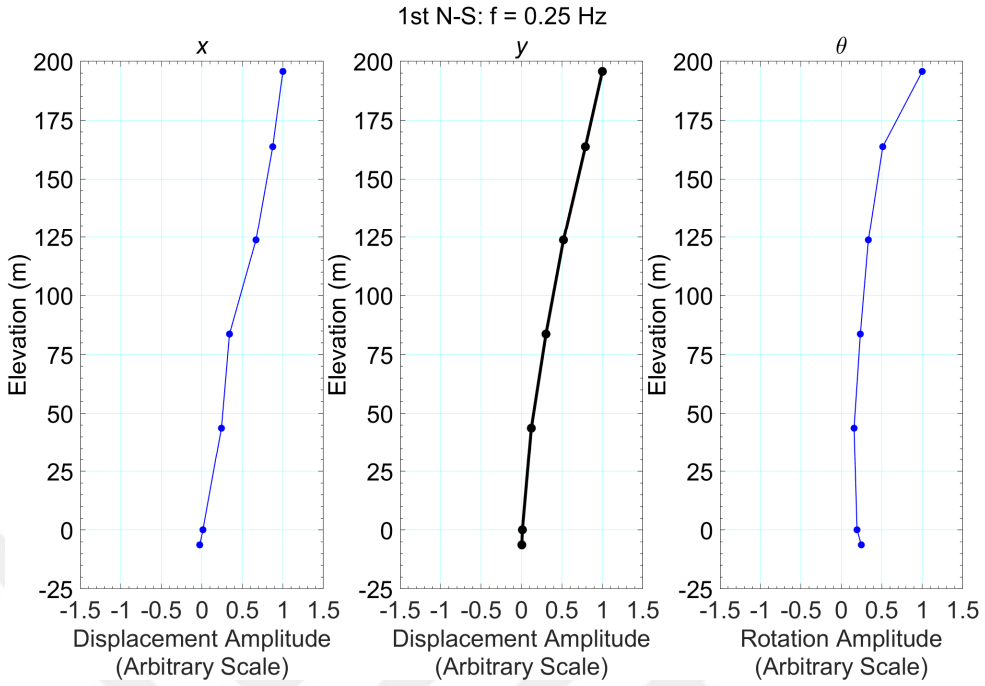

(a)

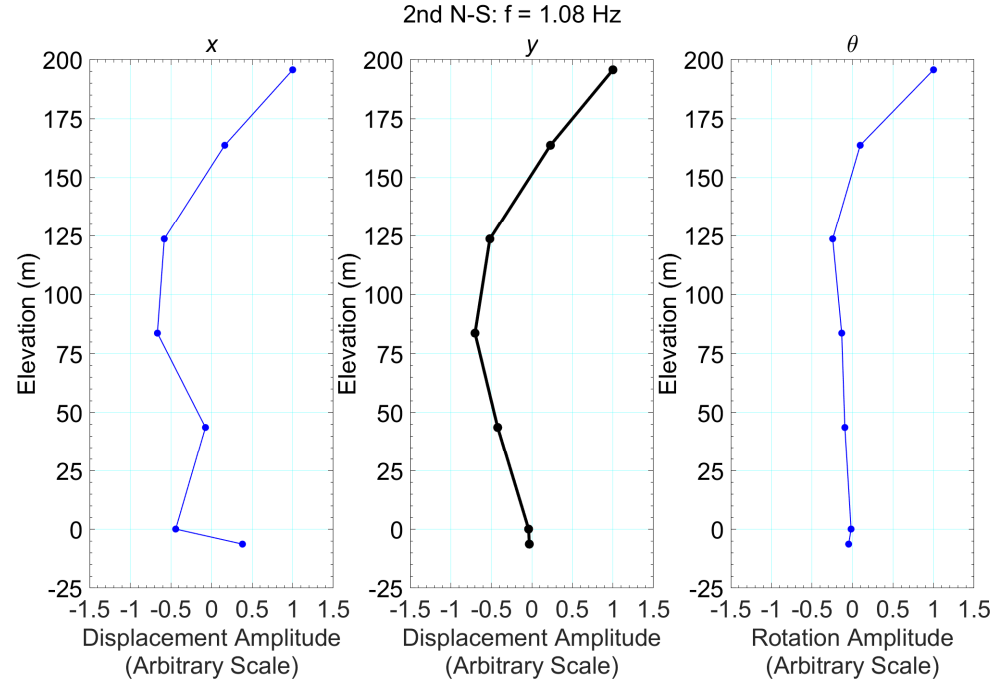

(b)

Figure 4.7 N-S translational vibration mode shapes: (a) 1st mode, (b) 2nd mode, (c) 3rd mode and (d) 4th mode.

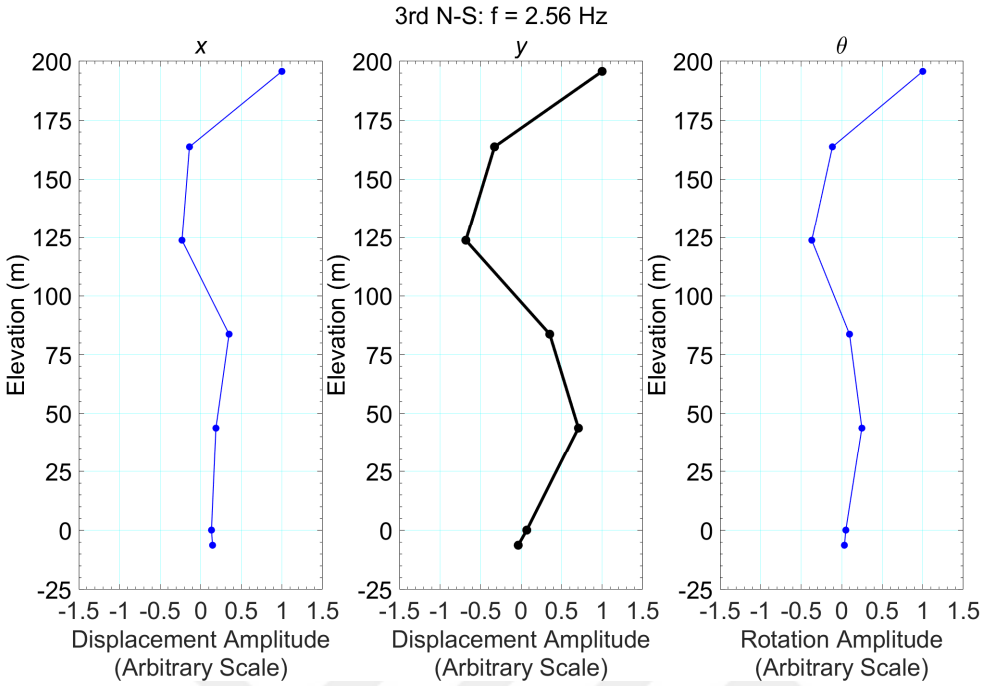

(c)

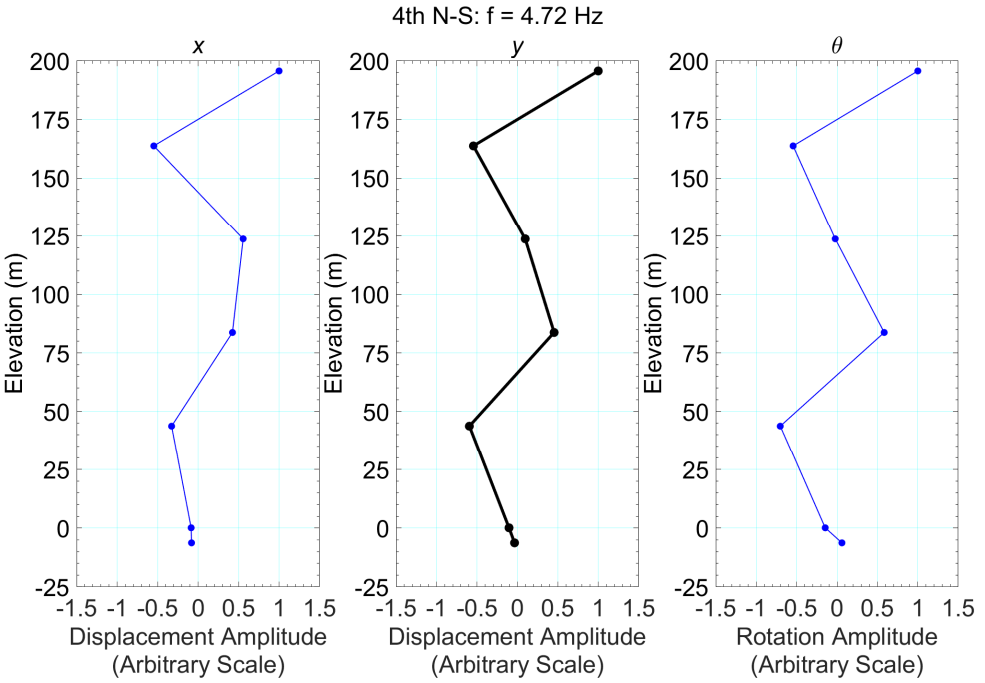

(d)

Figure 4.7 Continued.

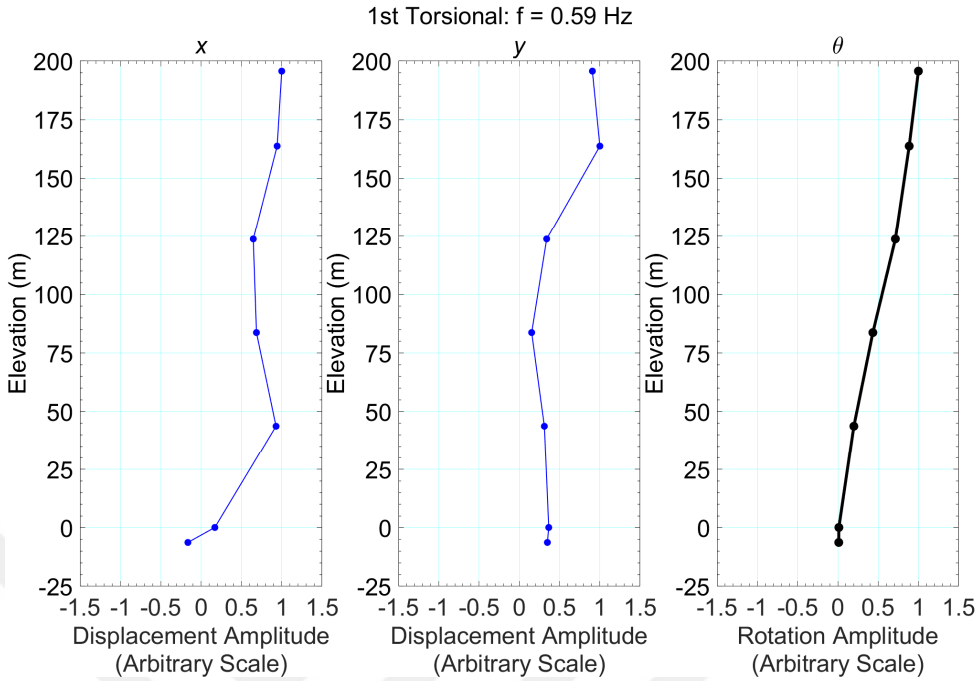

(a)

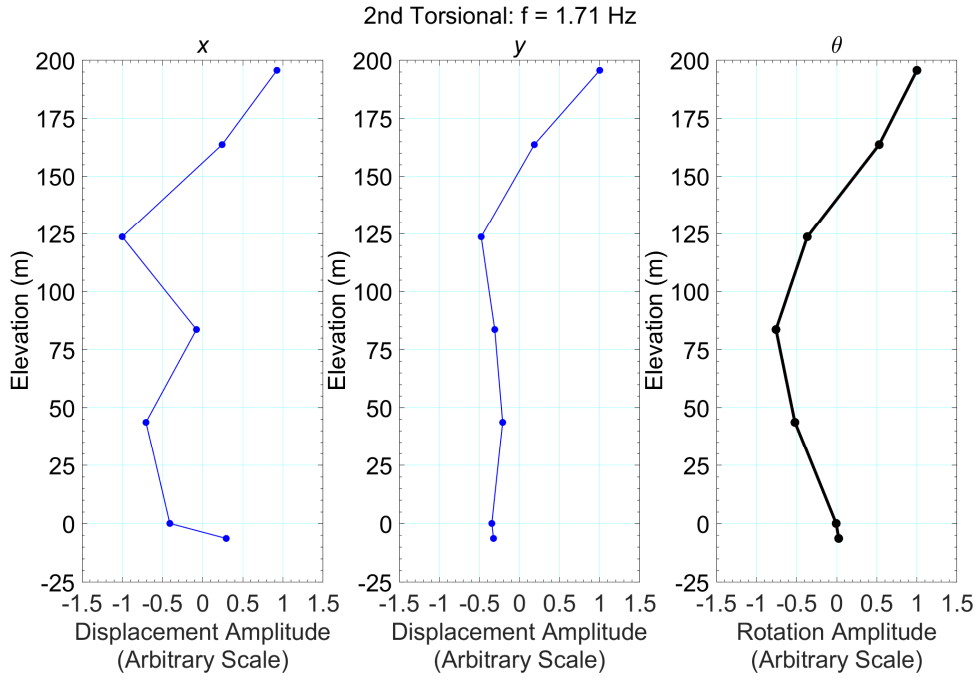

(b)

Figure 4.8 Torsional vibration mode shapes: (a) 1st mode, (b) 2nd mode, (c) 3rd mode and (d) 4th mode.

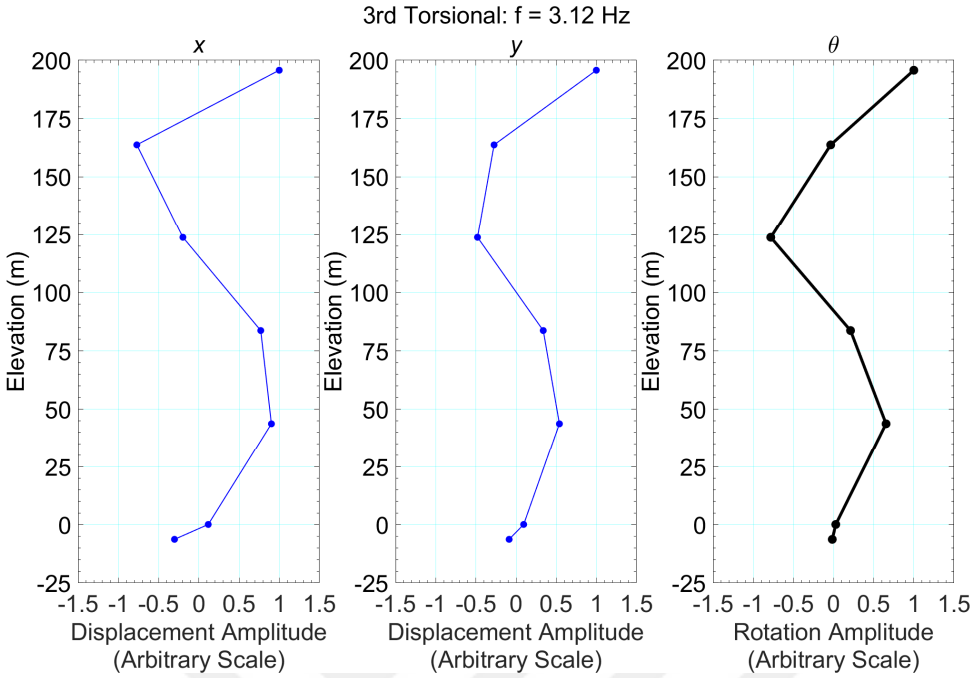

(c)

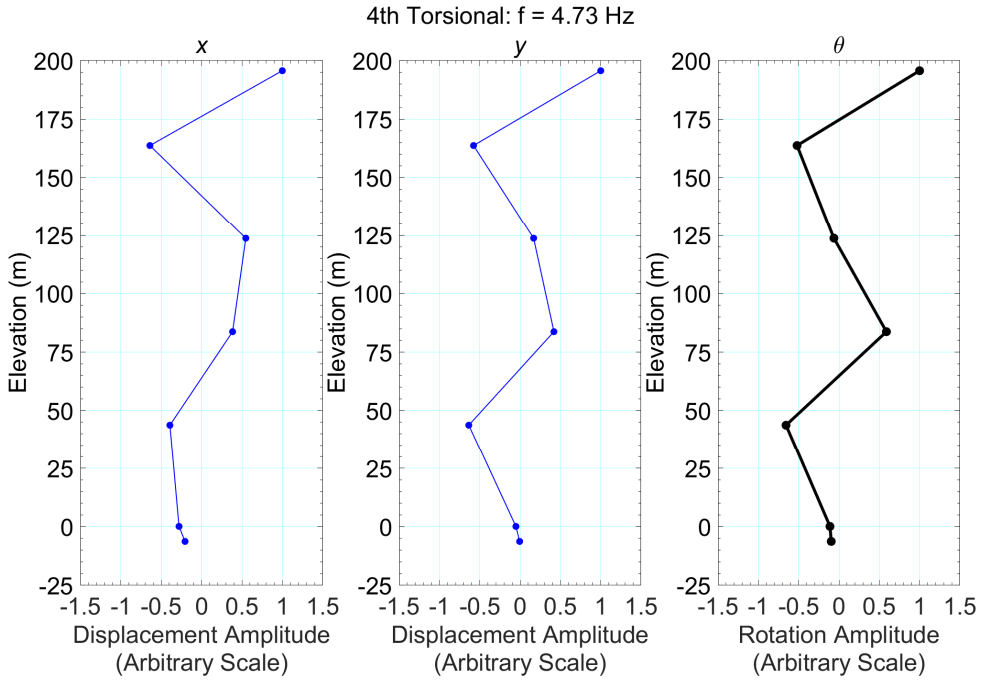

(d)

Figure 4.8 Continued.

bandwidth and the logarithmic decrement methods are the most commonly used methods in frequency and time domains, respectively, for damping estimation (Safak and Cakti, 2014). The half-power bandwidth method is the best for a single-degree-of-freedom harmonic oscillator with stationary data (Casiano, 2016). However, non-stationary responses of a multi-degree-of-freedom system are of concern in this study. Hence, the logarithmic decrement method was used for damping estimation. This method uses the auto-correlation function, narrow band-pass filtering and exponential curve fitting. An algorithm that was written based on this method is summarized below:

1. Divide the signal into sub-segments using a moving window of 8 minutes (480 seconds; 48,000 data points) with 50% overlapping. The window size is an essential parameter for accurate estimation of the damping ratio. The selection of the window size will be explained subsequently.
2. Apply the Hanning window to each sub-segment to eliminate possible aliasing problems ("Hann" function in MATLAB).
3. Narrow band-pass filter each sub-segment around each identified natural vibration frequency with a bandwidth three times the frequency resolution, $3 \times 1/(N \cdot \Delta t)$ where N is the number of data points in the sub-segment.
4. Calculate the autocorrelation function for each filtered sub-segment ("xcorr" function in MATLAB).
5. Determine the damping ratio by a least-squares fit to the peaks (between 90% and 20% of the maximum amplitude; Magalhaes et al., 2010) of the natural logarithm of the autocorrelation function, $R(\tau)$, for each sub-segment:

$$\ln[R(\tau)] = -\xi\omega_0\tau + \ln C \tag{4.2}$$

   where τ is time lag (s), ξ is the damping ratio, ω_0 is the angular natural frequency (Hz) and C is a constant (Safak and Cakti, 2014).
6. Calculate the mean damping ratio associated with each identified natural frequency.

The above algorithm was used for all instrumented floor accelerations except the acceleration records of the ground and basement floors, where the amplitudes were relatively small. Table 4.3 presents the median modal damping ratios associated with each identified natural vibration frequency listed in Table 4.1.

The selection of the window size used in the algorithm is important in estimating accurate damping ratios. The sub-segments of the signal should be long enough to avoid leakage errors and the number of sub-segments should be sufficient for the damping averaging process (Kareem and Tamura, 2013). Figure 4.9 shows the variation of damping values with different window sizes. The damping ratios are

Table 4.3 Modal damping ratios (%): 02.02.2019 00:00:00 GMT.

Mode	x (E-W)	y (N-S)	θ
1	0.48	0.56	0.23
2	0.17	0.12	0.10
3	0.09	0.05	0.04
4	0.05	0.03	0.03

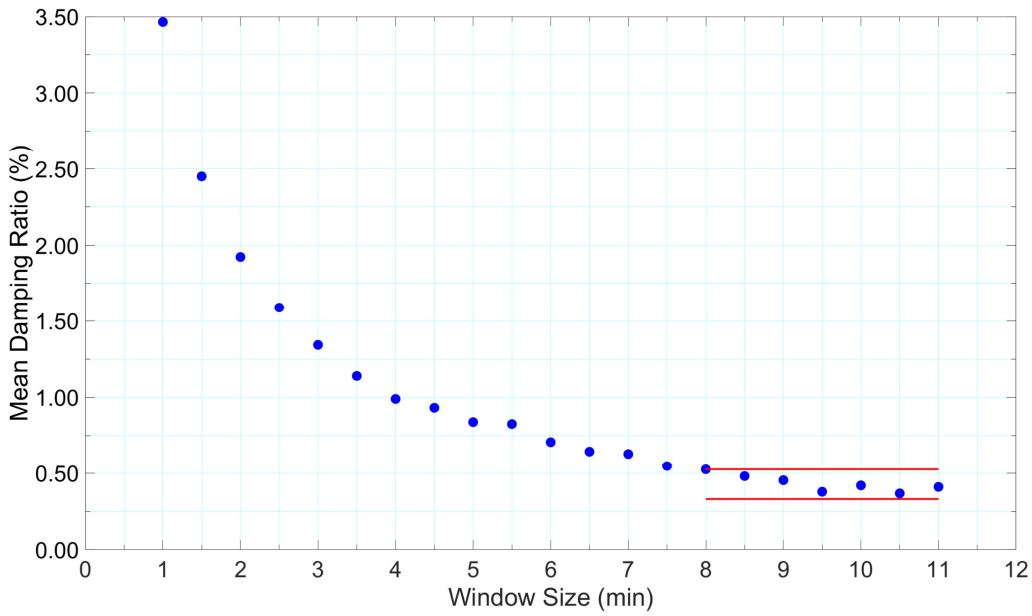

Figure 4.9 Mean damping ratio vs. window size.

getting smaller as the window size increases, which leads to an increase in frequency resolution. The leakage error, which is proportional to the square of the frequency resolution (Zhang et al., 2004), can be reduced by increasing the frequency resolution. The calculated damping ratio starts to converge when the window size is greater than 8 minutes (48,000 data points) as shown in Figure 4.9. Hence, the window size was selected as 8 minutes for damping calculations in this study.

4.3 Long-Term Monitoring

The algorithms developed for system identification were implemented for long-term monitoring of the dynamic properties. Continuous vibration records of the building in 2019 (since February) were analyzed. Each dataset includes 60-minutes-long time-series that were recorded by 27 channels of accelerometers installed throughout the building. The system identification was performed for the first four translational modes in both E-W and N-S directions and the first four torsional modes, lying within the 0.1–6.0 Hz frequency range.

Figures 4.10 and 4.11 present the long-term monitoring of the natural vibration frequencies and damping ratios, respectively, for first four translational modes in both E-W and N-S directions and the first four torsional modes. Table 4.4 lists the means and coefficients of variation (COV) of the natural vibration frequencies and damping ratios that were identified from the analysis of 11-months data. It is clear that all first four modes except the fourth N-S translational and torsional modes were not significantly sensitive to factors such as environmental effects, daily human activities or traffic. However, there were fluctuations for the fourth N-S translational and torsional modes. The frequencies of these modes were closely spaced and the Fourier amplitudes at frequencies close to these frequencies spread out as shown in Figure 4.12. The coefficient of variation was less than 0.02 for all frequencies and was between 0.08 and 0.12 for the associated damping ratios. Although damping values are known to be highly uncertain, the identified damping ratios for the first translational modes in both E-W and N-S directions were all consistently in between

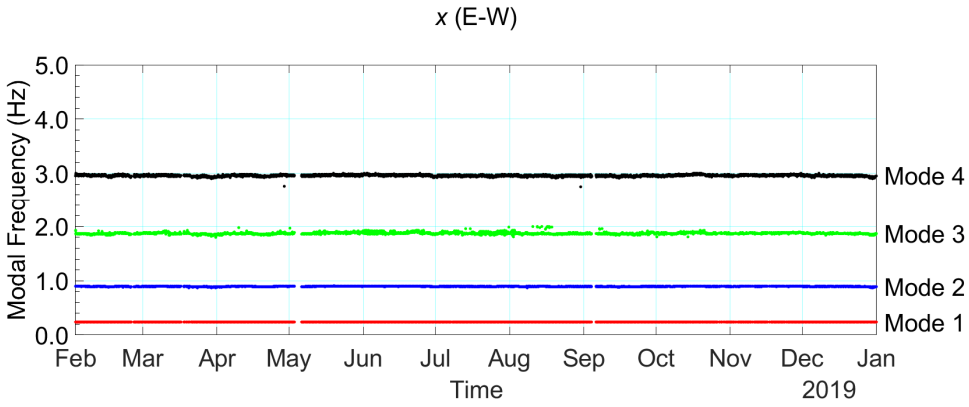

(a)

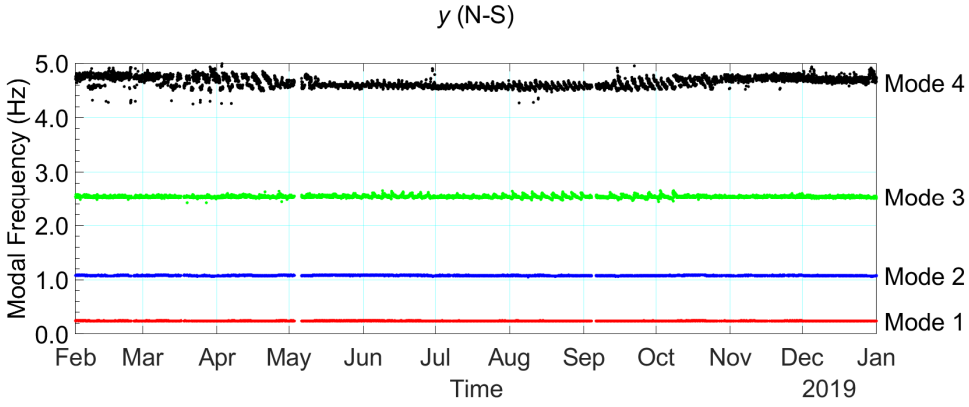

(b)

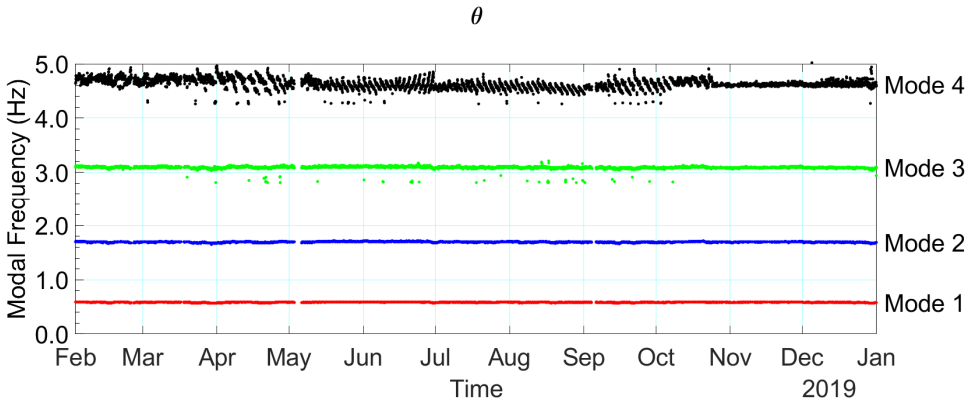

(c)

Figure 4.10 Long-term monitoring of the natural vibration frequencies in 2019: (a) E-W translational, (b) N-S translational and (c) torsional.

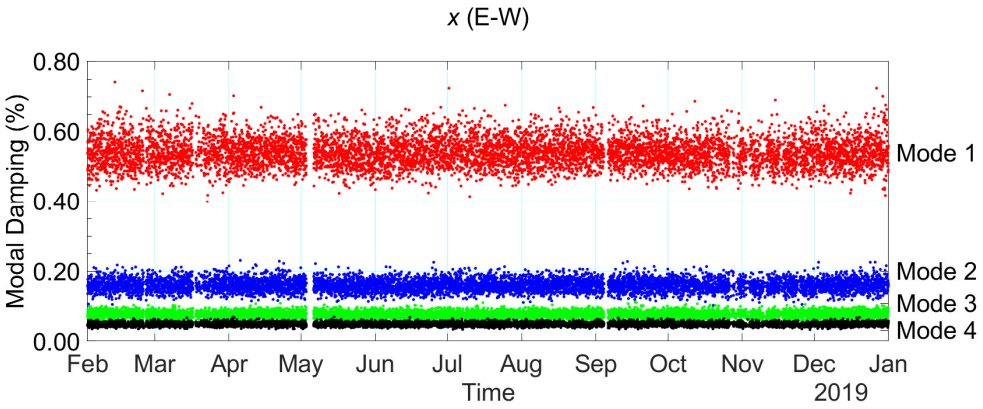

(a)

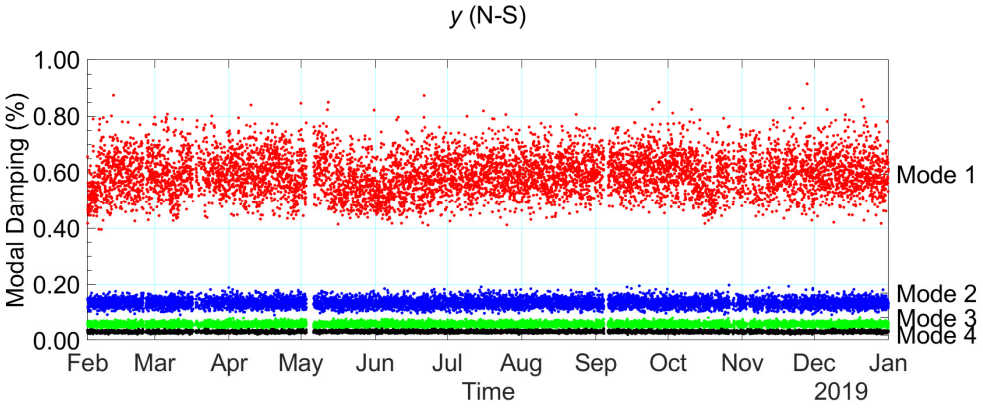

(b)

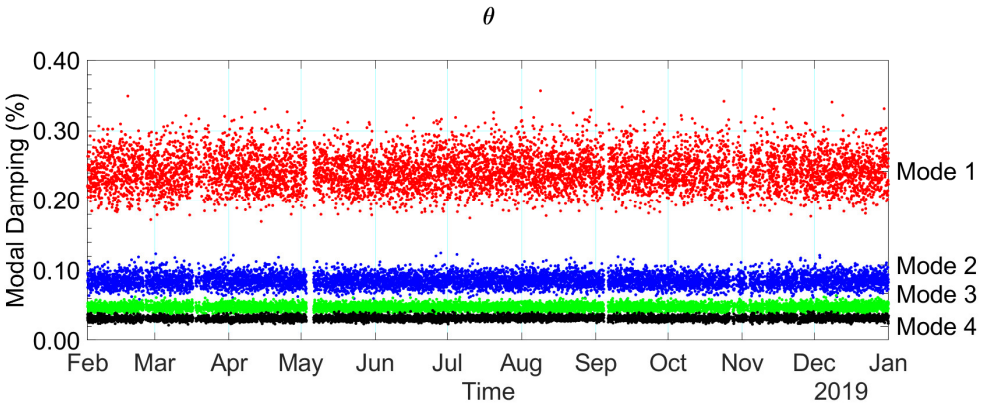

(c)

Figure 4.11 Long-term monitoring of the modal damping ratios in 2019: (a) E-W translational, (b) N-S translational and (c) torsional.

Table 4.4 System identification results of continuous monitoring.

Mode		Natural vibration frequency		Modal damping ratios	
Dir.	No.	Mean (Hz)	COV	Mean (%)	COV
x (E-W)	1	0.24	0.00	0.54	0.08
	2	0.90	0.01	0.16	0.11
	3	1.88	0.01	0.08	0.11
	4	2.96	0.01	0.05	0.10
y (N-S)	1	0.24	0.01	0.59	0.12
	2	1.08	0.01	0.13	0.11
	3	2.55	0.01	0.06	0.11
	4	4.65	0.02	0.03	0.10
θ (torsion)	1	0.59	0.01	0.24	0.10
	2	1.70	0.01	0.09	0.10
	3	3.09	0.01	0.05	0.09
	4	4.63	0.02	0.03	0.09

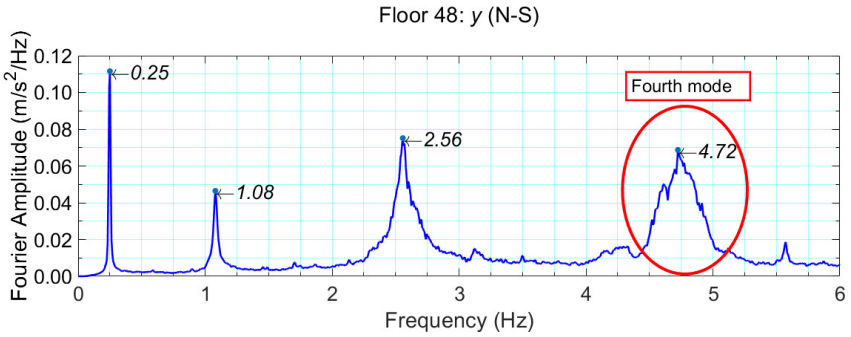

(a)

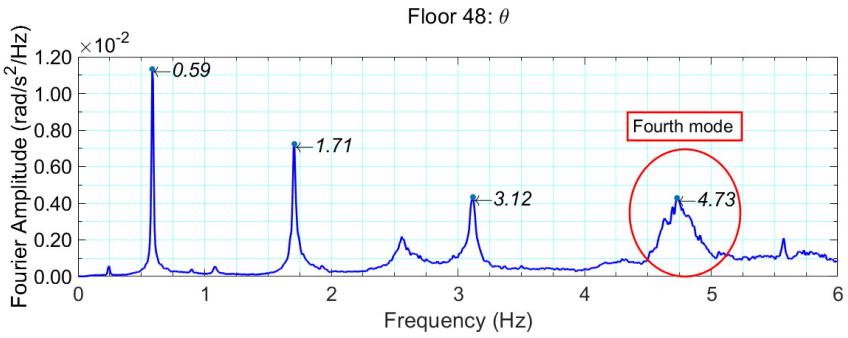

(b)

Figure 4.12 Fourier amplitude spectra of the 48th floor accelerations from 02.02.2019 00:00:00 GMT: (a) N-S translational and (b) torsional.

0.4% and 0.8%. Figures 4.13–4.15 present the vibration mode shapes as identified from a-day-long records, a-month long records (based on the average values of each monitored day) and a-year-long records (based on the average values of each monitored month). The vibration mode shapes were mostly coherent within a tolerable range during the period of continuous monitoring in 2019.

4.4 Summary

In this chapter, the algorithms used for data retrieval and system identification were presented and their implementation on a selected reference dataset was shown. Then, the modal dynamic properties of the building were identified for the selected datasets. Finally, the algorithms developed were implemented for long-term monitoring of the dynamic properties between February to December in 2019 to observe the possible changes in the modal properties and to validate the algorithms developed.

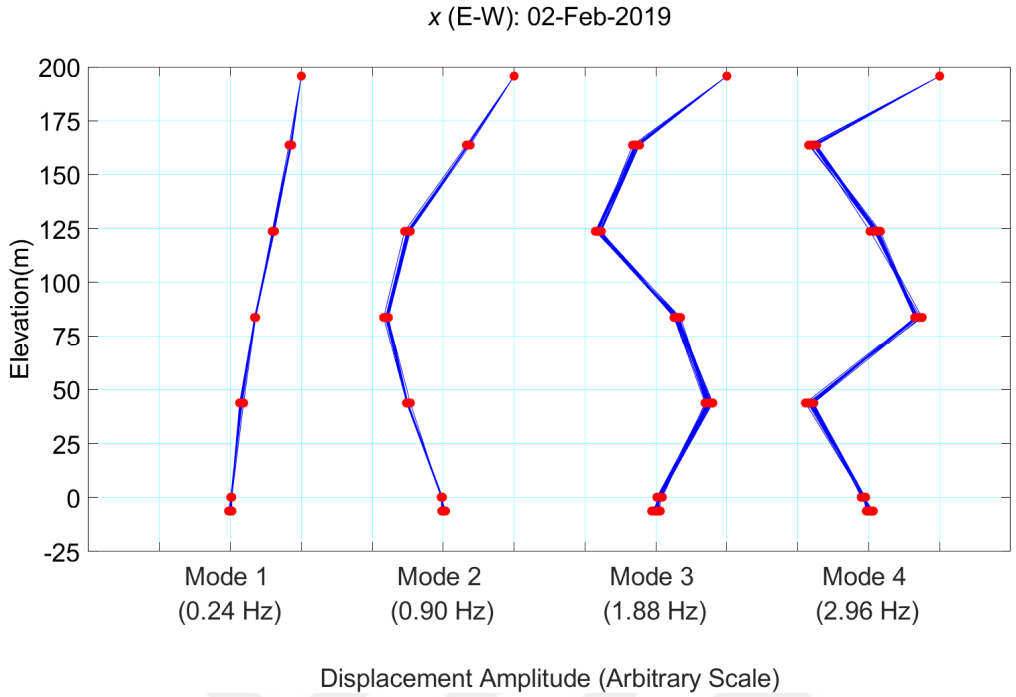

(a)

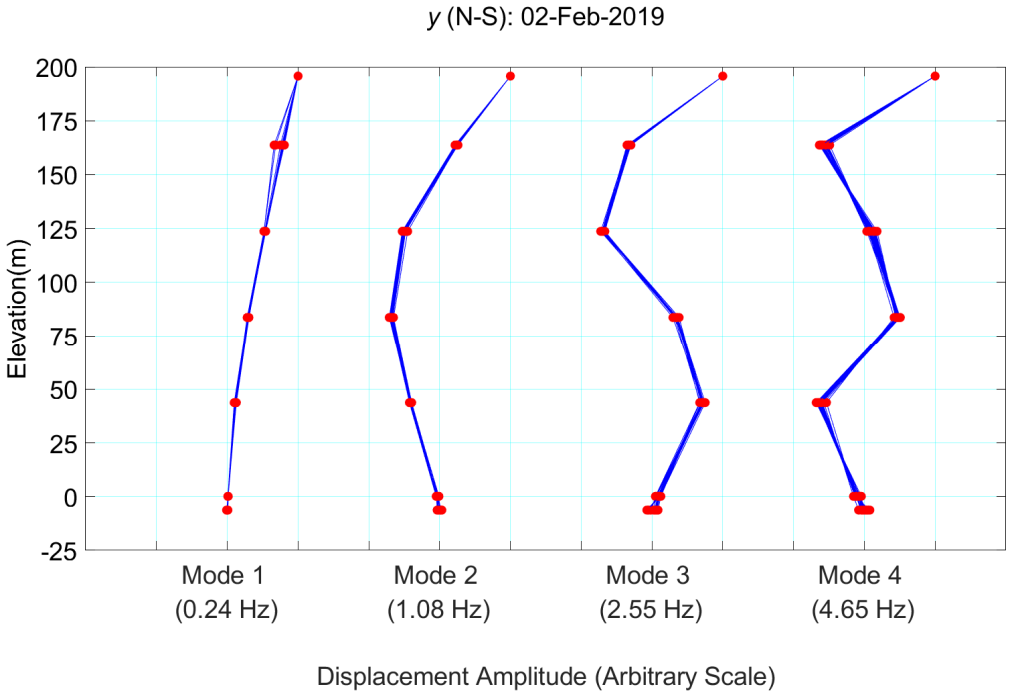

(b)

Figure 4.13 Vibration mode shapes identified from a-day-long records (02.02.2019): (a) E-W translational, (b) N-S translational and (c) torsional.

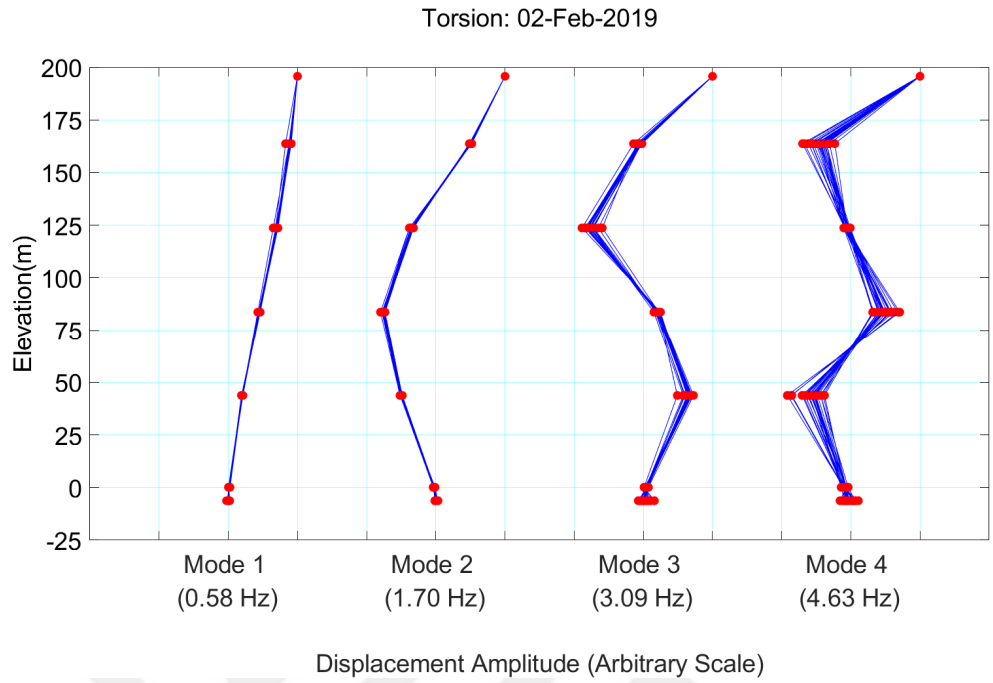

(c)

Figure 4.13 Continued.

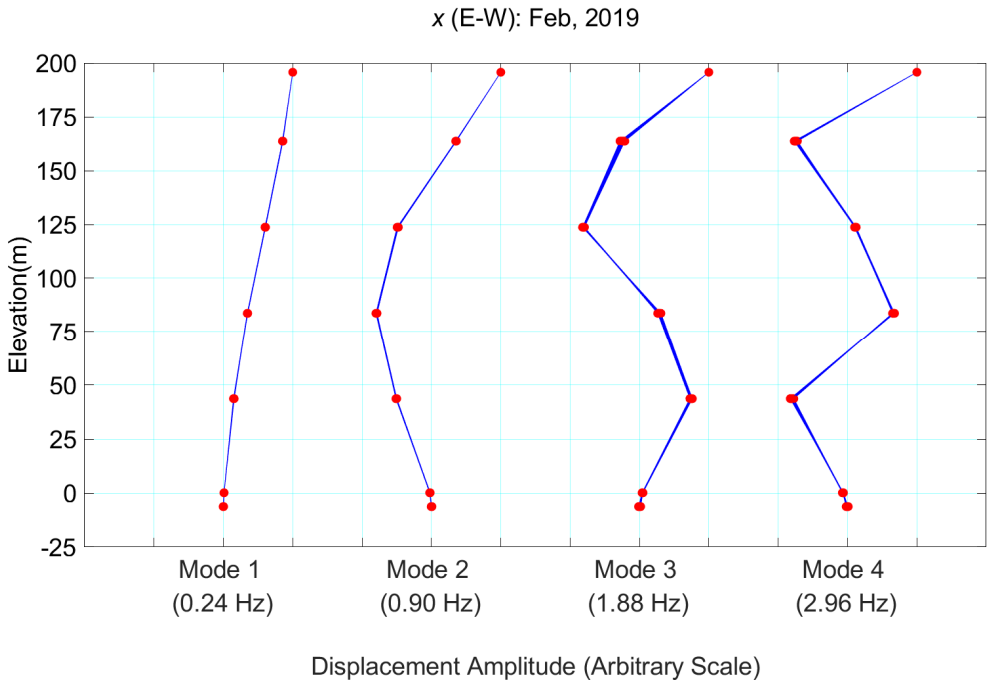

(a)

Figure 4.14 Vibrational mode shapes identified from a-month-long records (February, 2019): (a) E-W translational, (b) N-S translational and (c) torsional.

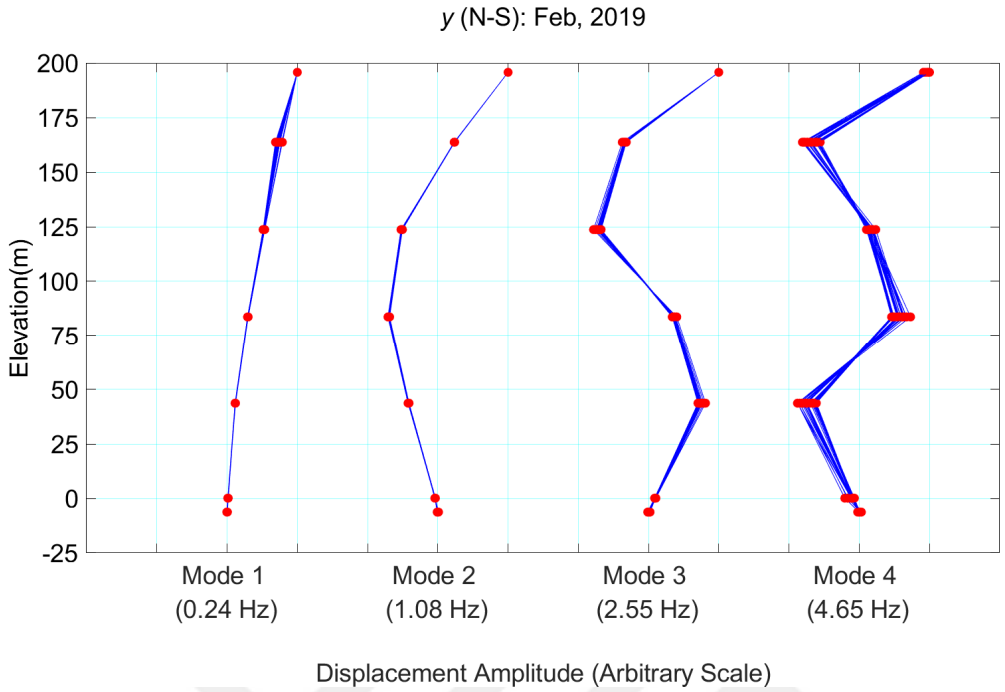

(b)

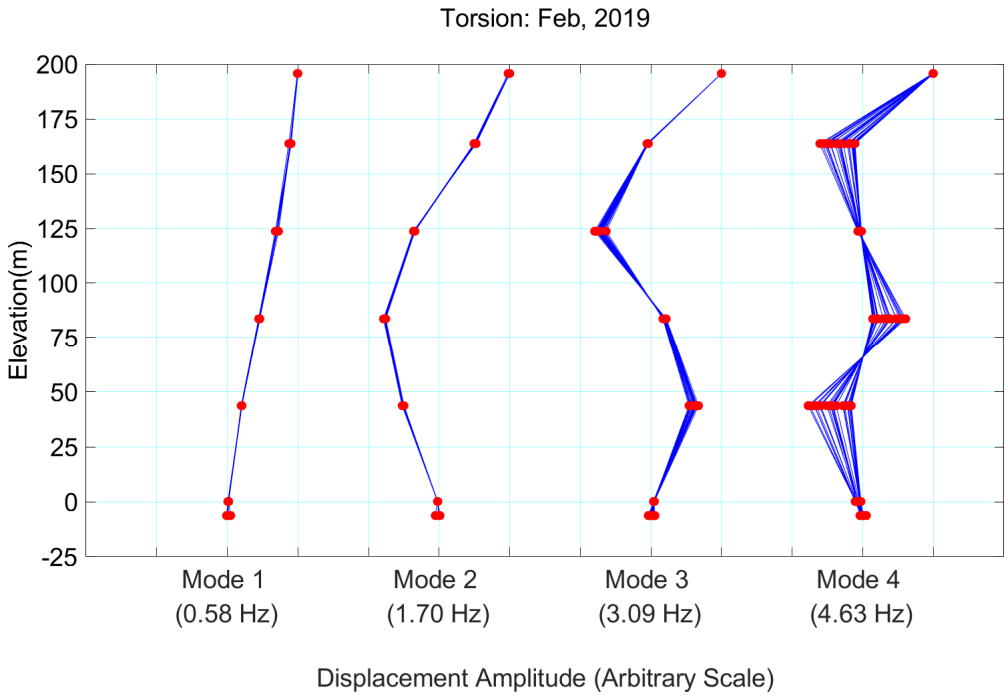

(c)

Figure 4.14 Continued.

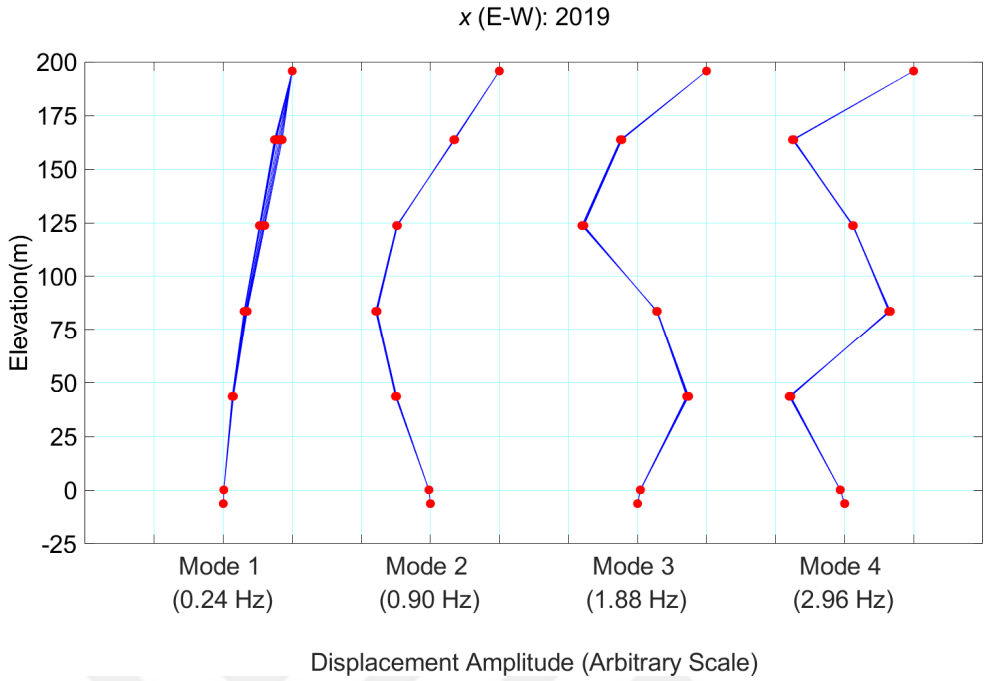

(a)

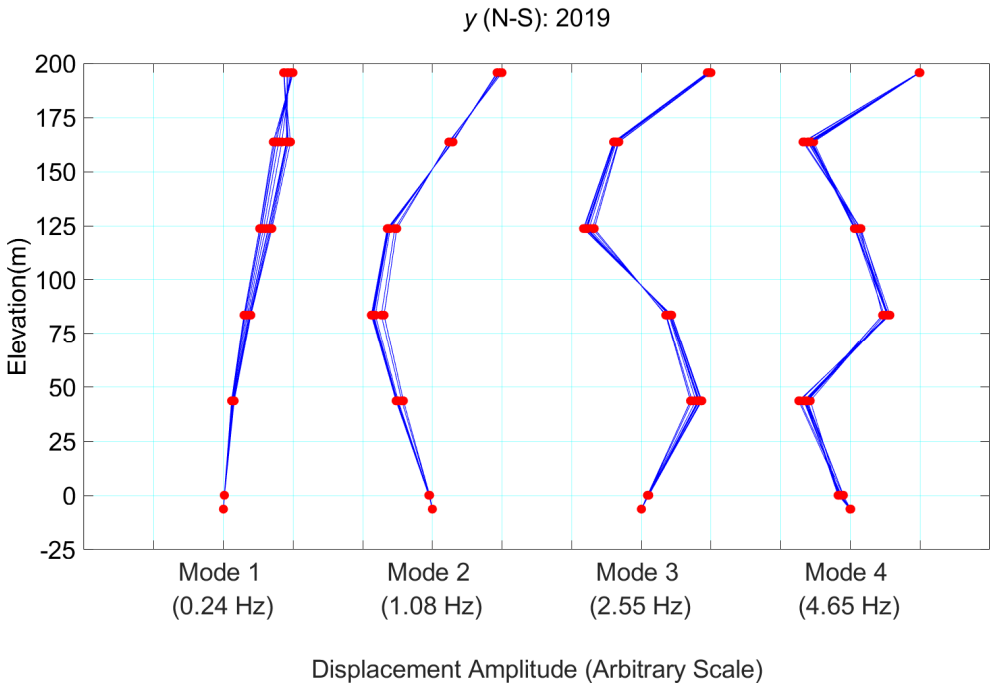

(b)

Figure 4.15 Vibrational mode shapes from a-year-long records (February to December, 2019): (a) E-W translational, (b) N-S translational and (c) torsional.

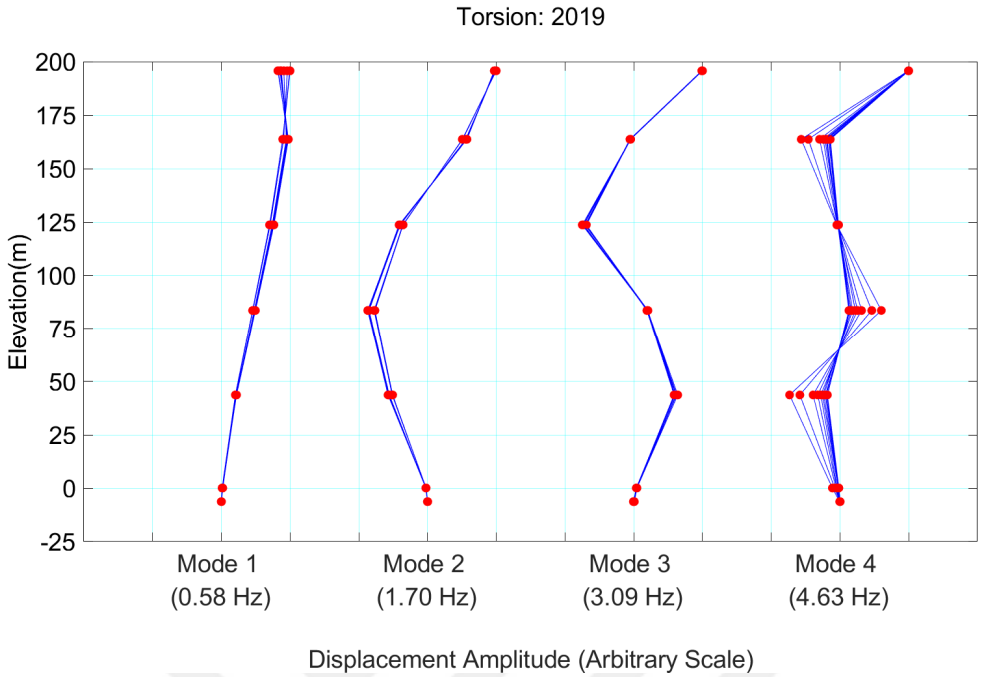

(c)

Figure 4.15 Continued.

CHAPTER 5

EARTHQUAKE RESPONSE RECORDS

5.1 General

The structural responses of the building were recorded during the earthquakes that occurred after January 27, 2019. Different events were recorded in this period; however, only building responses during earthquakes with moment magnitudes M_w greater than 3.5 at epicentral distances less than 50 km, with $M_w > 4.0$ at epicentral distances between 50 km and 100 km, and with $M_w > 5.0$ at epicentral distances greater than 100 km were presented in this chapter. Table 5.1 shows the list of the earthquakes with M_w 3.9–6.0 and epicentral distances of 15–283 km that occurred in 2019.

5.2 Building Responses During Earthquakes

Building responses during earthquakes listed in Table 5.1 were presented in this section. First, floor acceleration and displacement time histories, maximum roof and

Table 5.1 List of the selected earthquakes that occurred in 2019.

Date	Local Time	Epicenter	M_w	Distance (km)	Latitude (° N)	Longitude (° E)
Jan 27	06:16:47	Menemen	3.9	15	38.5591	27.0886
Feb 20	21:23:28	Ayvacik	5.0	144	39.6011	26.4261
Mar 20	09:34:27	Acipayam	5.5	228	37.4313	29.4385
Aug 08	11:39:08	Kusadasi	4.8	57	37.9720	26.9535
Aug 08	14:25:30	Bozkurt	6.0	222	37.8500	29.6016
Sep 26	13:59:25	Marmara	5.8	283	40.8718	28.1928

base accelerations, and maximum roof displacements were presented. Second, elastic 5% damped response spectra (spectral accelerations) of the free field ground motions, if available, and the building base motions were presented. Then, the short-time Fourier transforms (STFTs) of the 48th floor (roof) accelerations were presented. STFTs were calculated ("stft" function in MATLAB) using a moving window of 10.24 s (1024 data points) with 75% overlapping. Finally, the damping ratios were identified from the free decay of the earthquake displacement records (Clough and Penzien, 2003) using the developed algorithm summarized below:

1. Select the free vibration portion of the record following the earthquake event.
2. Narrow band-pass filter the record around each identified natural vibration frequency with a bandwidth three times the frequency resolution.
3. Determine the peaks between 90% and 20% of the maximum amplitude (Magalhaes et al., 2010).
4. Determine the damping ratio by a least-squares fit to the peaks, as explained in Section 4.2.3.

5.2.1 27.01.2019 M_w 3.9 Menemen, Izmir earthquake

The structural response of the building was recorded during the M_w 3.9 Menemen, Izmir (38.5591° N, 27.0886° E) earthquake that occurred on January 27, 2019 at 06:16:47 local time, with epicenter 15 km away from the building (Figure 5.1). The recorded floor accelerations and displacements are shown in Figures 5.2 and 5.3, respectively. The maximum accelerations at the roof and base were 0.016 g and 0.009 g, respectively, whereas the maximum roof displacement was 1 mm. Figure 5.4 shows the elastic 5% damped response spectra (spectral accelerations) of the building base motions. The STFTs of the roof accelerations in Figure 5.5 show that contributions of higher modes, particularly the second mode, to the building response during the earthquake. The building response was essentially in the first mode following the earthquake. The identified damping ratio associated with the first E-W

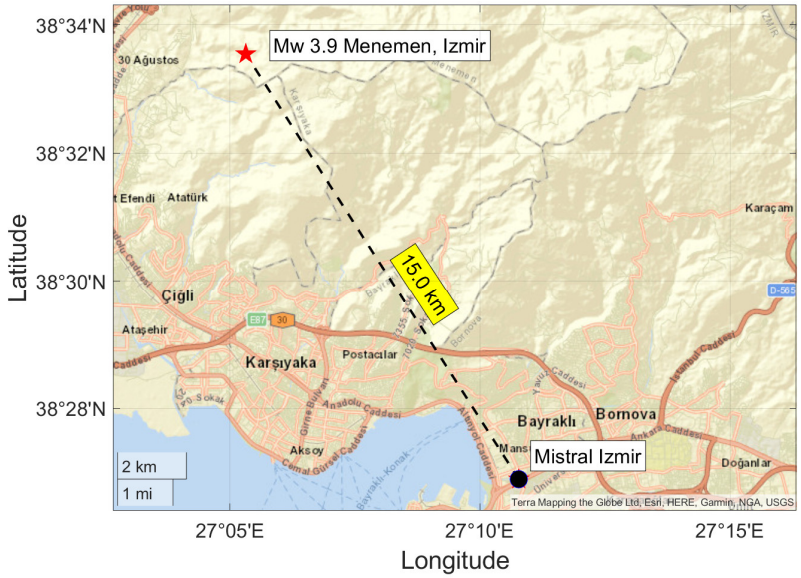

Figure 5.1 Epicenter of the 27.01.2019 06:16:47 TR M_w 3.9 Menemen, Izmir earthquake.

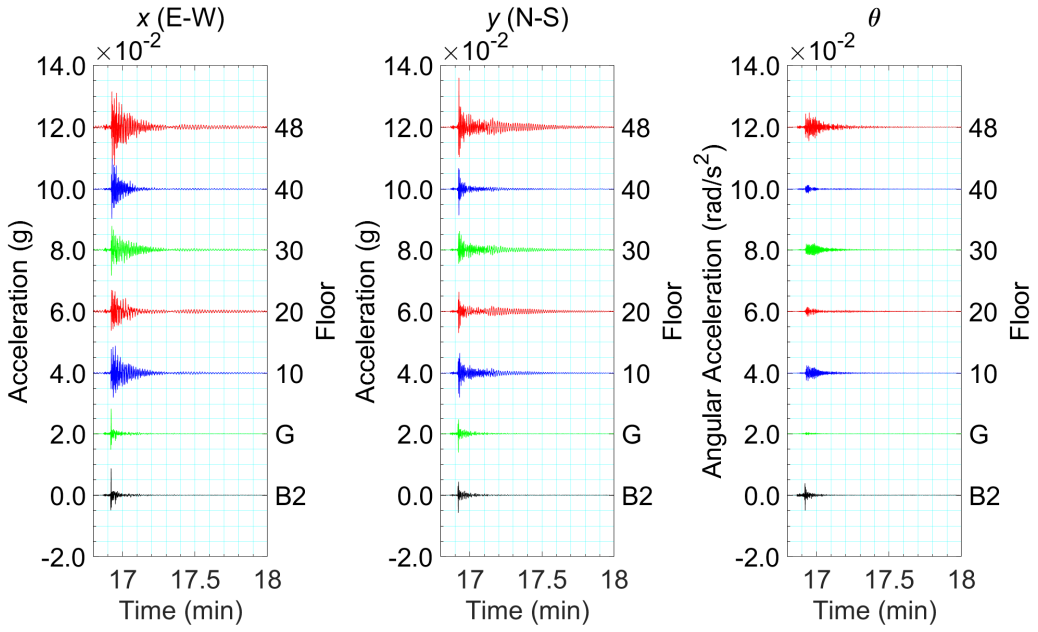

Figure 5.2 Floor acceleration time histories: 27.01.2019 06:16:47 TR M_w 3.9 Menemen, Izmir earthquake.

translational mode was 1.0%, which is almost two times the damping ratio identified from ambient vibrations (0.54%).

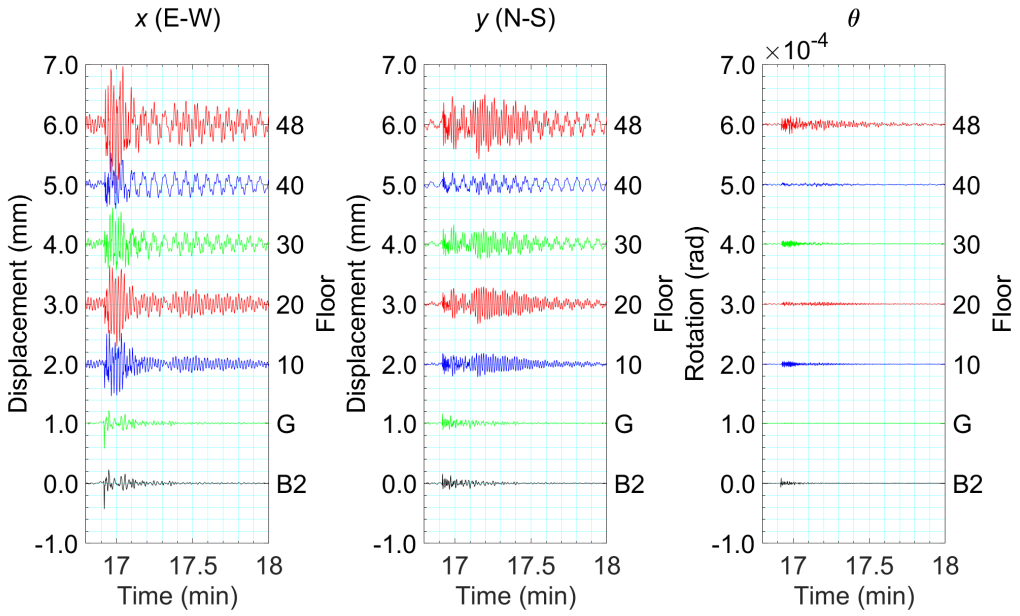

Figure 5.3 Floor displacement time histories: 27.01.2019 06:16:47 TR M_w 3.9 Menemen, Izmir earthquake.

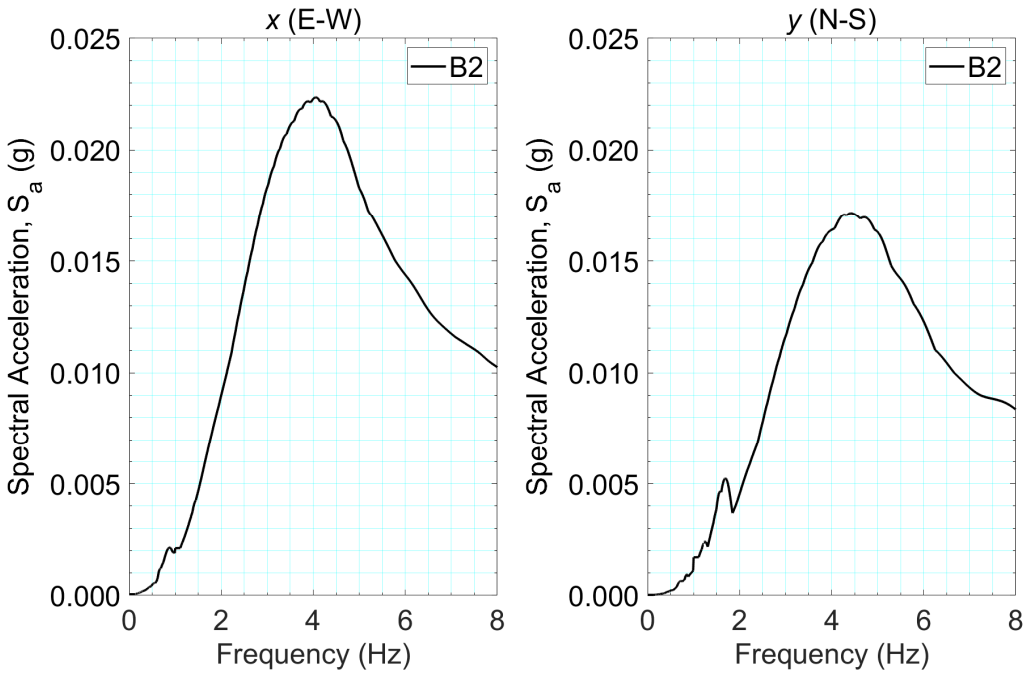

Figure 5.4 Elastic 5% damped response spectra of the building base motions.

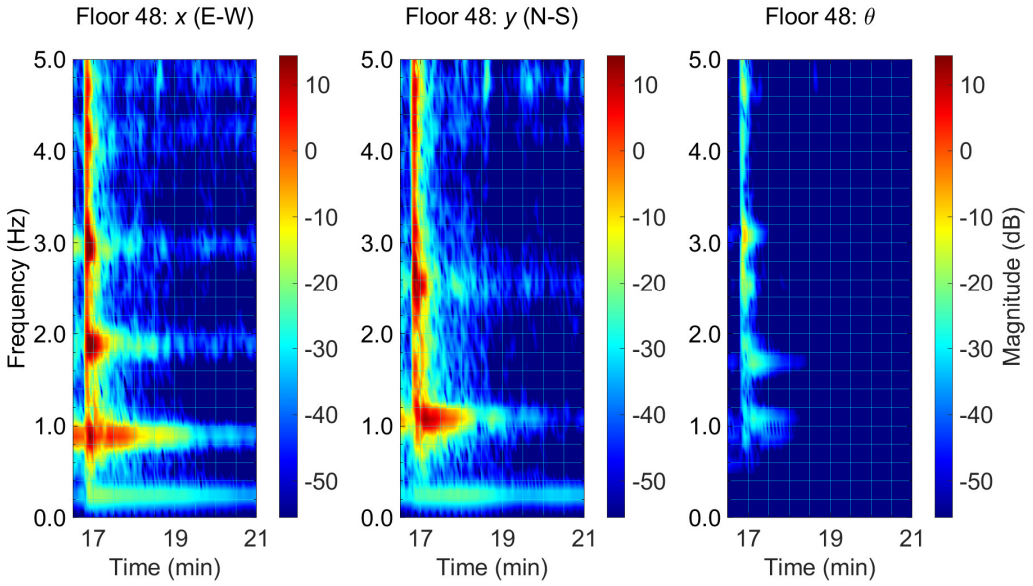

Figure 5.5 STFTs of the 48th floor accelerations: 27.01.2019 06:16:47 TR M_w 3.9 Menemen, Izmir earthquake.

5.2.2 20.02.2019 M_w 5.0 Ayvacik, Canakkale earthquake

The structural response of the building was recorded during the M_w 5.0 Ayvacik, Canakkale (38.6011° N, 26.4261° E) earthquake that occurred on February 20, 2019 at 21:23:28 local time, with epicenter 144 km away from the building (Figure 5.6). The recorded floor accelerations and displacements are shown in Figures 5.7 and 5.8, respectively. The maximum accelerations at the roof and base were 0.009 g and 0.004 g, respectively, whereas the maximum roof displacement was 5 mm. Figure 5.9 shows the elastic 5% damped spectral accelerations of the free field ground motions and building base motions. The STFTs of the roof accelerations in Figure 5.10 show that contributions of higher modes, particularly the second mode, to the building response during the earthquake. The building response was essentially in the first mode following the earthquake. The identified damping ratio associated with the first E-W translational mode was 1.5%, which is almost three times the damping ratio identified from ambient vibrations (0.54%).

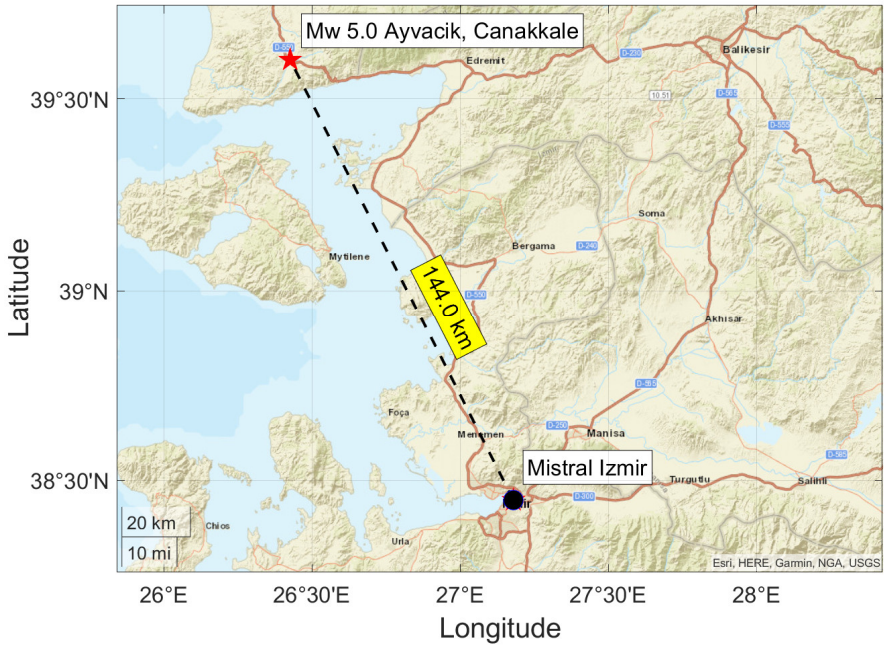

Figure 5.6 Epicenter of the 20.02.2019 21:23:28 TR M_w 5.0 Ayvacik, Canakkale earthquake.

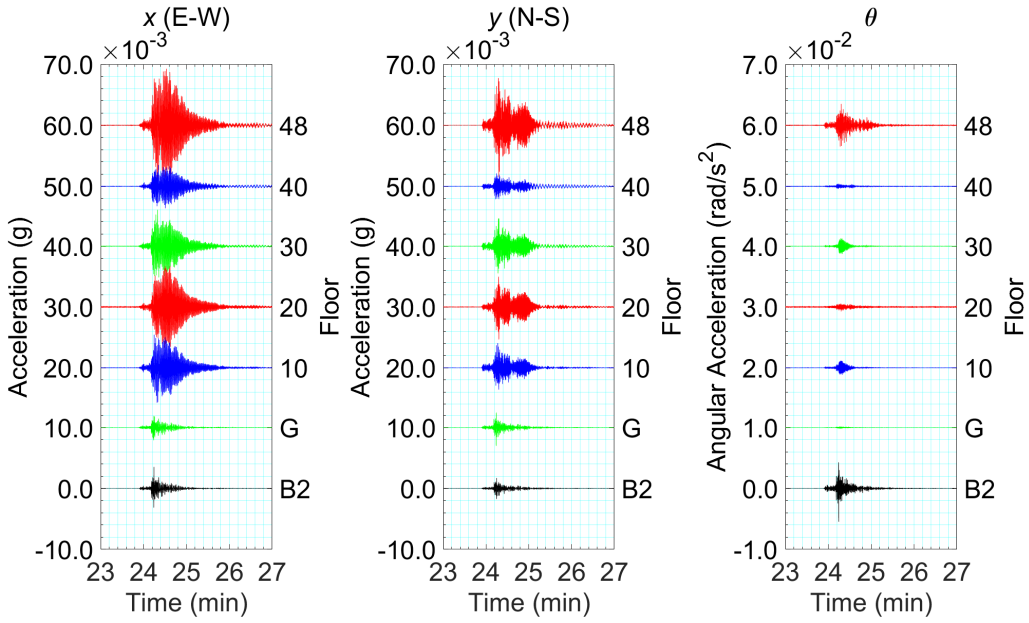

Figure 5.7 Floor acceleration time histories: 20.02.2019 21:23:28 TR M_w 5.0 Ayvacik, Canakkale earthquake.

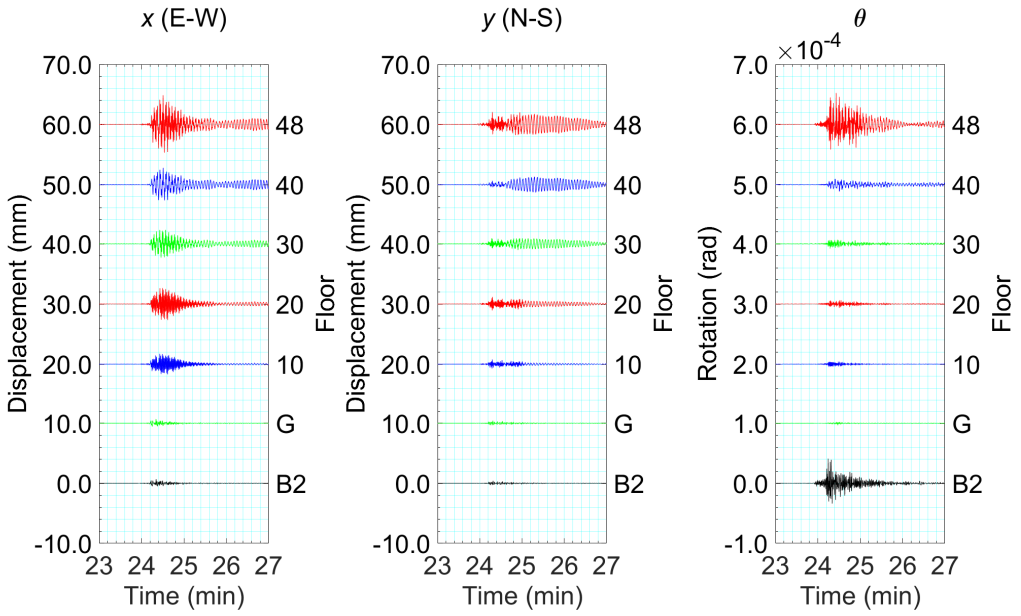

Figure 5.8 Floor displacement time histories: 20.02.2019 21:23:28 TR M_w 5.0 Ayvacik, Canakkale earthquake.

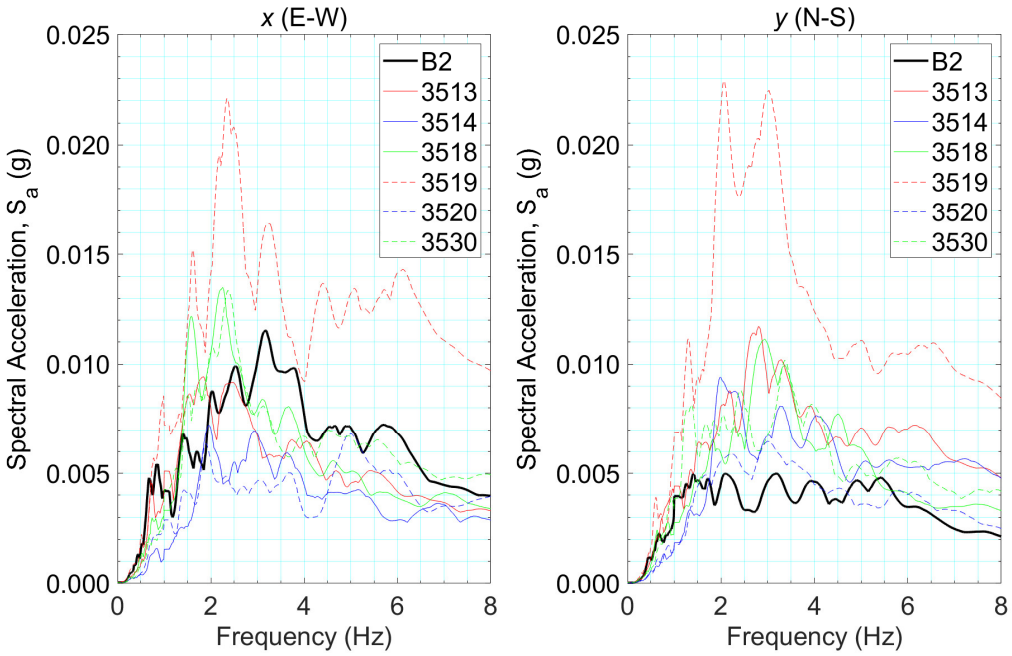

Figure 5.9 Elastic 5% damped response spectra of the free field ground motions and building base motions.

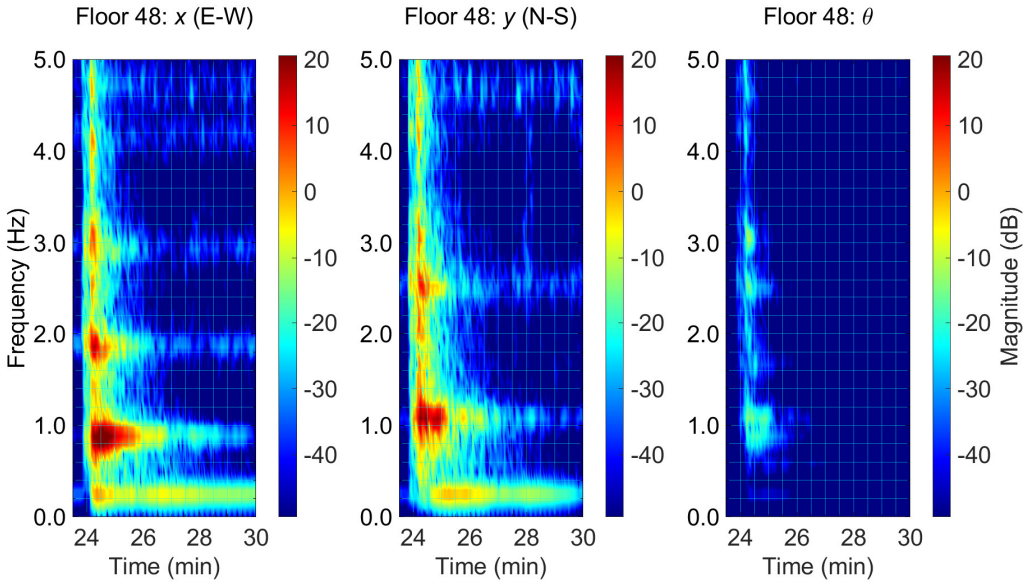

Figure 5.10 STFTs of the 48th floor accelerations: 20.02.2019 21:23:28 TR M_w 5.0 Ayvacik, Canakkale earthquake.

5.2.3 20.03.2019 M_w 5.5 Acipayam, Denizli earthquake

The structural response of the building was recorded during the M_w 5.5 Acipayam, Denizli (37.4313° N, 29.4385° E) earthquake that occurred on March 20, 2019 at 09:34:27 local time, with epicenter 228 km away from the building (Figure 5.11). The recorded floor accelerations and displacements are shown in Figures 5.12 and 5.13, respectively. The maximum accelerations at the roof and base were 0.017 g and 0.002 g, respectively, whereas the maximum roof displacement was 8 mm. Figure 5.14 shows the elastic 5% damped spectral accelerations of building base motions. The STFTs of the roof accelerations in Figure 5.15 show that contributions of higher modes, particularly the second mode, to the building response during the earthquake. The building response was essentially in the first mode following the earthquake. The identified damping ratio associated with the first E-W translational mode was 0.8%, which is slightly higher than the damping ratio identified from ambient vibrations (0.54).

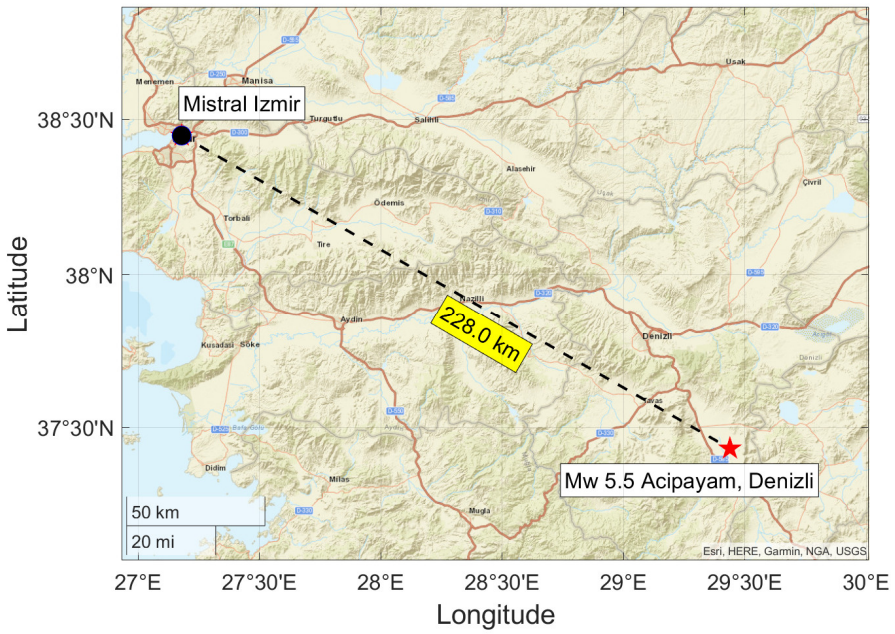

Figure 5.11 Epicenter of the 20.03.2019 09:34:27 TR M_w 5.5 Acipayam, Denizli earthquake.

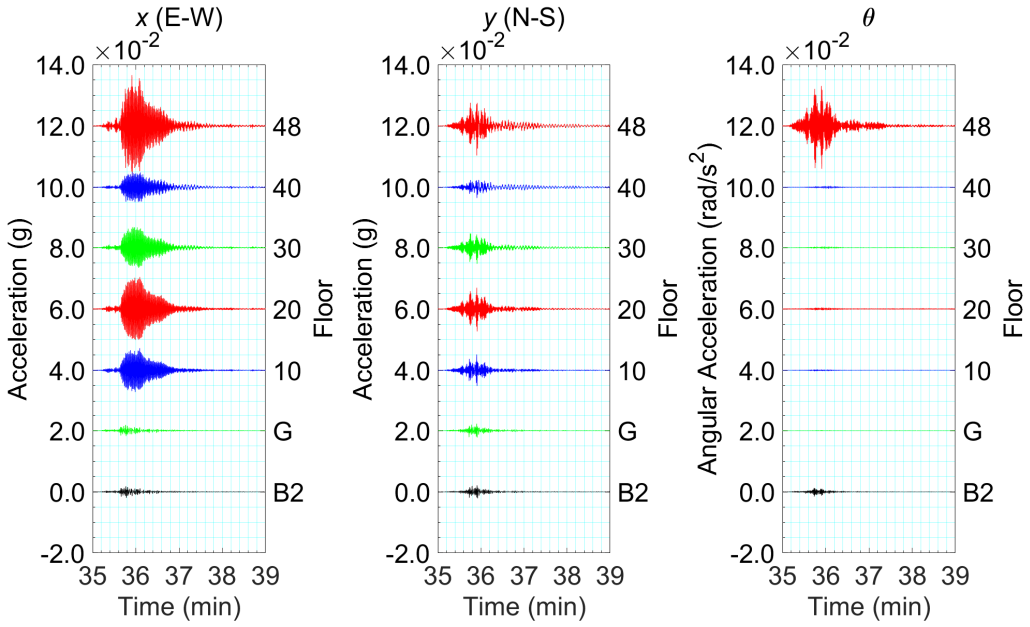

Figure 5.12 Floor acceleration time histories: 20.03.2019 09:34:27 TR M_w 5.5 Acipayam, Denizli earthquake.

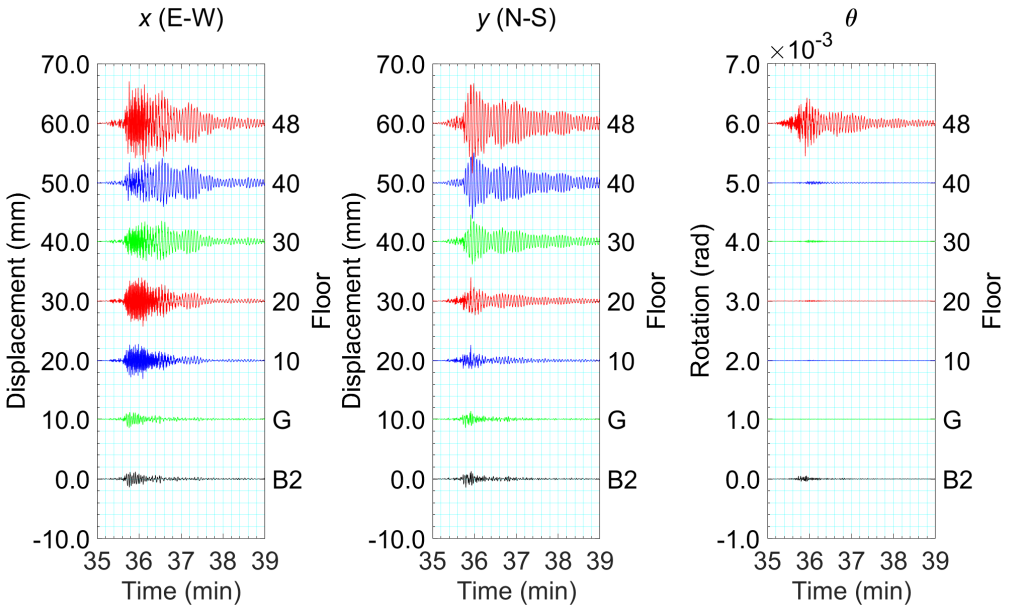

Figure 5.13 Floor displacement time histories: 20.03.2019 09:34:27 TR M_w 5.5 Acipayam, Denizli earthquake.

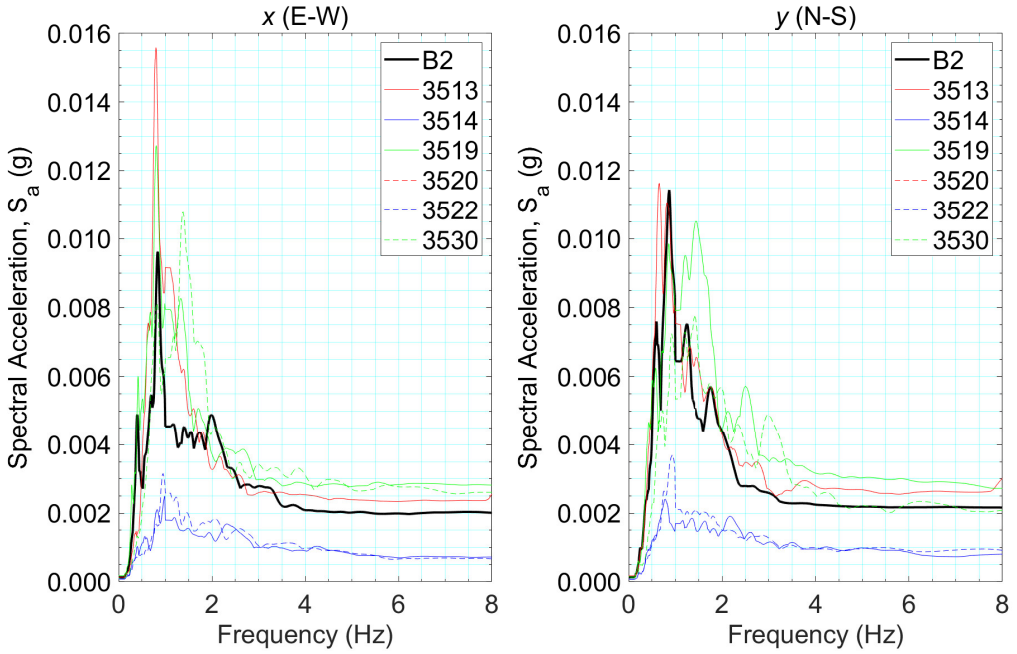

Figure 5.14 Elastic 5% damped response spectra of the free field ground motions and building base motions.

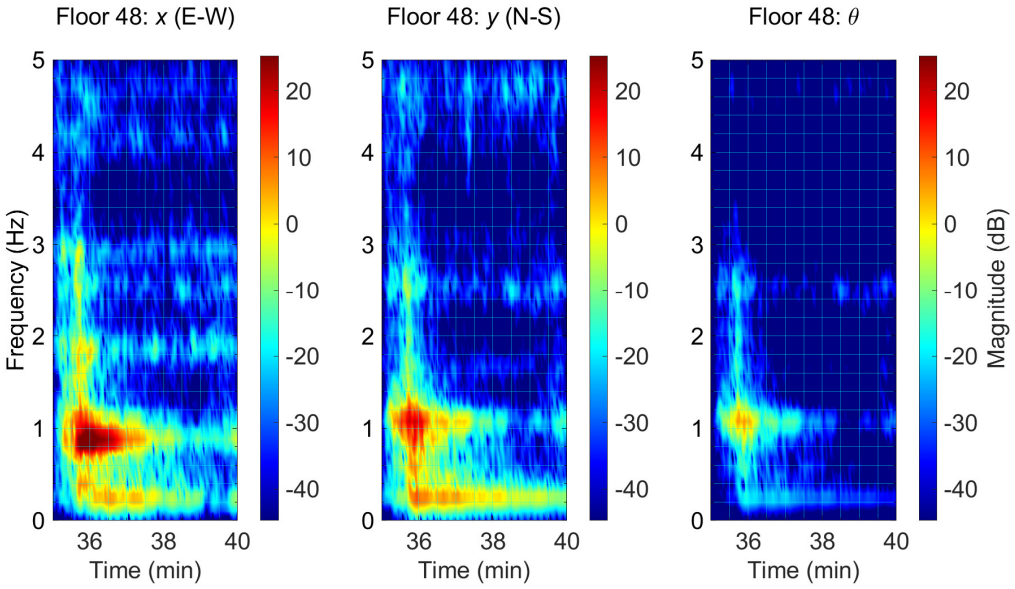

Figure 5.15 STFTs of the 48th floor accelerations: 20.03.2019 09:34:27 TR M_w 5.5 Acipayam, Denizli earthquake.

5.2.4 08.08.2019 M_w 4.8 Kusadasi Bay, Aydin earthquake

The structural response of the building was recorded during the M_w 4.8, Kusadasi Bay, Aydin (37.9720° N, 26.9535° E) earthquake that occurred on August 08, 2019 at 11:39:08 local time, with epicenter 57 km away from the building (Figure 5.16). The recorded floor accelerations and displacements are shown in Figures 5.17 and 5.18, respectively. The maximum accelerations at the roof and base were 0.012 g and 0.005 g, respectively, whereas the maximum roof displacement was 3 mm. Figure 5.19 shows the elastic 5% damped response spectra of building base motions. The STFTs of the roof accelerations in Figure 5.20 show that contributions of higher modes, particularly the second mode, to the building response during the earthquake. The building response was essentially in the first mode following the earthquake. The identified damping ratio associated with the first E-W translational mode was 1.3%, which is more than two times the damping ratio identified from ambient vibrations (0.54%).

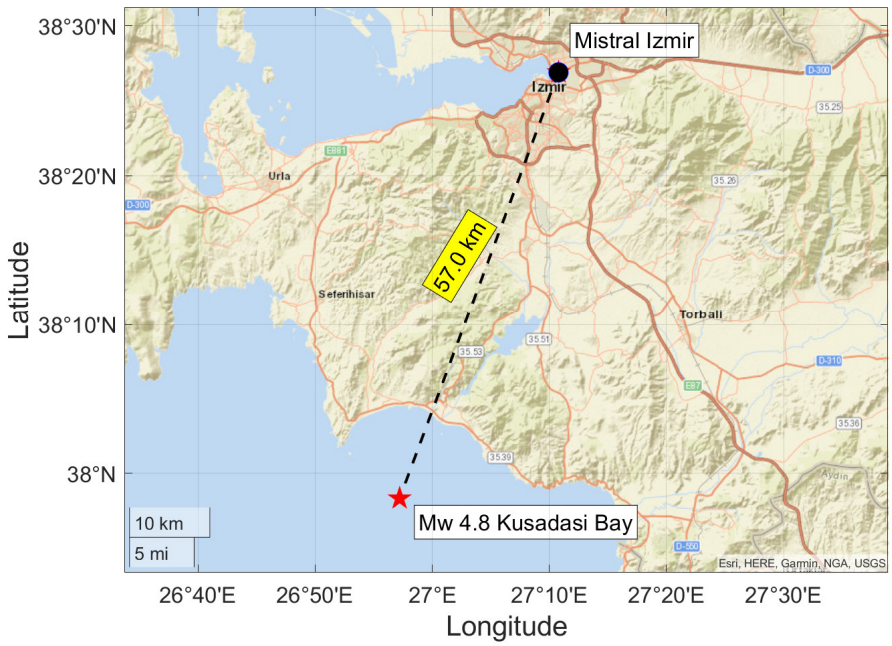

Figure 5.16 Epicenter of the 08.08.2019 11:39:08 TR M_w 4.8 Kusadasi Bay, Aydin earthquake.

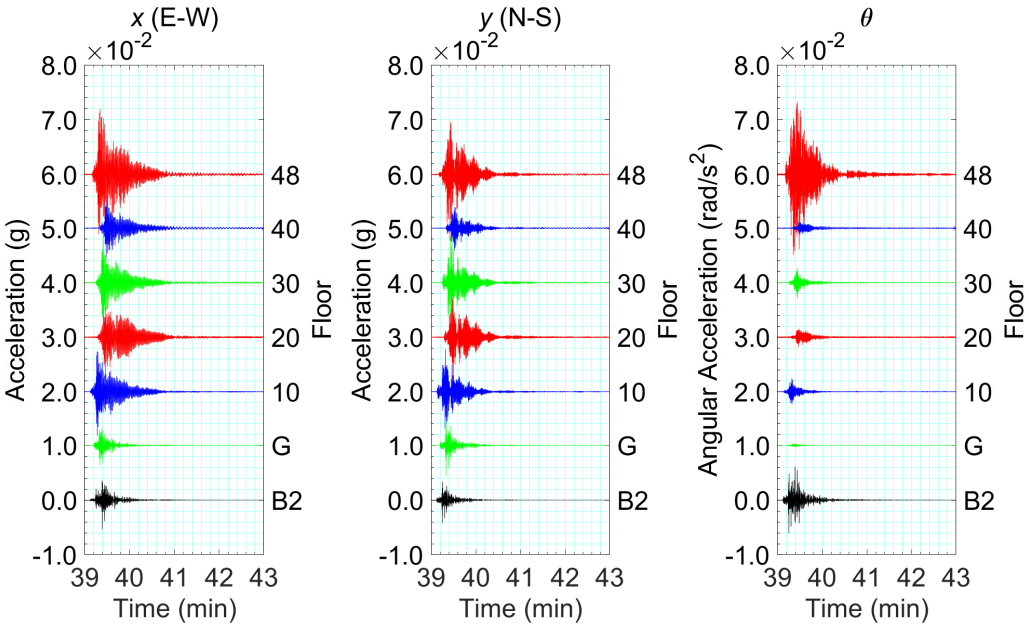

Figure 5.17 Floor acceleration time histories: 08.08.2019 11:39:08 TR M_w 4.8 Kusadasi Bay, Aydin earthquake.

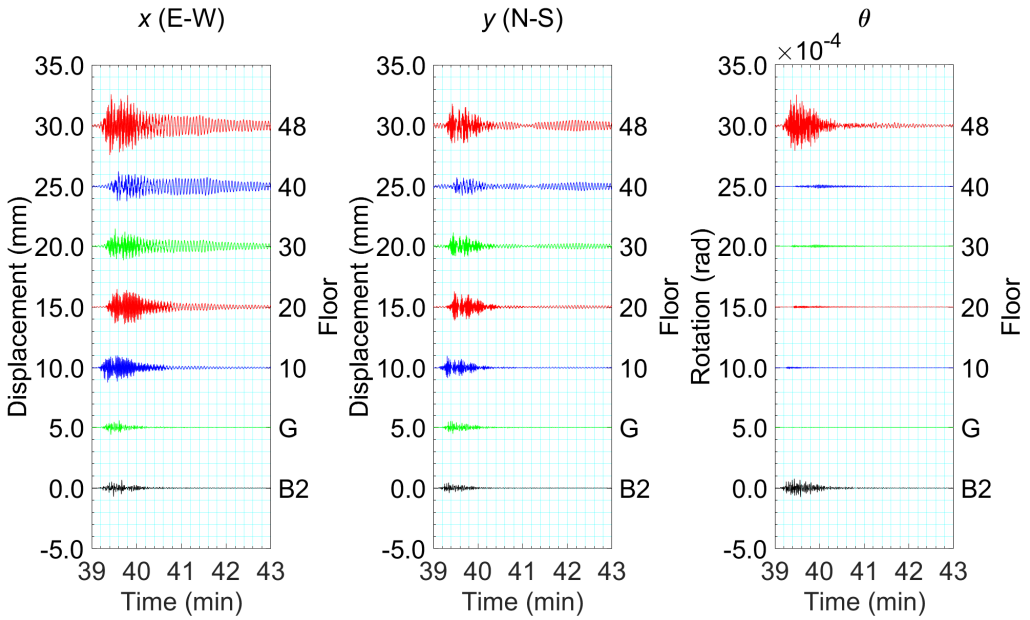

Figure 5.18 Floor displacement time histories: 08.08.2019 11:39:08 TR M_w 4.8 Kusadasi Bay, Aydin earthquake.

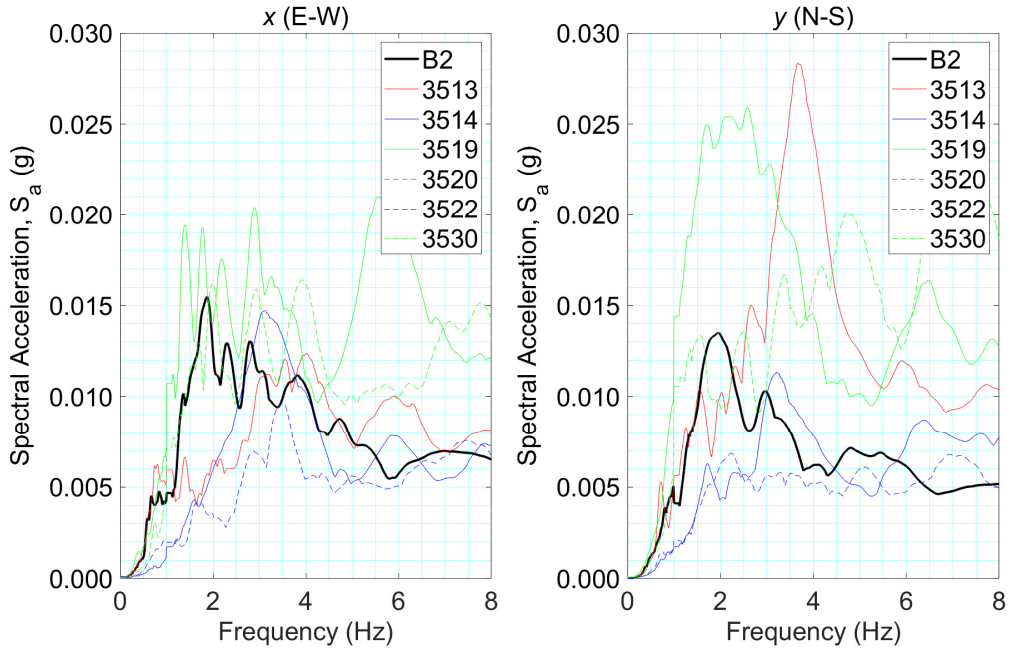

Figure 5.19 Elastic 5% damped response spectra of the free field ground motions and building base motions.

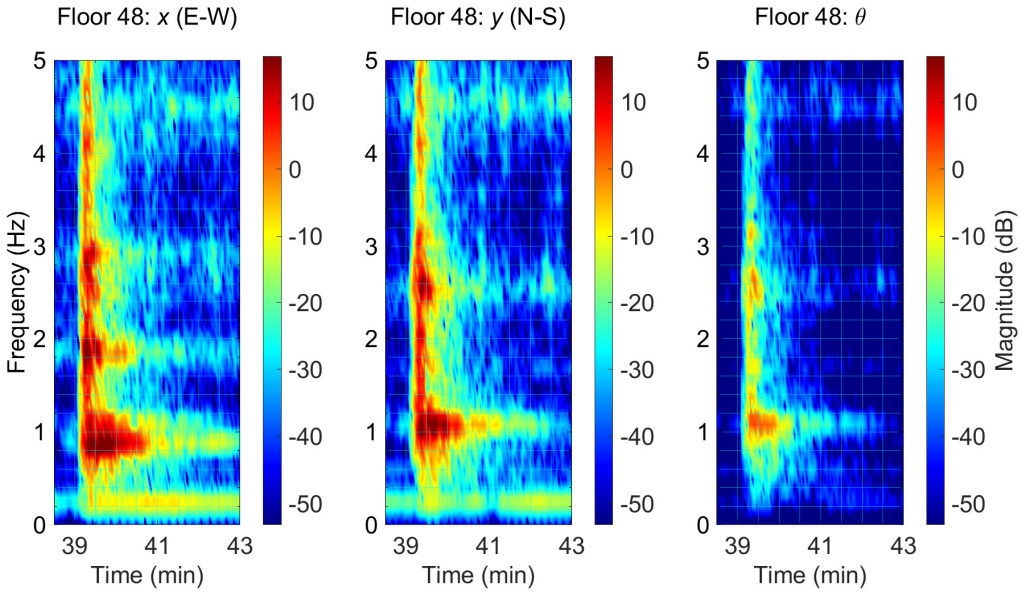

Figure 5.20 STFTs of the 48th floor accelerations: 08.08.2019 11:39:08 TR M_w 4.8 Kusadasi Bay, Aydin earthquake.

5.2.5 08.08.2019 M_w 6.0 Bozkurt, Denizli earthquake

The structural response of the building was recorded during the M_w 6.0, Bozkurt, Denizli (37.8500° N, 29.6016° E) earthquake that occurred on August 08, 2019 at 14:25:30 local time, with epicenter 222 km away from the building (Figure 5.21). The recorded floor accelerations and displacements are shown in Figures 5.22 and 5.23, respectively. The maximum accelerations at the roof and base were 0.006 g and 0.001 g, respectively, whereas the maximum roof displacement was 4 mm. Figure 5.24 shows the elastic 5% damped spectral accelerations of building base motions. The STFTs of the roof accelerations in Figure 5.25 show that contributions of the first two modes to the building response during the earthquake. The building response was essentially in the first mode following the earthquake. The identified damping ratio associated with the first E-W translational mode was 1.7%, which is almost three times the damping ratio identified from ambient vibrations (0.54%).

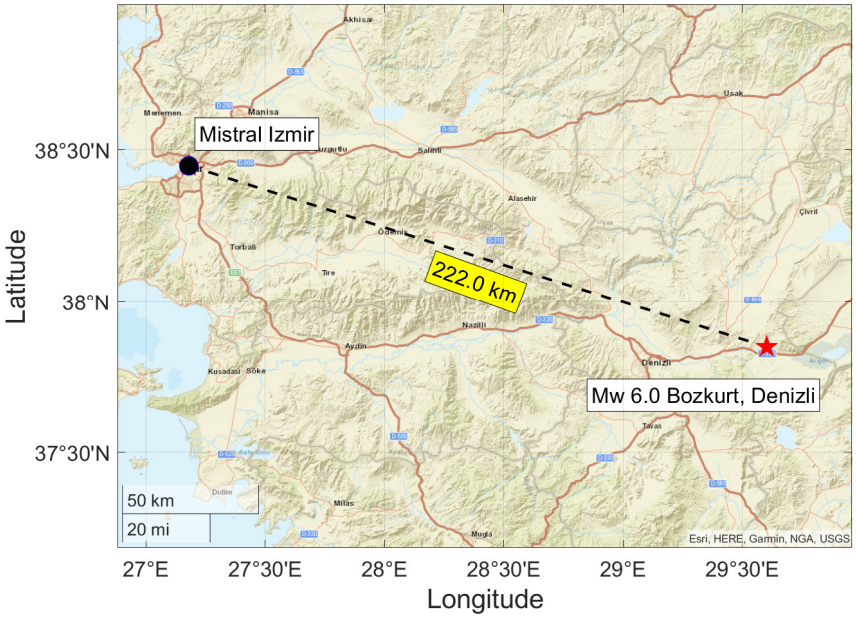

Figure 5.21 Epicenter of the 08.08.2019 14:25:30 TR M_w 6.0 Bozkurt, Denizli earthquake.

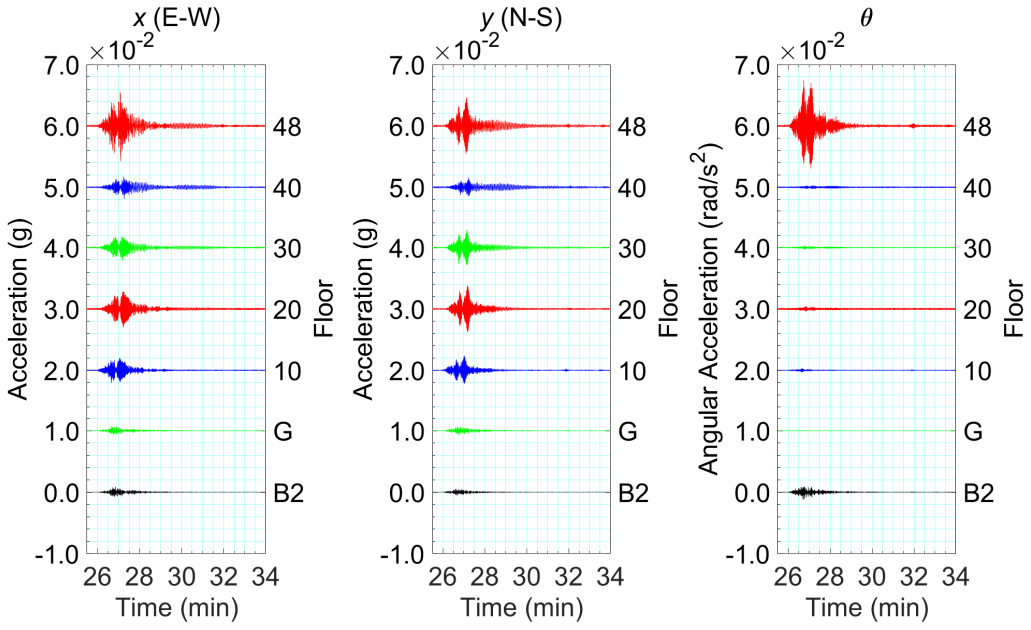

Figure 5.22 Floor acceleration time histories: 08.08.2019 14:25:30 TR M_w 6.0 Bozkurt, Denizli earthquake.

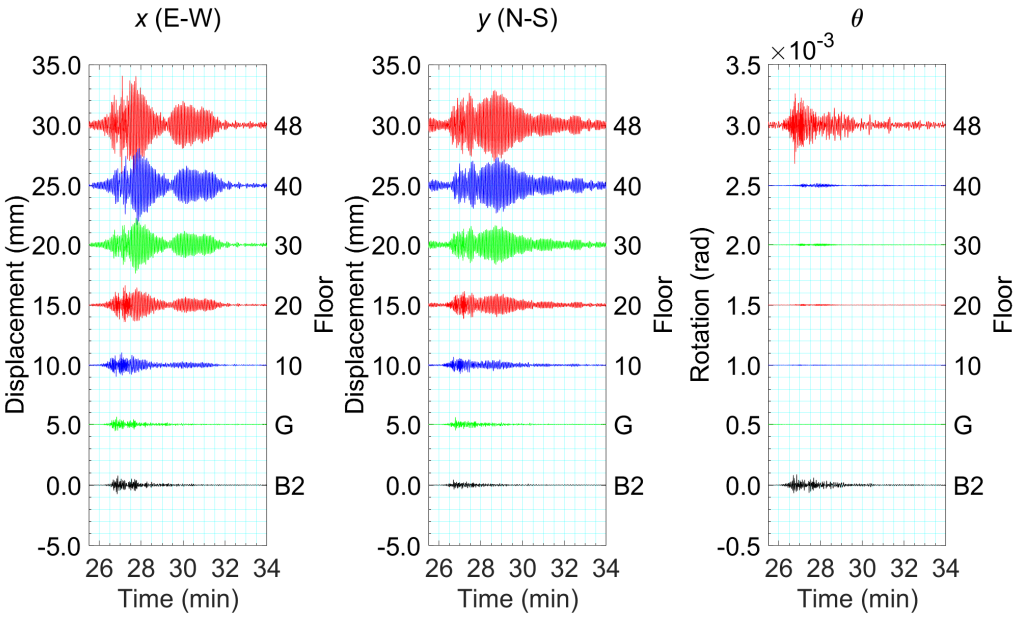

Figure 5.23 Floor displacement time histories: 08.08.2019 14:25:30 TR M_w 6.0 Bozkurt, Denizli earthquake.

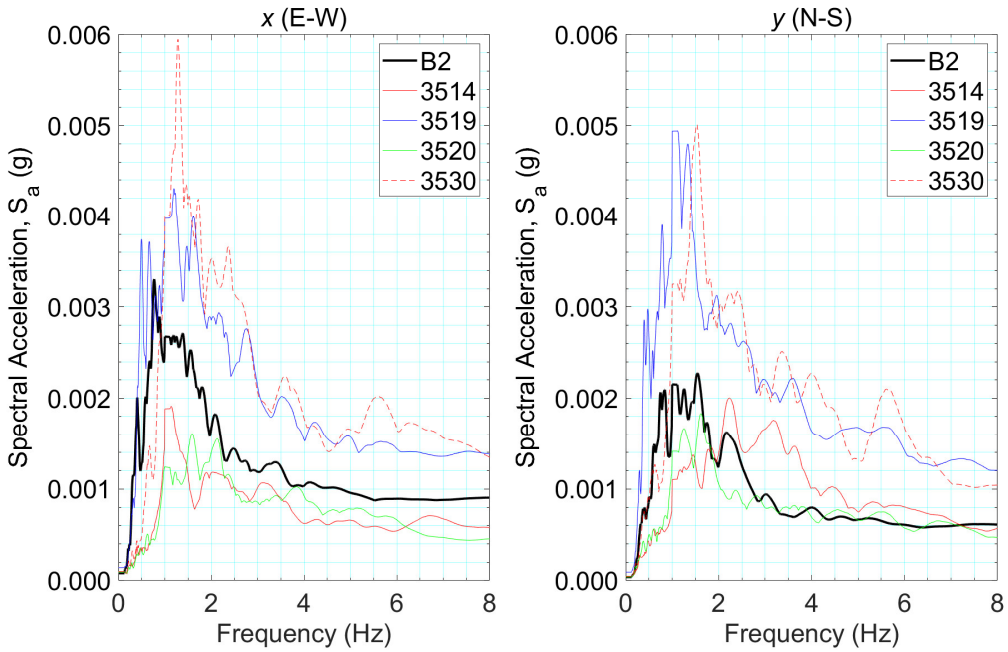

Figure 5.24 Elastic 5% damped response spectra of the free field ground motions and building base motions.

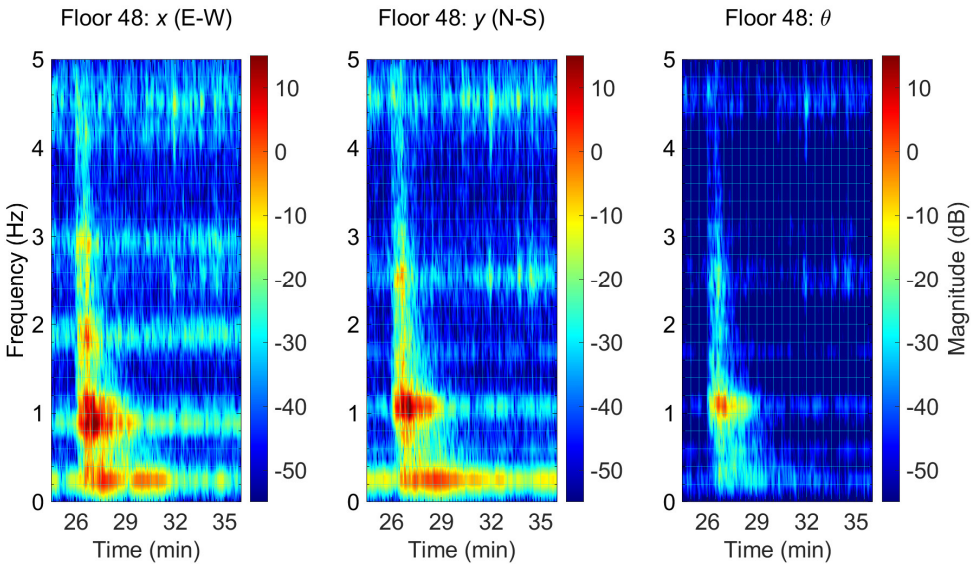

Figure 5.25 STFTs of the 48th floor accelerations: 08.08.2019 14:25:30 TR M_w 6.0 Bozkurt, Denizli earthquake.

5.2.6 26.09.2019 M_w 5.8 the Marmara Sea, Istanbul earthquake

The structural response of the building was recorded during the M_w 5.8, the Marmara Sea, Istanbul (40.8718° N, 28.1928° E) earthquake that occurred on September 26, 2019 at 13:59:25 local time, with epicenter 283 km away from the building (Figure 5.26). The recorded floor accelerations and displacements are shown in Figures 5.27 and 5.28, respectively. The maximum accelerations at the roof and base were 0.004 g and 0.001 g, respectively, whereas the maximum roof displacement was 4 mm. Figure 5.29 shows the elastic 5% damped spectral accelerations of building base motions. The STFTs of the roof accelerations in Figure 5.30 show that contributions of the first two modes to the building response during the earthquake. There were also considerable oscillations in the higher modes. The building response was essentially in the first mode following the earthquake. The identified damping ratio associated with the first E-W translational mode was 1.5%, which is almost two times the damping ratio identified from ambient vibrations (0.54%).

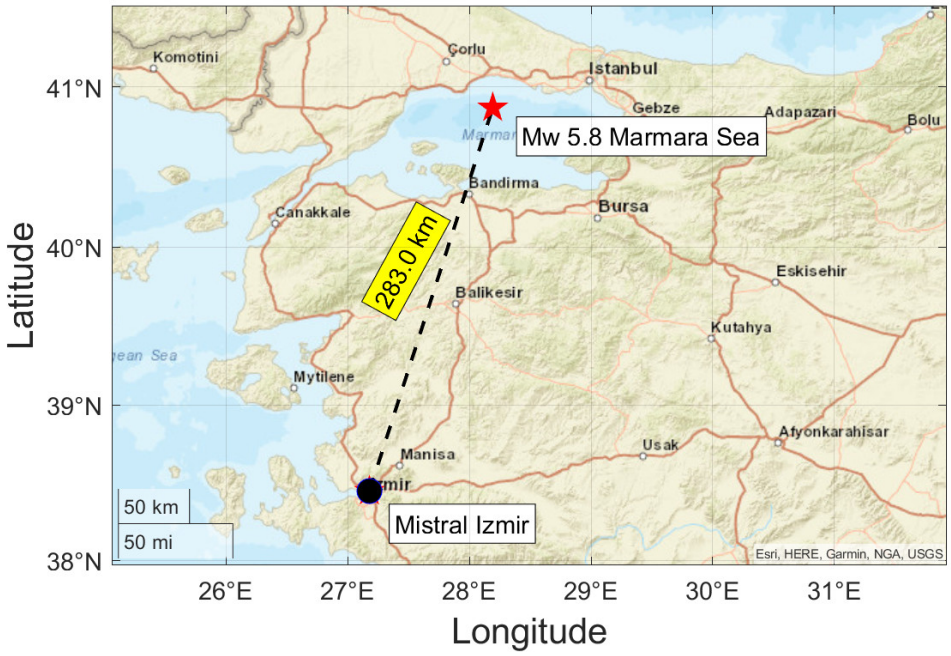

Figure 5.26 Epicenter of the 26.09.2019 13:59:25 TR M_w 5.8 Marmara Sea, Istanbul earthquake.

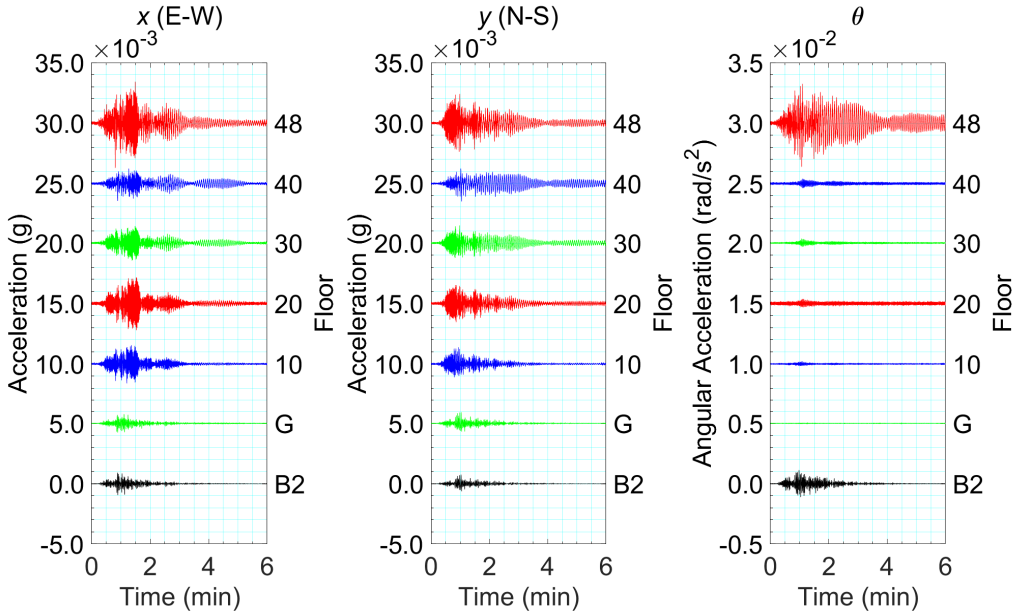

Figure 5.27 Floor acceleration time histories: 26.09.2019 13:59:25 TR M_w 5.8 Marmara Sea, Istanbul earthquake.

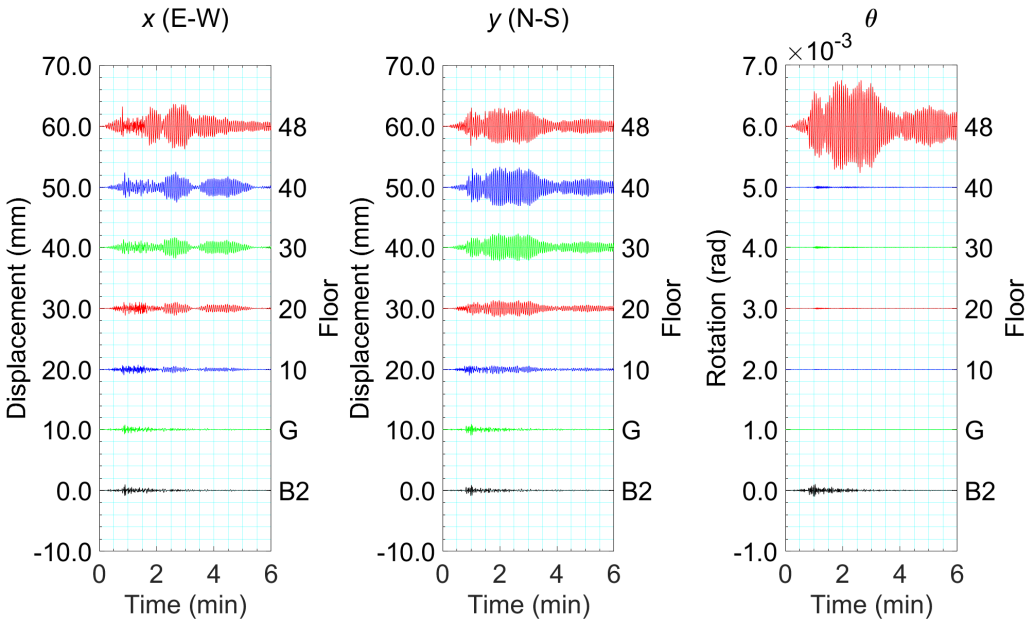

Figure 5.28 Floor displacement time histories: 26.09.2019 13:59:25 TR M_w 5.8 Marmara Sea, Istanbul earthquake.

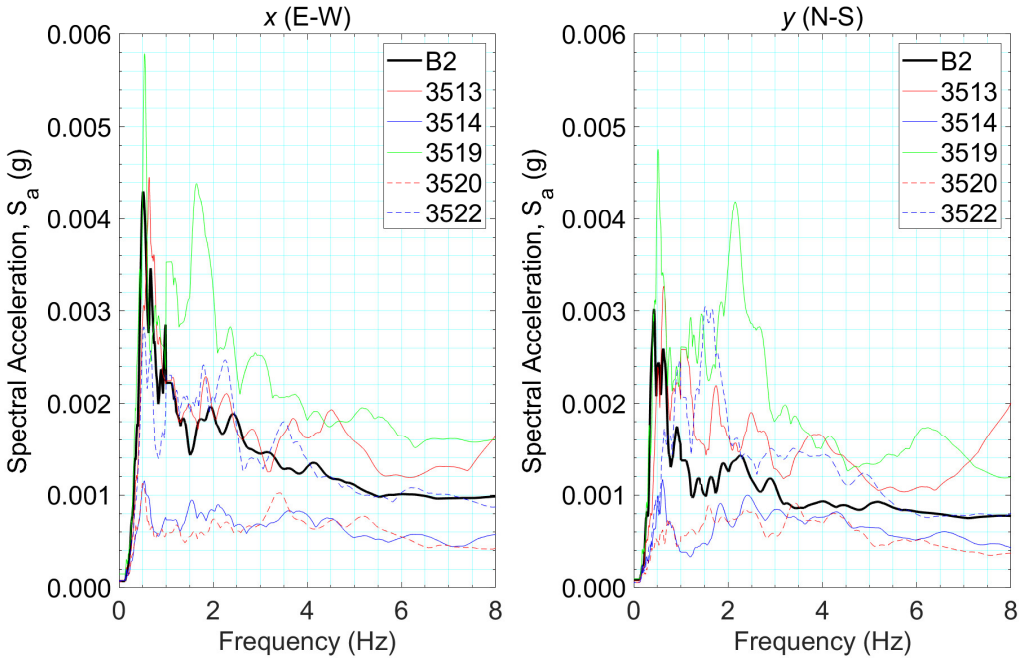

Figure 5.29 Elastic 5% damped response spectra of the free field ground motions and building base motions.

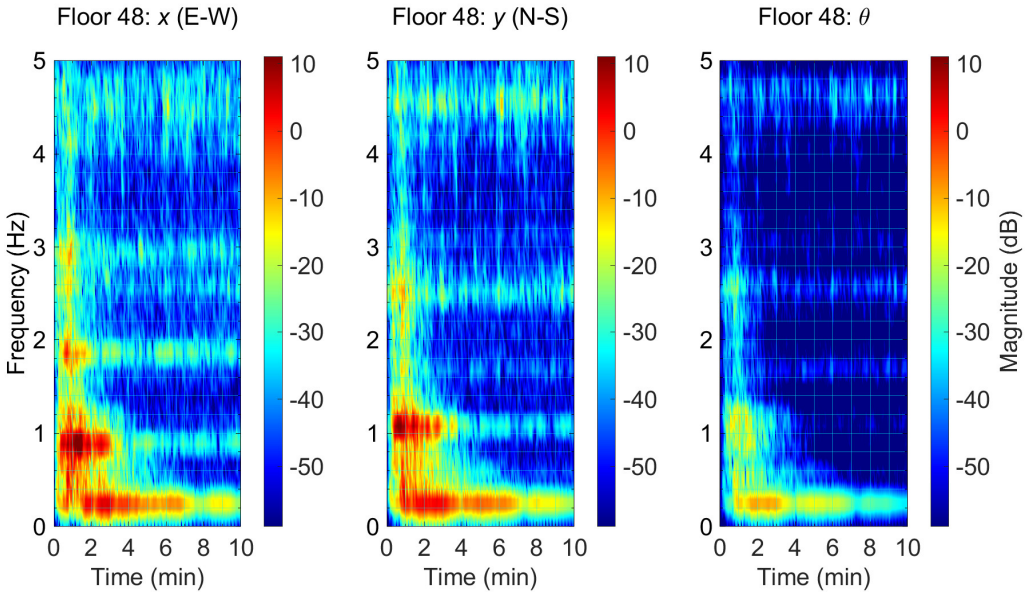

Figure 5.30 STFTs of the 48th floor accelerations: 26.09.2019 13:59:25 TR M_w 5.8 Marmara Sea, Istanbul earthquake.

5.2.7 Summary of the earthquake responses

Table 5.2 summarizes the building responses during the earthquakes in 2019. The maximum acceleration was 0.017 g at the roof and 0.009 g at the building base, where base-to-roof amplifications were in the range of 1.8–8.6. The maximum roof displacement was 8 mm. The identified modal damping ratios were in the range of 0.8–1.7%. Higher-mode effects were observed during the earthquakes; the building response was essentially in the first translational modes following the earthquakes.

5.3 SSI and Rocking Responses

SSI and rocking responses were investigated using the 2019 M_w 5.5 Acipayam, Denizli earthquake response records since the largest roof acceleration among all earthquakes in 2019 was recorded during this earthquake.

Table 5.2 Building responses during the earthquakes in 2019.

Date	Epicenter	M_w	Distance (km)	Max. Acceleration (g)		Max. Roof Disp. (mm)	ξ (%)
				Base	Roof		
Jan 27	Menemen	3.9	15	0.009	0.016	1	1.0
Feb 20	Ayvacik	5.0	146	0.004	0.009	5	1.5
Mar 20	Acipayam	5.5	228	0.002	0.017	8	0.8
Aug 08	Kusadasi	4.8	57	0.005	0.012	3	1.3
Aug 08	Bozkurt	6.0	222	0.001	0.006	4	1.7
Sep 26	Marmara	5.8	284	0.001	0.004	4	1.5

The presence of SSI can be identified by comparing the dominant frequencies of the base-to-roof transfer functions and the Fourier amplitude spectra of the roof responses (Safak and Cakti, 2014). The transfer functions were calculated by dividing the Fourier amplitude spectra of the roof accelerations (Figure 5.31) by those of the base motions and were presented in Figure 5.32. The dominant frequencies in Figures 5.31 and 5.32 are equal; hence, SSI effects were not present.

The rocking responses were calculated as the differences between the vertical acceleration responses at the base (Celebi and Safak, 1991; Safak and Cakti, 2014; Cha et al., 2016) as presented in Figure 5.33a. The Fourier amplitude spectra of these responses were presented in Figure 5.33b. There were peaks at frequencies 0.87 Hz and 1.07 Hz, which are the second translational modes in E-W and N-S directions (identified in Chapter 4), respectively. These common frequencies were the rocking frequencies. Figures 5.34 and 5.35 present the 48th floor displacements, the displacements at this floor due to rocking — calculated by multiplying the rocking rotation by the elevation difference between floor 48 and the basement, and their difference (i.e., horizontal displacements free of rocking effects). These figures show that the contribution of rocking in both E-W and N-S displacements was not significant, not more than 10% and 8% of the maximum displacements, respectively.

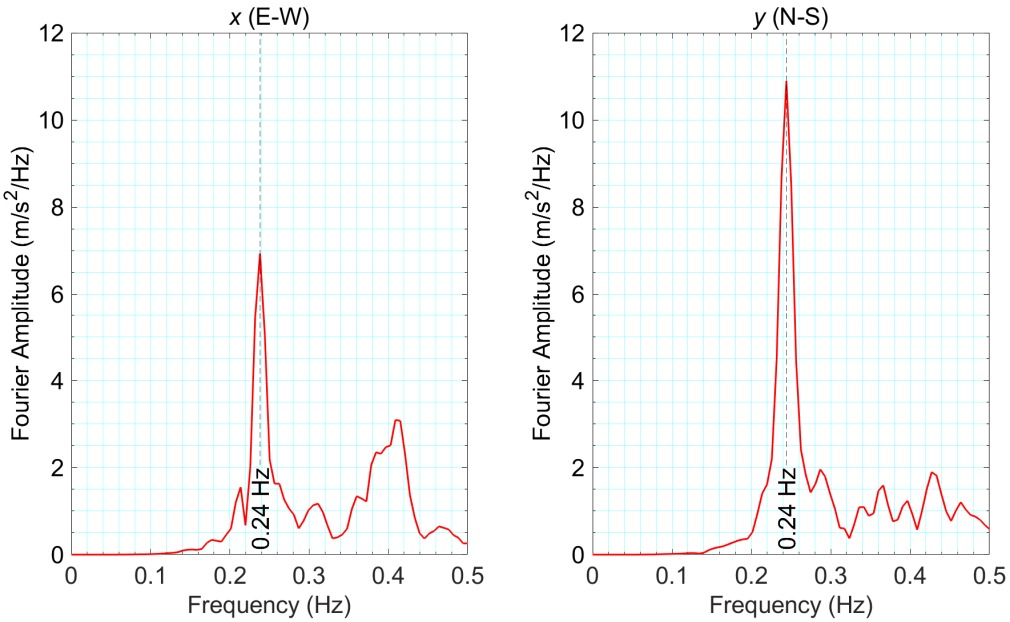

Figure 5.31 Fourier amplitude spectra of the roof accelerations: 2019 M_w 5.5 Acipayam, Denizli earthquake.

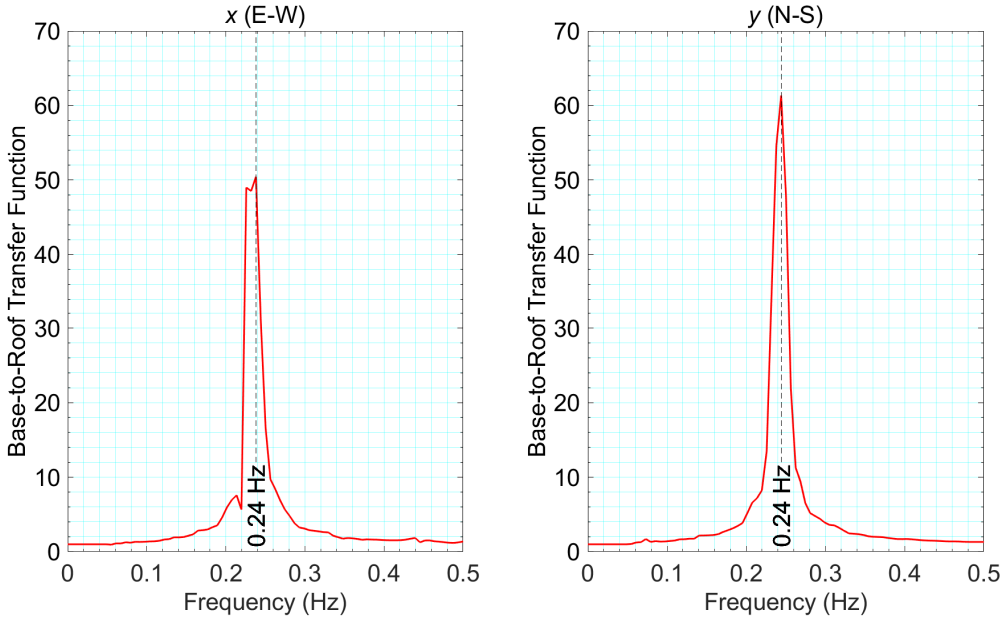

Figure 5.32 Base-to-roof transfer functions: 2019 M_w 5.5 Acipayam, Denizli earthquake.

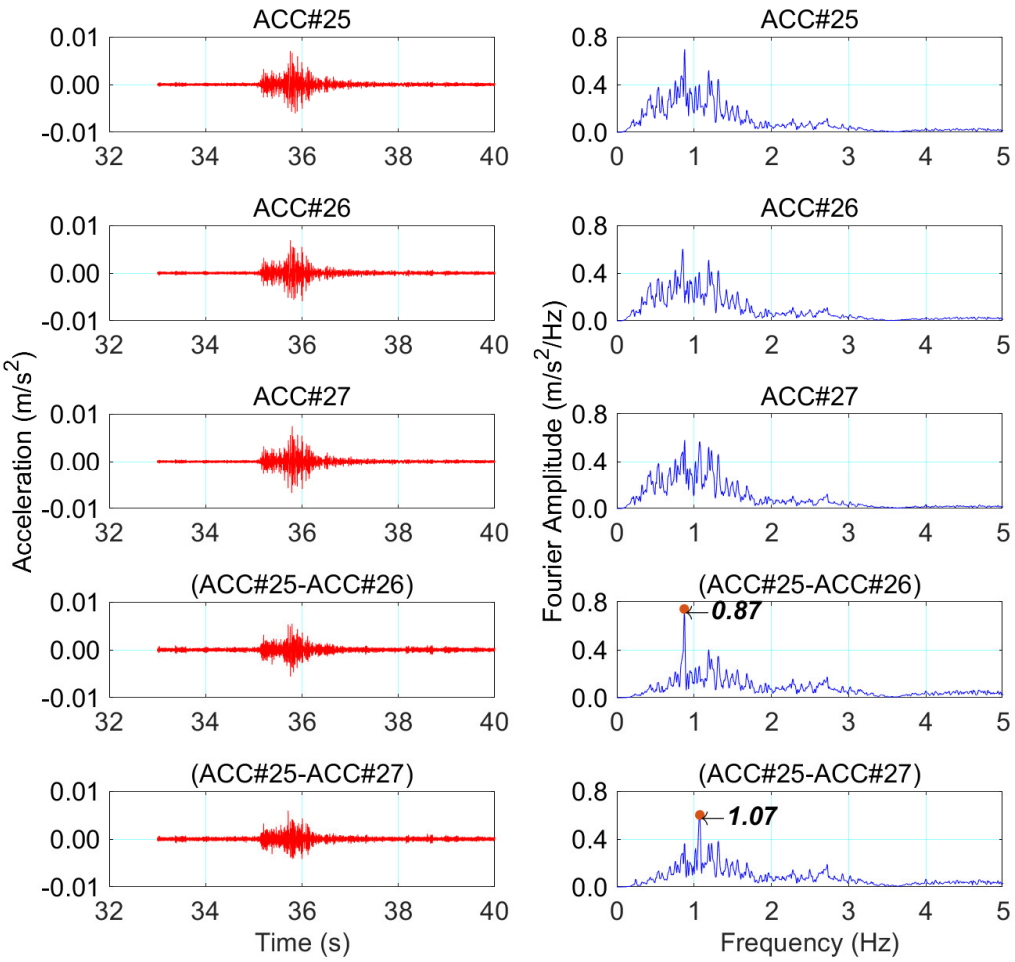

Figure 5.33 (a) Time histories and (b) Fourier amplitude spectra of the vertical accelerations at three corners of the basement and their difference: 2019 M_w 5.5 Acipayam, Denizli earthquake.

To sum up, SSI and rocking responses were considered negligible. However, detailed investigation of SSI and rocking responses by advanced system identification methods is a subject of future research.

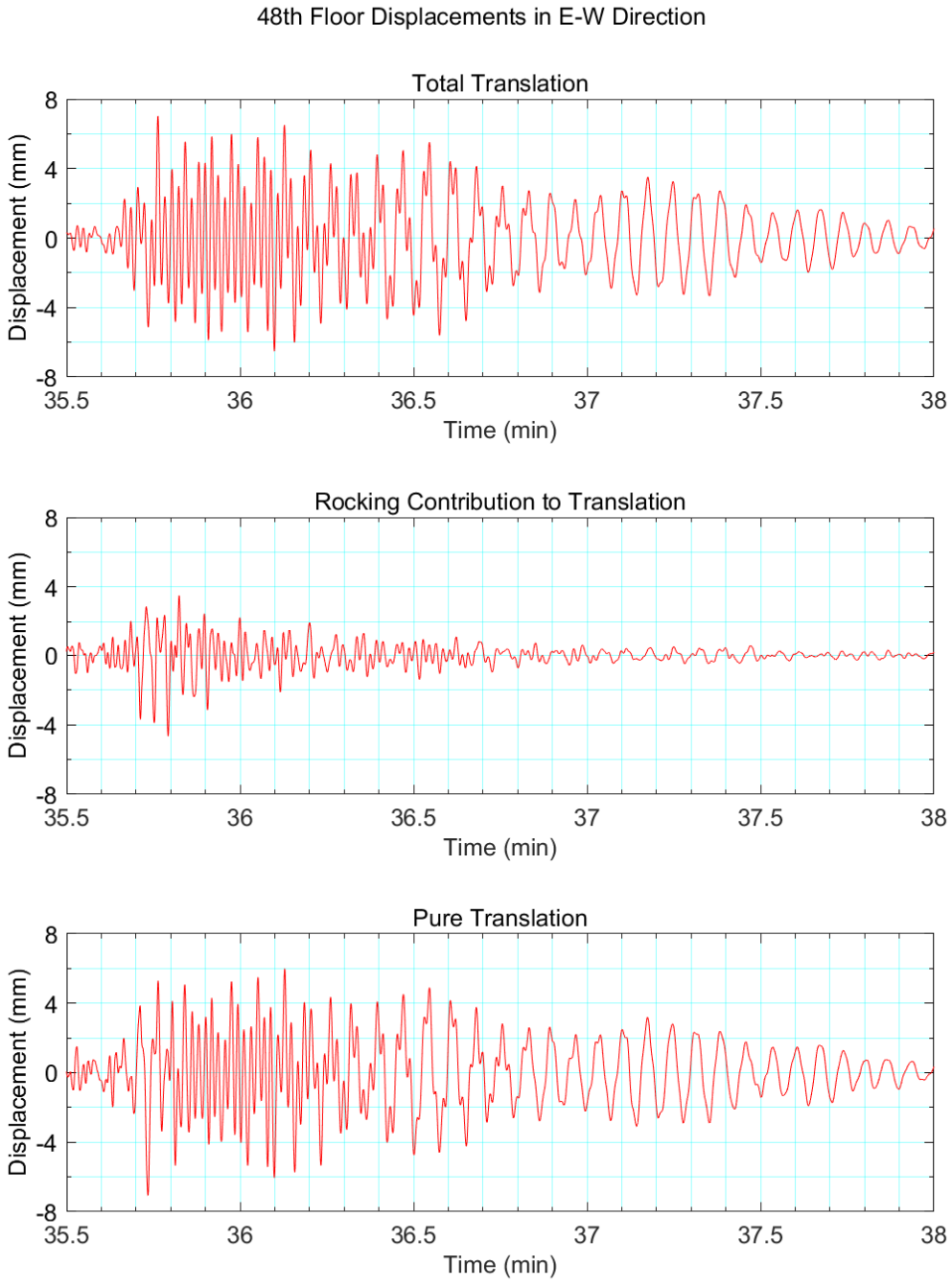

Figure 5.34 Rocking contribution to the 48th floor E-W translation (rocking rotation around N-S axis): March 20, 2019 M_w 5.5 Acipayam earthquake.

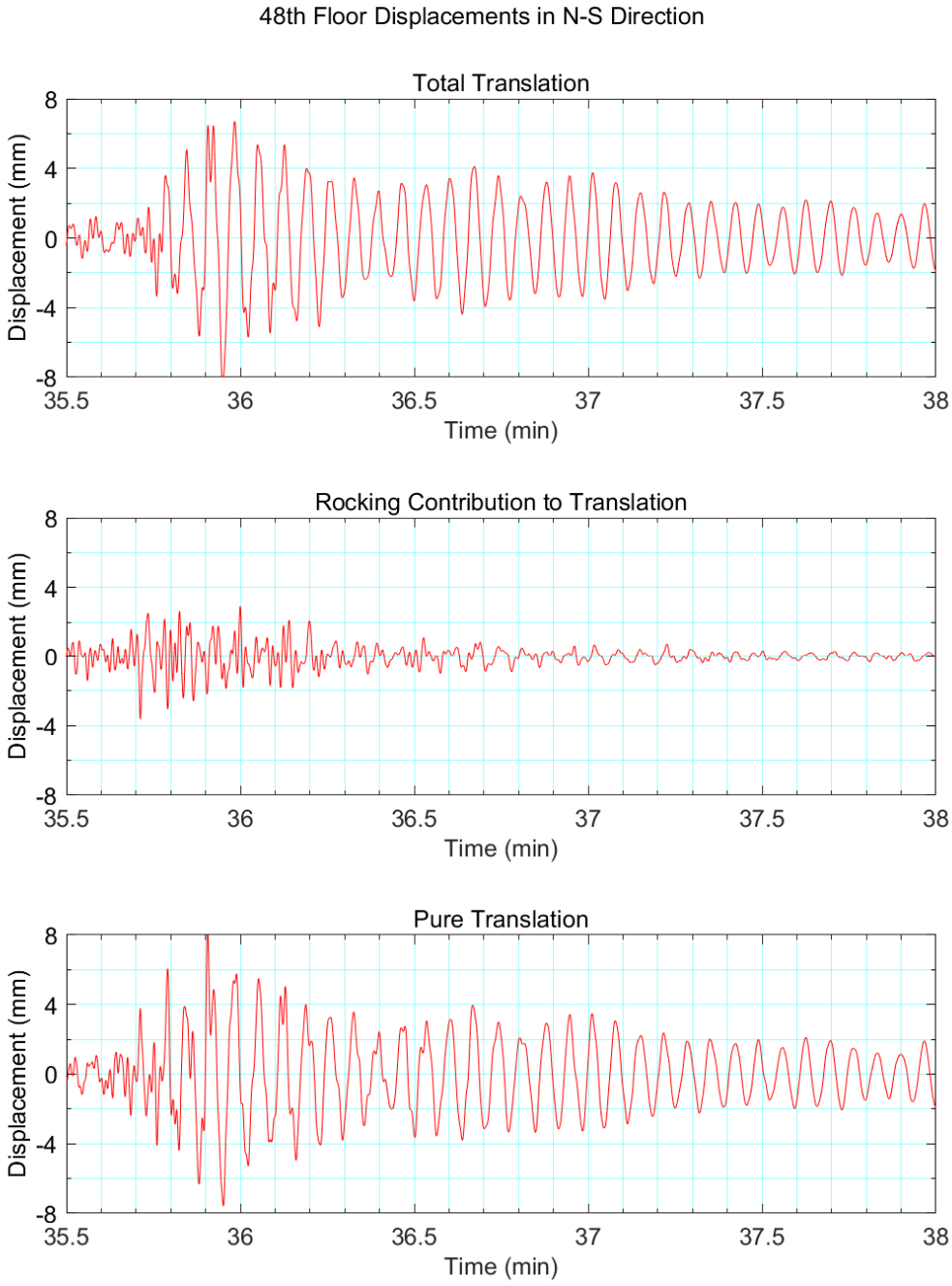

Figure 5.35 Rocking contribution to the 48th floor N-S translation (rocking rotation around E-W axis): March 20, 2019 M_w 5.5 Acipayam earthquake.

5.4 Summary

This chapter presented the analyses of the structural response records during earthquakes with moment magnitudes M_w 3.9–6.0 and epicenters 15–285 km away from the building. SSI and rocking responses were investigated using response records from one of the earthquake events listed in Table 5.1.

CHAPTER 6

FINITE ELEMENT STRUCTURAL MODEL

6.1 Structural Model

A three-dimensional linear elastic finite element structural model of the instrumented building was developed based on its architectural and structural drawings using ETABS (Computers and Structures, Inc., 2018b). Figures 6.1–6.3 show the three-dimensional views of the building, the podium floor plan and the typical tower floor plan, respectively, which were extracted from the model.

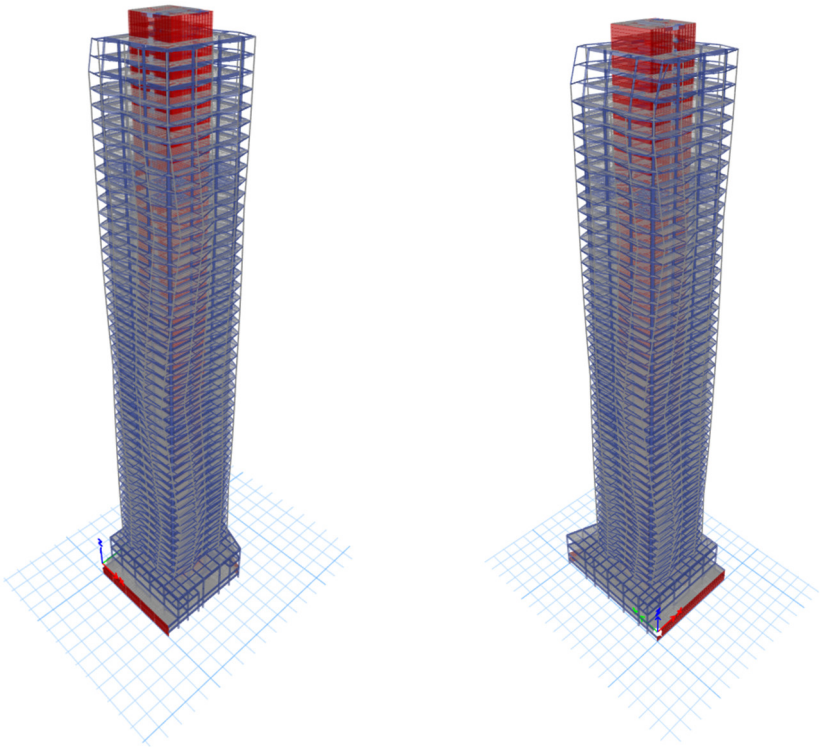

(a) (b)

Figure 6.1 Three-dimensional views of the building from the (a) SE and (b) SW corners.

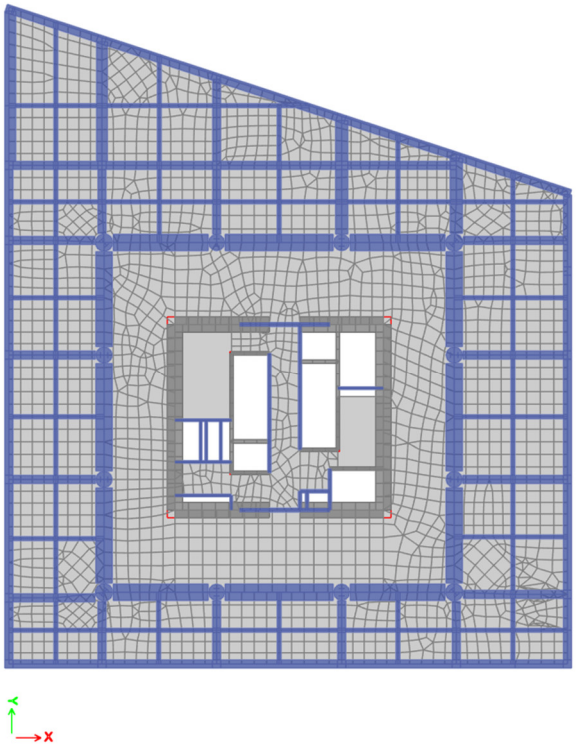

Figure 6.2 2nd podium floor plan.

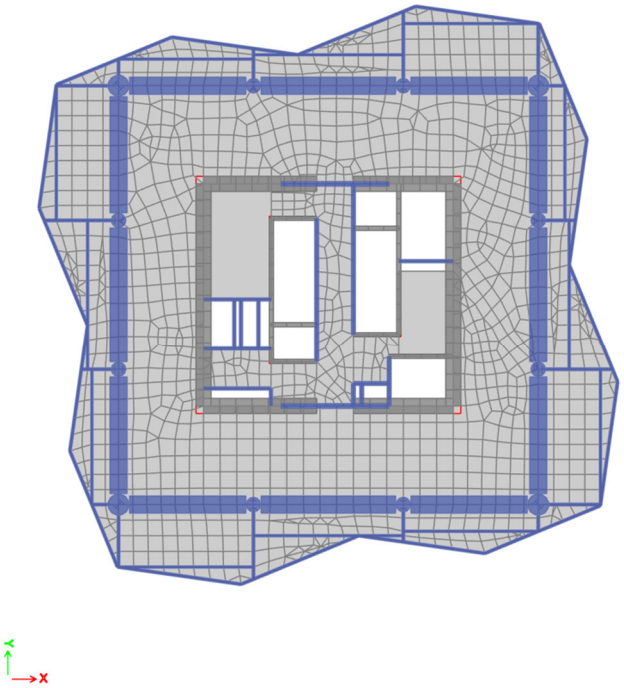

Figure 6.3 Typical tower floor plan (floor 10).

Frame elements were used in modeling the beams and columns based on centerline dimensions. Rigid offsets were defined at beam and column ends (Computers and Structures, Inc., 2018a). Shell elements, which combine independent membrane and thin-plate behavior, were used in modeling the floor and wall systems. Rectangular meshes of typically 1 m × 1 m in size were used. Elevator openings in flat plates were considered. Stairways were modeled using membrane elements for automatic calculation of the stairway loads.

BRBs at floors 19 and 39 were modeled using truss elements with cross-sectional areas of 0.04 m^2 and moduli of elasticity of 200,000 MPa. Concentric X-braced steel frames (with tube sections and plates) encased in RC core shear walls at floors 18–20 and 38–40 were modeled with fully restrained moment connections (Figure 6.4).

The properties of concrete and steel materials were defined per TS 500 (Turkish Standards Institute, 2000) and EN 1993-1-1 (European Committee for Standardization, 2005), respectively, as presented in Tables 6.1 and 6.2.

P-Delta effects were considered in the finite element structural model. SSI effects were shown to be negligible in Chapter 5; therefore, fixed support conditions were defined at the basement level shear walls and columns.

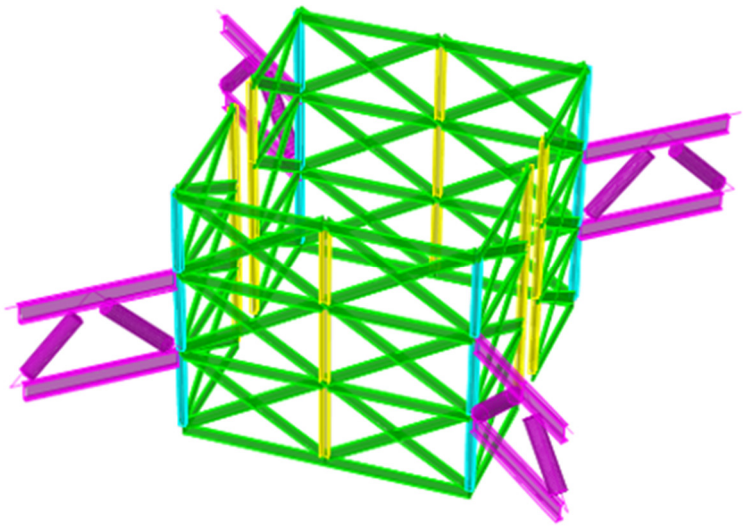

Figure 6.4 BRB-outrigger system.

Table 6.1 Material properties of concrete.

Material	Unit Weight kN/m^3	Compressive Strength MPa	Modulus of Elasticity MPa
C30	24	30	32000
C40	24	40	34000
C50	24	50	37000

Table 6.2 Material properties of steel.

Material	Unit Weight kN/m^3	Yield Strength MPa	Modulus of Elasticity MPa
S275	77	275	210000
S355	77	355	210000
S460	77	460	210000

6.2 Eigenvalue Analysis

Eigenvalue analysis of the building was performed to determine the natural vibration frequencies and the corresponding mode shapes. Mass and stiffness parameters used in the finite element model of the building, the two most important inputs for the eigenvalue analysis, are presented below.

The building mass consists of dead loads (self weight, superimposed dead load and cladding load) and live loads. The weights of the typical tower floor and the building in total were calculated as 9100 kN and 505,000 kN, respectively, based on the load combination $1.0D + 0.3L$ (D and L stand for dead and live loads, respectively; TBEC

2019). The ratio of the live load to the dead load is 0.12. The unit weight of concrete was taken as 24 kN/m^3, whereas that of structural steel was taken as 77 kN/m^3 in the structural model. The self weight of all members was then calculated by the finite element program. Superimposed dead loads and live loads (TS 498; Turkish Standards Institute, 1997) were assigned as area loads on slabs. The cladding loads, which consist of the weights of the glass panels and aluminum framing, were assigned as line loads on the beams at the perimeter of the building. Steel framing on the roof was not explicitly modeled; however, its weight was assigned as a line load on the perimeter roof beams. Tables 6.3 and 6.4 present the dead and live load values, respectively.

Table 6.3 Dead loads (kN/m^2).

Superimposed Loads*	
Offices	2.35
Corridors	1.90
Roof	2.00
Ground	1.35
Basements	1.35
Cladding Load†	1.00

*Superimposed loads include the weights of floor cover, mechanical and plumbing equipment, partition walls, elevated slab and insulation material.

†Cladding load consists of the weights of glass panels and aluminum framing.

Table 6.4 Live loads (kN/m^2).

Offices	2.00
Corridors	5.00
Parking	5.00
Mechanical floors	7.50

There are four different sets of stiffness parameters used in the structural model:

Model 1 is the initially developed model with the gross section properties.

Model 2 uses the cracked section properties defined in TBEC 2019 for tall buildings under service and frequent earthquakes. Table 6.5 presents the effective section stiffness multipliers for use in modeling RC members. For composite columns, the stiffness multiplier was calculated using the following procedure:

1. Determine the gross moment of inertia of the transformed section for each composite column in the structural model. ETABS provides this value by transforming the encased steel section into an equivalent concrete section:

$$I_{gt} = I_c + nI_s \tag{6.1}$$

where I_c and I_s are the moments of inertia of the concrete and steel sections, respectively, and n is the modular ratio.

Table 6.5 TBEC 2019 effective section stiffness multipliers under service and frequent earthquakes.

Shear Wall – Slab (In Plane)	Axial	Shear
Shear wall	0.75	1.00
Basement shear wall	1.00	1.00
Slab	0.50	0.80
Shear Wall – Slab (Out of Plane)	**Flexural**	**Shear**
Shear wall	1.00	1.00
Basement shear wall	1.00	1.00
Slab	0.50	1.00
Frame Member	**Flexural**	**Shear**
Beam	0.70	1.00
Column	0.90	1.00
Composite column*	0.92	1.00

* See Eq. 6.4.

2. Calculate the cracked moment of inertia of the transformed section:

$$I_{cr} = 0.90I_c + nI_s \tag{6.2}$$

3. Solve for I_c from Eq. 6.1 and insert into Eq. 6.2:

$$I_{cr} = 0.90\left(I_g - nI_s\right) + nI_s = 0.90I_g + 0.10nI_s \tag{6.3}$$

4. Calculate the effective section stiffness multiplier for each composite column:

$$\alpha = 0.90 + 0.10nI_s/I_{gt} \tag{6.4}$$

5. Use the mean stiffness multiplier for all composite columns.

Model 3 uses the cracked section properties calculated using the equations in TS 500 and ACI 435 (ACI Committee 435, 1978). Calculations for the shear walls, composite columns, beams and slabs are summarized below.

- Tensile stresses (maximum 3.5 MPa) in the shear walls under service loads (1.0D + 0.3L) shown in Figure 6.5 do not exceed the flexural tensile strength (5.0 MPa) calculated based on TS 500 for grade C50 concrete. Hence, gross section properties were used for the shear walls.
- Tensile stresses in the composite columns due to bending moments:

$$\sigma = My/I_{gt} \tag{6.5}$$

do not overcome the compressive stresses due to axial compression forces:

$$\sigma = P/A_{gt} \tag{6.6}$$

where P and M are the axial compression forces and bending moments, respectively, under service gravity loads, y is the distance from the centroid to the tension face and A_{gt} is the gross area of the transformed section. Hence, gross section properties were used for the composite columns.

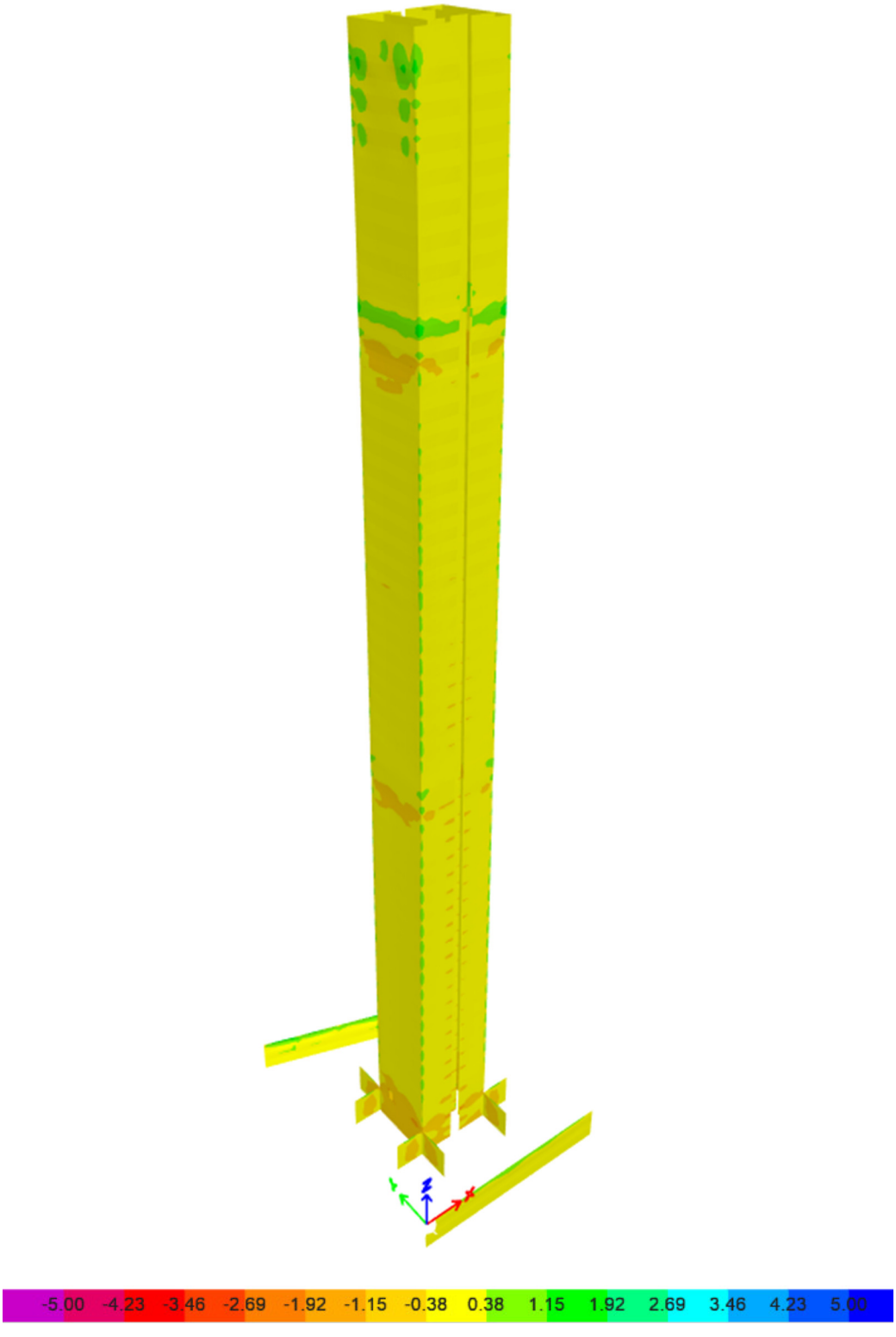

Figure 6.5 Stresses in shear walls (MPa).

- For beams, the cracking moments at the midspan and supports were calculated (TS 500):

$$M_{cr} = 2.5 f_{ctd} I_g / y \tag{6.7}$$

where f_{ctd} is the concrete design tensile strength and I_g is the gross moment of inertia. Then, the effective moments of inertia at the midspan and supports were calculated (TS 500):

$$I_{eff} = (M_{cr}/M_{max})^3 I_g + [1 - (M_{cr}/M_{max})^3] I_{cr} \tag{6.8}$$

where M_{max} is the maximum moment under service gravity loads. Finally, the average effective moment of inertia for each beam was calculated (ACI Committee 435, 1978):

$$I_{eff,avg} = 0.70 I_{eff,m} + 0.15(I_{eff,1} + I_{eff,2}) \tag{6.9}$$

where $I_{eff,m}$ is the effective moment of inertia at the midspan, and $I_{eff,1}$ and $I_{eff,2}$ are the effective moments of inertia at the supports. Table 6.6 presents the effective section stiffness multipliers:

$$\alpha = I_{eff,avg}/I_g \tag{6.10}$$

Note that midspan moments do not exceed cracking moments except for the beams at ground floor.

- Tensile stresses in the slabs between the ground floor and floor 5 shown in Figure 6.6 do not exceed the flexural tensile strength; hence, gross section properties were used. However, tensile stresses in the upper floor slabs exceed the flexural tensile strength at the midspan and supports; hence, cracked section properties for slabs (see Table 6.5) were used based on TBEC 2019.

Model 4 uses the cracked section properties defined in TBEC 2019 for the design earthquake calculations. Table 6.7 presents the effective section stiffness multipliers for use in modeling RC members. For composite columns, the stiffness multiplier was calculated as explained previously.

Table 6.6 Effective section stiffness multipliers for the beams according to TS 500 and ACI Committee 435.

Floor	Beam sizes (cm)	M_{cr} (kN·m)		M_{max} (kN·m)		α
		Midspan	Support	Midspan	Support	
20–48	100/60	690	271	101	286	0.97
4–19	105/60	720	283	101	286	0.99
3	120/60	815	320	116	369	0.91
2	120/110	3560	1070	371	810	1.00
1	120/60	815	321	248	320	1.00
G	140/60	797	371	984	874	0.46
B1	140/60	797	371	620	510	0.83

6.3 Comparison with System Identification Results

6.3.1 Natural vibration frequencies

The natural vibration frequencies identified from ambient vibration records in Chapter 4 and those determined from all four finite element models with different gross/cracked section properties are tabulated in Table 6.8. There are no significant differences between the identified frequencies from ambient vibration records and those determined from Model 1, which uses the gross section properties. The differences are generally less than 2% with a few exceptions such as the fourth mode in the N-S direction, where the difference is 6%. When the frequencies from Model 2, which uses the cracked section properties explicitly stated in TBEC 2019 for tall buildings under service and frequent earthquakes, are compared with the identified frequencies, the differences are in the order of 10%. This indicates that the building has not even been subjected to service-level excitations. Hence, Model 3, which uses

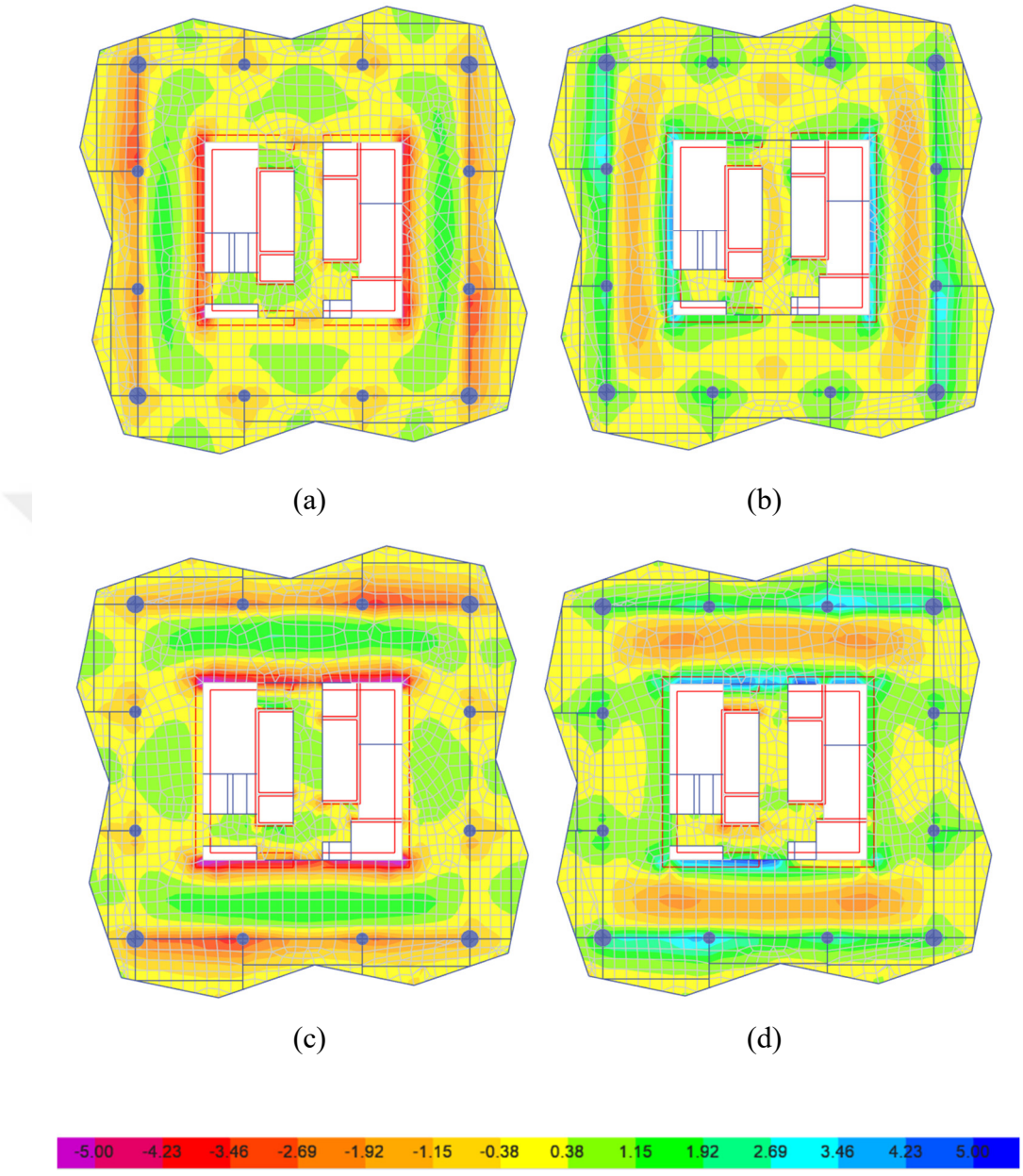

Figure 6.6 Stresses along x-axis direction at (a) bottom face and (b) top face; y-axis direction at (c) bottom face and (d) top face of the 5th floor slab (MPa).

the calculated cracked section properties, was developed. Model 3 frequencies are almost identical to Model 1 frequencies, which proves that minor cracking in some beams and slabs do not change the natural vibration frequencies significantly. Model

Table 6.7 TBEC 2019 effective section multipliers for earthquake load calculations.

Shear wall – Slab (In-plane)	Axial	Shear
Shear wall	0.50	0.50
Basement shear wall	0.80	0.50
Slab	0.25	0.25
Shear wall – Slab (Out of plane)	Flexural	Shear
Shear wall	0.25	1.00
Basement shear wall	0.50	1.00
Slab	0.25	1.00
Frame member	Flexural	Shear
Beam	0.35	1.00
Column	0.70	1.00
Composite column	0.75	1.00

3 was selected as the baseline finite element structural model that represents the current status of the building. Table 6.9 presents the modal mass participation ratios for the first four vibration modes. Furthermore, the frequencies from Model 4, which uses the cracked section properties explicitly stated in TBEC 2019 for the design earthquake calculations, are also presented in Table 6.7. The frequencies decrease significantly by about 30% for all modes.

6.3.2 Vibration mode shapes

The three-dimensional vibration mode shapes determined from the baseline finite element structural model for the first four translational modes in the E-W and N-S directions and the first four torsional modes are presented in Figures 6.7–6.9, respectively. These mode shapes are compared with those identified from the

Table 6.8 Comparison of natural vibration frequencies.

Mode		Natural vibration frequencies (Hz)				
Dir.	No.	System ID	FEM			
			Model 1	Model 2	Model 3	Model 4
x (E-W)	1	0.24	0.24	0.22	0.24	0.18
	2	0.90	0.89	0.80	0.88	0.67
	3	1.87	1.92	1.73	1.88	1.43
	4	2.99	2.95	2.67	2.89	2.17
y (N-S)	1	0.25	0.24	0.22	0.24	0.18
	2	1.08	1.08	0.96	1.08	0.77
	3	2.56	2.57	2.29	2.56	1.81
	4	4.72	4.45	4.09	4.42	3.04
θ	1	0.59	0.58	0.55	0.57	0.45
	2	1.71	1.70	1.59	1.67	1.29
	3	3.12	3.05	2.88	3.01	2.31
	4	4.73	4.56	4.30	4.52	3.18

Table 6.9 Modal mass participation ratios.

Mode	x (E-W)	y (N-S)	θ
1	0.55	0.52	0.54
2	0.17	0.17	0.10
3	0.05	0.06	0.04
4	0.03	0.04	0.02

ambient vibration records in Figures 6.10–6.12 in two-dimensional space. They are all in good agreement.

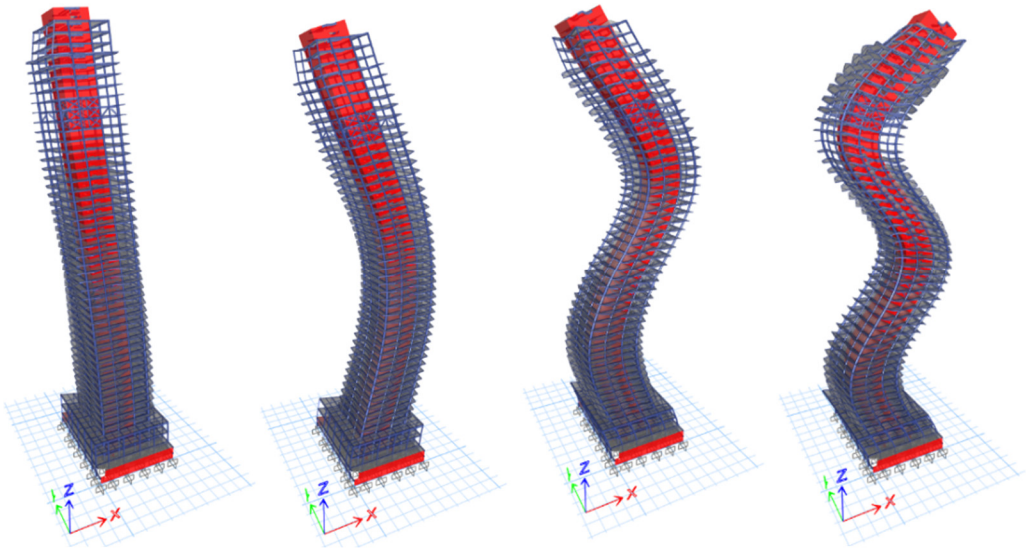

(a) (b) (c) (d)

Figure 6.7 E-W translational vibration mode shapes: (a) 1st, (b) 2nd, (c) 3rd and (d) 4th modes.

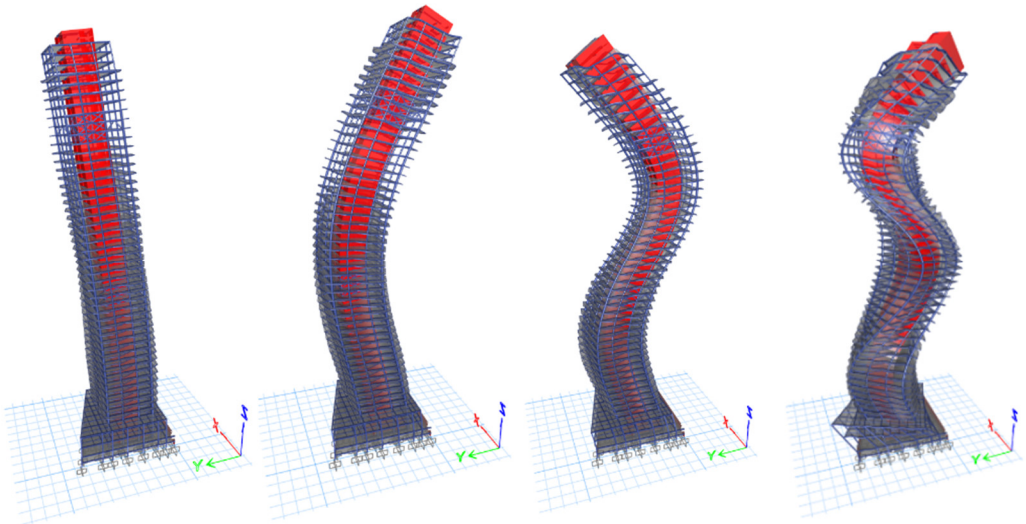

(a) (b) (c) (d)

Figure 6.8 N-S translational vibration mode shapes: (a) 1st, (b) 2nd, (c) 3rd and (d) 4th modes.

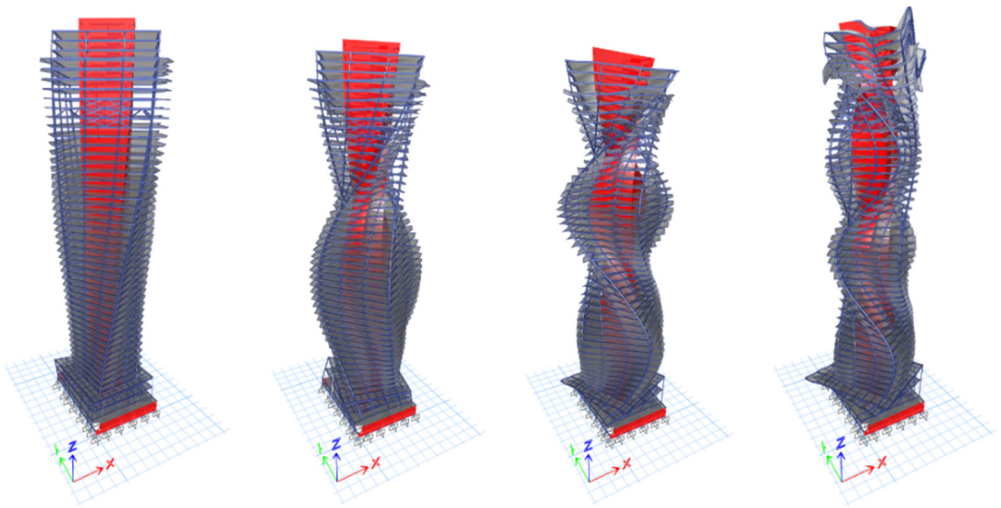

(a) (b) (c) (d)

Figure 6.9 Torsional vibration mode shapes: (a) 1st, (b) 2nd, (c) 3rd and (d) 4th modes.

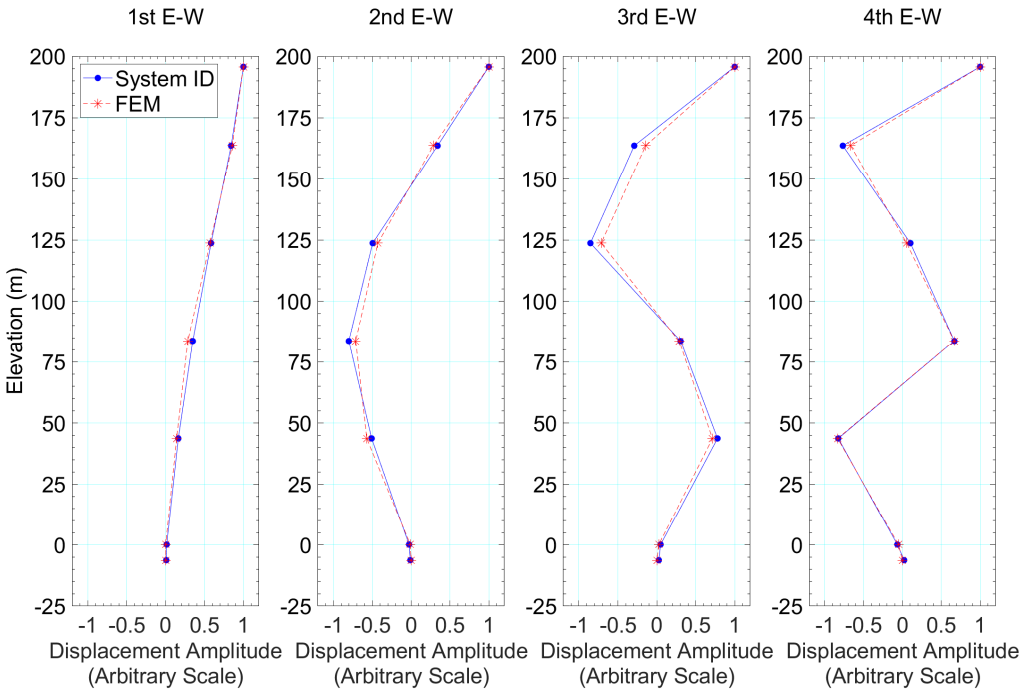

Figure 6.10 E-W translational vibration mode shapes: system ID (02.02.2019 00:00:00 GMT) vs. FEM.

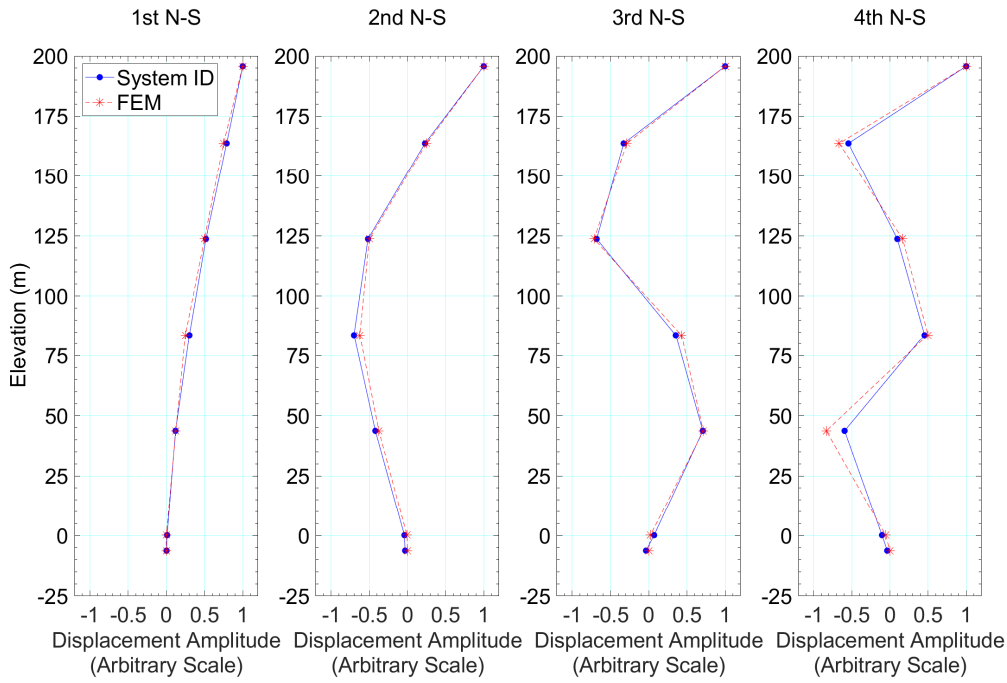

Figure 6.11 N-S translational vibration mode shapes: system ID (02.02.2019 00:00:00 GMT) vs. FEM.

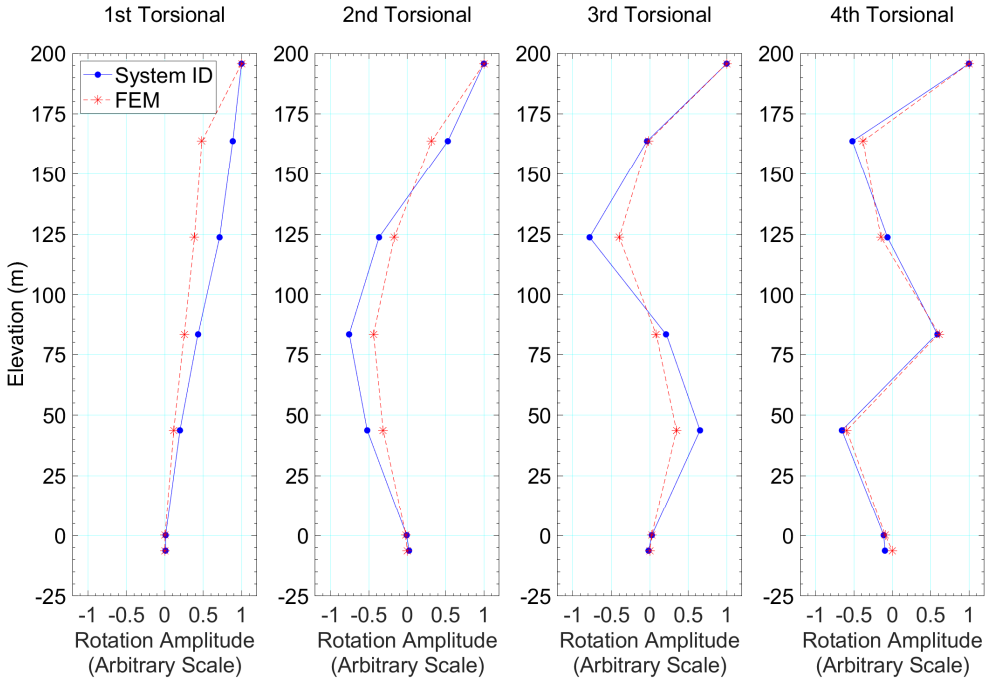

Figure 6.12 Torsional vibration mode shapes: system ID (02.02.2019 00:00:00 GMT) vs. FEM.

6.4 Summary

The three-dimensional finite element structural model of the instrumented building was developed. Mass and stiffness parameters used for the eigenvalue analysis were described. Natural vibration frequencies and mode shapes identified from the ambient vibration records and the finite element model were compared. The finite element model that uses the modulus of elasticity for concrete in TS 500 and the cracked section properties calculated according to TS 500 and ACI Committee 435 predicted the natural vibration frequencies well. The vibration mode shapes were also in good agreement. It is concluded that the building's mass and stiffness were accurately modeled and the fixed support condition assumption was deemed appropriate.

CHAPTER 7

GUIDELINES FOR STRUCTURAL HEALTH MONITORING SYSTEMS ON TALL BUILDINGS

7.1 Development Process

The new Turkish Building Earthquake Code has made the installation of SHM systems on tall buildings mandatory. It is a positive development for the earthquake engineering profession in Turkey. SHM systems enable recording earthquake-induced structural vibrations and continuous monitoring of ambient vibrations (e.g., due to wind). From the recorded structural responses, structural system dynamic properties during the strong earthquake ground motions can be identified and they can be compared with those identified before and after the earthquake events. These comparisons provide essential information about tall buildings. To collect reliable information, guidelines regulating the installation, management and operation of the SHM systems on tall buildings are required.

Initially, two draft guidelines were prepared by METU and Bogazici University researchers within the scope of two concurrent research projects at these universities funded by AFAD (see Chapter 1). Existing SHM guidelines and instrumented buildings were examined in preparing the draft guidelines (see Chapter 2). Then, AFAD compiled these two documents and prepared the first draft of the SHM Guidelines for Tall Buildings. The first draft was critically reviewed by academicians and participants from state and private sectors in a workshop organized by AFAD in Istanbul on October 25, 2018. The following issues were noted for the revision of the draft guidelines:

- the number of recording channels
- sampling rate
- accelerometer specifications

- time synchronization
- monitoring mode (continuous, trigger)
- installation, maintenance and budget
- security of the recorded data
- reporting of the system identification results
- inspection and management
- implementation on existing tall buildings and other essential buildings

The second draft was presented in an another workshop organized by AFAD in Ankara on June 25, 2019. Eventually, AFAD published the Guidelines for SHM Systems on Tall Buildings on January 9, 2020 (Disaster and Emergency Management Presidency of Turkey, 2020). The main sections of the Guidelines are presented in the next section.

7.2 Guidelines for SHM Systems on Tall Buildings

7.2.1 Minimum requirements for system installation and specifications

ARTICLE 4 - (1) Accelerometers of the SHM system will be synchronously connected to a minimum 24-bit digital recorder with GPS (Global Positioning System) timing. The digital recorder will continuously record the building vibrations and transfer the data in real time to the specified centers via internet, modem, satellite or similar connections. In case of power or connection problems, the system will be able to operate and store the data for at least a week.

(2) Precautions will be taken to protect the accelerometers, digital recorders and other equipment in the SHM system against fire and mechanical shocks.

ARTICLE 5 - (1) Time synchronization of all devices of the SHM system will be ensured. Cables should be preferred for connecting the accelerometers to the digital recorders. If a wireless connection is used, it should be ensured that there is no time

synchronization problem. Cables will not distort the recorded data and their lengths are preferred to be not longer than 100 m.

(2) A GPS antenna will be located on the roof of the building for universal time (UTC) synchronization of the accelerometers. An NTP server can also be used for time synchronization. Digital recorders should be connected directly to the building network via ethernet cables. The noise level given in Table 7.1 should not be exceeded at the digitizer output.

(3) Cables should conform with the first paragraph of Article 83 of the Regulation on the Fire Protection of Buildings, which was published in the Official Gazette No. 26735 on December 19, 2007.

ARTICLE 6 - (1) Digital recorders should be able to record data in both continuous and trigger modes. In the trigger mode, the trigger level will be 0.005 g (5 gals) at the basement level and the acceleration record will include 300 s before and 600 s after the earthquake.

(2) Immediately after an earthquake event, AFAD can have the building owner check whether the system is up and running and request the data to be transferred to the center by other means in case of an outage.

ARTICLE 7 - (1) The minimum number of accelerometer channels is given in Table 7.2.

Table 7.1 Accelerometer specifications.

Dynamic range	>144 dB+
Frequency range	0.01–200 Hz
Noise level	<1 μg RMS
Measurement range	± 2 g

Table 7.2 Minimum number of accelerometers.

Building height above ground	Minimum channel number
105–155	16
156–205	24
>205	32

(2) Accelerometer deployment in the building should be made at least in the numbers and locations as specified below (Figure 7.1). AFAD can increase the number of accelerometers depending on the building characteristics.

a) Three accelerometers (two parallel and one perpendicular to these) on each of the top floor and two floors with the highest modal displacements.
b) Two accelerometers in perpendicular directions on the ground floor.
c) Five accelerometers in total at the foundation level, three vertical accelerometers to determine the rocking motions along both axes of the building and two horizontal accelerometers in perpendicular directions to record the earthquake ground motion acting on the building.

ARTICLE 8 - (1) Accelerometers should conform with the technical specifications in Table 7.1 as a minimum.

ARTICLE 9 - (1) Data from each channel of the SHM system should at least be sampled at 200 samples per second (200 Hz). For special structural systems/buildings, AFAD can request the sampling rate be increased to 500 Hz and the building owner will take the necessary precautions immediately.

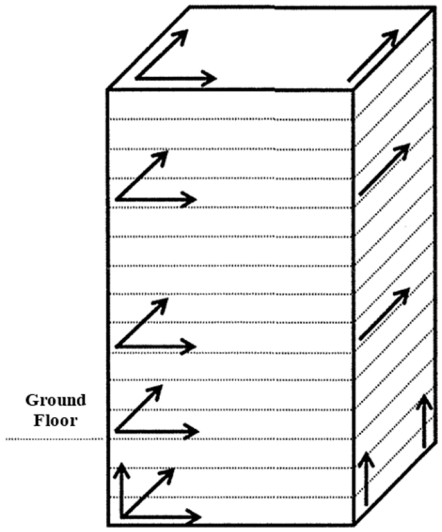

Figure 7.1 Accelerometer layout.

7.2.2 Responsibility, acceptance, control and inspection of the system

Responsibility

ARTICLE 10 - (1) The building owner is responsible for the installation, maintenance, repair, data communication cost and protection of the SHM system.

(2) The building owner will undertake the data transfer to AFAD, evaluation and reporting of the SHM data, and will take precautions against possible risks based on the outcome of the analysis of the SHM data.

ARTICLE 11 - (1) The instrumentation of the building will be according to Article 7. However, AFAD can impose changes.

(2) The building owner will submit the documents listed in Article 12 for approval of the SHM system when applying for the Occupancy Permit. These documents are kept by the building owner to be submitted to AFAD when deemed necessary.

Documentation of the SHM system

ARTICLE 12 - (1) The following documents will be submitted by the building owner for approval of the SHM system:

a) Building plans.
b) SHM system marked on building drawings.
c) Connection and network settings of the SHM system.
d) Official document signed by AFAD stating that the SHM data have been transferred to AFAD.

Check and Inspection

ARTICLE 13 - (1) The check and inspection of the SHM system will be carried out according to the legislations of the institution authorizing the building license.

7.2.3 Evaluation and reporting of the data

Evaluation of the Data

ARTICLE 14 - (1) The company in charge of the installation of the SHM system will be responsible for the identification of the modal properties (frequencies, mode shapes and damping ratios) of the building from the SHM data. The following should be provided about this system identification:

a) The methods used for the identification.
b) At least the first three translational modes in two directions and the first three torsional modes (nine modes in total).
c) A monthly database of the modal values identified from the recorded ambient vibration data and percent changes of these values.
d) Changes in the modal values from the recorded pre- and post-earthquake data.

(2) The outcome of the system identification should be approved by academicians in universities who are experts in the SHM field.

Reporting of the Data

ARTICLE 15 - (1) The company in charge of the installation of the SHM system will prepare a report based on the recorded ambient vibration data and/or earthquake data every three months, and submit both the soft and hard copies of the report to both the building owner and AFAD. The report should include the following information:

a) A sketch of the structural form of the building and a short description of the building including the number of floors, the construction date and the structural system.
b) The instrumentation scheme (the distances and directions indicated).
c) Clear pictures of the SHM system (accelerometers, digital recorders, etc.).
d) Technical specifications of the accelerometers and digital recorders.
e) The recording dates of the SHM data.
f) System identification report defined in the first paragraph of Article 14.

7.3 Summary

This chapter presented the development process of the Guidelines for SHM Systems on Tall Buildings required per the new Turkish Building Earthquake Code and the main sections of the Guidelines.

CHAPTER 8

SUMMARY, CONCLUSIONS AND FUTURE RESEARCH

8.1 Summary

The new Turkish Building Earthquake Code requires real-time monitoring of the structural response of tall buildings. Guidelines regulating the installation, management and operation of SHM systems to be installed on tall buildings was developed within the scope of two concurrent research projects at METU and Bogazici University, which were funded by AFAD. The research project at METU inspired this thesis study. First, the historical development of structural response monitoring and the existing SHM guidelines for buildings were reviewed. Following critical appraisal of strong motion instrumentation examples of buildings, SHM Guidelines for Tall Buildings in Turkey was developed. In parallel to this effort, a 27-channel SHM system was installed on the tallest building in Izmir, a 216 m tall composite building with BRBs. The building has been continuously monitored since January 27, 2019. The dynamic structural properties were identified and the recorded earthquake responses of the building were analyzed by the developed system identification algorithm. The finite element structural model of the building was also developed and validated using the system identification results from ambient vibration records.

8.2 Results and Conclusions

Guidelines for SHM Systems on Tall Buildings in Turkey was developed. AFAD published the SHM Guidelines on January 9, 2020 as an attachment to the new Code. The SHM system installed on the case study building in Izmir, which complies with

the developed guidelines, was shown to provide the data required for the system identification of the building.

Structural system dynamic properties of the instrumented building were identified using ambient vibration records for the first four translational modes in both E-W and N-S directions and the first four torsional modes. The fundamental natural vibration periods are 4.17 s and 4.00 s in the E-W and N-S directions, respectively, and 1.71 s for the torsional mode. The associated modal damping ratios were identified as 0.5%, 0.6% and 0.2%, respectively. Damping calculations were sensitive to the signal processing algorithms. Long-term monitoring between February 1, 2019 and December 31, 2019 showed no significant changes in the dynamic properties due to daily and seasonal temperature variations and daily and weekly occupancy variations.

Four finite element structural models were developed using different sets of stiffness parameters:

- gross section properties (Model 1)
- cracked section properties defined in the new Code for service and frequent earthquakes (Model 2)
- cracked section properties calculated using the equations in TS 500 and ACI 435 (Model 3)
- cracked section properties defined in the new Code for the design earthquake calculations (Model 4)

The modulus of elasticity for concrete in all these models was defined per TS 500. There were no significant differences between the identified frequencies from ambient vibration records and those determined from Model 1. Model 3 frequencies were almost identical to Model 1 frequencies, which proved that minor cracking in some beams and slabs do not change the natural vibration frequencies significantly. Model 4, which was developed to predict the frequencies under the design earthquake, pointed to about 30% reduction in the frequencies due to cracking in structural members.

The structural response records of the building during earthquakes in 2019 with moment magnitudes M_w 3.9–6.0 and epicenters 15–285 km away from the building were analyzed. The maximum acceleration was 0.017 g at the roof (during the M_w 5.5 Acipayam, Denizli earthquake) and 0.009 g at the building base (during the M_w 3.9 Menemen, Izmir earthquake), whereas the maximum roof displacement was 8 mm (during the M_w 5.5 Acipayam, Denizli earthquake). The identified modal damping ratios were in the range of 0.8–1.7%. Higher-mode effects were observed during the earthquakes; the building response was essentially in the first translational modes following the earthquakes. SSI and rocking responses of the building were identified as negligible.

8.3 Future Research

The scope and limitations of this study point towards the following topics that can be addressed in the future:

- analysis of the building response and BRB performance during major earthquakes provided that the SHM system remains active
- damping calculation methods
- wave propagation methods for damage assessment
- detailed investigation of SSI and rocking responses
- human comfort criteria in tall buildings
- analysis of the building response with wind speed and temperature data by adding a weather station to the SHM system
- assessment of the pile foundation performance by adding borehole instrumentation to the SHM system
- identification of the structural system dynamic properties using advanced system identification methods

REFERENCES

2013 San Francisco Building Code (2014) *Procedures for Seismic Instrumentation of New Buildings*, *Administrative Bulletin AB-058*. San Francisco, California, USA. Available at: https://sfdbi.org//sites/default/files/Documents (Accessed: 2 December 2018).

ACI Committee 435 (1978) Proposed revisions by Committee 435 to ACI Building Code and Commentary provisions on deflections, *ACI Journal*, 68(6): 229–238.

Aktan A E, Catbas FN, Grimmelsman KA and Pervizpour M (2002) *Development of a Model Health Monitoring Guide for Major Bridges*. Report Submitted to FWHA, DOT/FHWA Solicitation: DTFH61-01-Q-00072.

ANSS Structural Instrumentation Guideline Committee (2005) *Guideline for ANSS Seismic Monitoring of Engineered Civil Systems—Version 1.0*, *ANSS Open-File Report 2005-1039*. U.S. Geological Survey, Menlo Park, California, USA.

ANSS Technical Integration Committee (2002) *Technical Guidelines for the Implementation of The Advanced National Seismic System*, *ANSS Open-File Report 02-92*. U.S. Geological Survey, Menlo Park, California, USA.

Aytulun E and Soyoz S (2019) Structural Monitoring Applications and Software Devolopment for Tall Buildings, in *Proceedings of the Fifth International Conference on Earthquake Engineering and Seismology, October 8–11*. Ankara, Turkey.

Bergmeister K, Aktan AE, Bucher C and Dorfmann L (2003) *fib Bulletin 22. Monitoring and safety evaluation of existing concrete structures*. fib. The International Federation for Structural Concrete (fib Bulletins). doi: 10.35789/fib.BULL.0022.

Brownjohn JMW (2007) Structural health monitoring of civil infrastructure,

Philosophical Transactions of the Royal Society A, 365: 589–622. doi: 10.1098/rsta.2006.1925.

Cakti E and Safak E (2014) Structural Health Monitoring Systems in Istanbul, in *Proceedings of the Second European Conference on Earthquake Engineering and Seismology, August 25–29*. Istanbul, Turkey.

Carder D S (1936) Observed Vibrations of Buildings, *Bulletin of the Seismological Society of America*, 116(201): 107–116.

Casiano MJ (2016) *Extracting Damping Ratio From Dynamic Data and Numerical Solutions*, *NASA/TM—2016–218227*. Huntsville, Alabama, USA. Available at: http://www.sti.nasa.gov (Accessed: 15 March 2020).

Celebi M, Safak E, Brady AG, Maley R and Sotoudeh V (1987) *Integrated Instrumentation Plan for Assessing the Seismic Response of Structures-A Review of the Current USGS Program*. U.S. Geological Survey, Menlo Park, California, USA. Available at: https://pubs.usgs.gov/circ (Accessed: 9 January 2019).

Celebi M, Nishenko S, Astill C and Chun RM (1998) *Seismic Instrumentation of Federal Buildings*, *Open-File Report 98-117*. U.S. Geological Survey, Menlo Park, California, USA.

Celebi M (2000) *Seismic Instrumentation of Buildings*, *USGS Report 00-157*. U.S. Geological Survey, Menlo Park, California, USA.

Celebi M (2002) *Seismic Instrumentation of Buildings (with Emphasis on Federal Buildings)*, *Special GSA/USGS Project, An Administrative Report*. U.S. Geological Survey, Menlo Park, California, USA.

Celebi M, Huang M, Shakal A, Hooper J and Klemencic R (2013) Ambient response of a unique performance-based design tall building with dynamic response modification features, *The Structural Design of Tall and Special Buildings*, 22(10): 816–829. doi: 10.1002/tal.1093.

Celebi M and Nishenko S (1997) *Seismic Instrumentation of Federal Buildings*,

Open-File Report 97-452. U.S. Geological Survey, Menlo Park, California, USA.

Celebi M and Safak E (1991) Seismic response of Transamerica Building. I: Data and preliminary analysis, *Journal of Structural Engineering*, 117(8): 2389–2404. doi: 10.1061/(ASCE)0733-9445(1991)117:8(2389).

Celik OC, Sucuoglu H and Akyuz U (2015) Forced vibration testing and finite element modeling of a nine-story reinforced concrete flat plate-wall building, *Earthquake Spectra*, 31(2): 1069–1081. doi: 10.1193/091212EQS287M.

Cha Y-J, Trocha P and Buyukozturk O (2016) Field measurement-based system identification and dynamic response prediction of a unique MIT building, *Sensors*, 16(7): 1016.

Clinton JF, Bradford SC, Heaton TH and Favela J (2006) The observed wander of the natural frequencies in a structure, *Bulletin of the Seismological Society of America*, 96(1): 237–257. doi: 10.1785/0120050052.

Clough RW and Penzien J (2003) *Dynamics of Structures*. Third Edit. Berkeley, California, USA: Computers & Structures, Inc.

Committee for the Future of the US National Strong-Motion Program (1997) *Vision fot he Future of the US National Strong-Motion Program*, *USGS Numbered Series Open-File Report 97-530*. U.S. Geological Survey, Reston, Virginia, USA. Available at: https://pubs.er.usgs.gov/publication/ofr97530B (Accessed: 20 October 2020).

Computers and Structures Inc. (2018a) CSI Analysis Reference Manual. Berkeley, California, USA. Available at: https://www.csiamerica.com (Accessed: 1 June 2018).

Computers and Structures Inc. (2018b) ETABS Version 18.0.1, Walnut Creek, California, USA. Available at: https://www.csiamerica.com/products/etabs (Accessed: 1 June 2018).

Crawford R and Ward HS (1964) Determination of the natural periods of buildings,

Bulletin of the Seismological Society of America, 54(6): 1743–1756.

Department of Public Works and Highway of the Philippines (2015) *Guidelines and Implementing Rules on Earthquake Recording Instrumentation for Buildings*. Manila, Philippines.

Disaster and Emergency Management Center (2018) Turkish Building Earthquake Code 2019, *Official Gazette, No: 30364 (in Turkish)*. Ankara, Turkey.

Disaster and Emergency Management Center (2020) Guidelines for SHM Systems on Tall Buildings *(in Turkish)*. Ankara, Turkey. Available at: https://www.afad.gov.tr/ yonerge (Accessed: 3 February 2021).

Dunand F, Rodgers JE, Acosta AV, Salsman M, Bard P and Celebi M (2004) *Ambient Vibration and Earthquake Strong-Motion Data Sets for selected USGS Extensively Instrumented Buildings*, *Open-File Report 2004-1375*. U.S. Geological Survey, Menlo Park, California, USA.

Erdik M, Celebi M, Mihailov V and Apaydin N (eds) (2001) *Strong Motion Instrumentation for Civil Engineering Structures*. Dordrecht, Netherlands: Springer. doi: 10.1007/978-94-010-0696-5.

European Committee for Standardization (2005) *EN 1993-1-1: Eurocode 3: Design of steel structures - Part 1-1: General rules and rules for buildings*. CEN, Brussels, Belgium.

Foutch DA, Housner GW and Jennings PC (1975) *Dynamic Responses of Six Multistory Buildings during the San Fernando Earthquake*, *Report No. EERL 75-02*. Pasadena, California, USA.

Garevski M (2013) *Earthquakes and Health Monitoring of Civil Structures*, *Springer Environmental Science and Engineering*. Edited by Mihail Garevski. Dordrecht, Netherlands: Springer (Springer Environmental Science and Engineering). doi: 10.1007/978-94-007-5182-8.

Ghahari SF, Abazarsa F, Avci O, Celebi M and Taciroglu E (2016) Blind identification of the Millikan Library from earthquake data considering soil-

structure interaction, *Structural Control and Health Monitoring*, 23(4): 684–706. doi: 10.1002/stc.1803.

Gumus O and Celik OC (2019) Structural Health Monitoring System on a 216 M Tall Building in Izmir Per the New Turkish Building Earthquake Code, in *Proceedings of the Fifth International Conference on Earthquake Engineering and Seismology, October 8–11*. Ankara, Turkey.

Guralp Systems Limited (2018) Seismic Monitoring Software. Calleva Park, England.

Hudson DE (ed.) (1971) *Strong-motion Instrumental Data on the San Fernando Earthquake of February 9, 1971*. California Institute of Technology, Pasadena, California, USA. Available at: https://authors. library .caltech.edu/26522/1/Hudson_1971.pdf (Accessed: 2 January 2020).

International Conference of Building Officials (1976) *1976 Uniform Building Code*. California, USA.

International Conference of Building Officials (1997) *1997 Uniform Building Code - Volume 1*. California, USA.

ISIS Canada (2001) *Guidelines for Structural Health Monitoring*. Design Manual No. 2. Manitoba, Canada.

Ivanovic SS, Trifunac MD, Novikova EI, Gladkov AA and Todorovska MI (2000) Ambient vibration tests of a seven-story reinforced concrete building in Van Nuys, California, damaged by the 1994 Northridge earthquake, *Soil Dynamics and Earthquake Engineering*, 19(6): 391–411. doi: 10.1016/S0267-7261(00)00025-7.

Ivanovic SS and Trifunac MD (1995) *Ambient Vibration Surveys of Full-Scale Structures Using Personal Computers - Examples for Kaprielian Hall*, *Report No. CE 95-05*. Los Angeles, California, USA.

Jennings PC and Housner GW (1971) *The San Fernando, California, Eartquake of February 9, 1971*. Pasadena, California, USA.

Johnson CM, Stepp CJ and Nigbor RL (eds) (2001) *Invited Workshop on Strong-Motion Instrumentation of Buildings*, *COSMOS NO. CP - 2001/04*. Emeryville, California, USA.

Kareem A and Tamura Y (eds) (2013) *Advanced Structural Wind Engineering*. Japan: Springer. doi: 10.1007/978-4-431-54337-4.

Kaynardag K and Soyoz S (2014) Structural Health Monitoring of a Tall Building, in *Proceedings of the Second European Conference in Earthquake Engineering and Seismology, August 25-29*. Istanbul, Turkey.

Li HN, Li AQ, Teng J, Yan WM, He XF and Yi TH (2012) *Design Standard for SHM Systems. China Engineering Construction Standardization Association, CECS 333-2012 (in Chinese).* China.

Los Angeles Tall Buildings Structural Design Council (2017) *An Alternative Procedure for Seismic Analysis and Design of Tall Buildings Located in the Los Angeles Region*. Los Angeles, California, USA.

Magalhaes F, Cunha A, Caetano E and Brincker R (2010) Damping estimation using free decays and ambient vibration tests, *Mechanical Systems and Signal Processing*, 24: 1274–1290.

Mao ZB, Peng MX, Liu JJ, Wang J, Zhang SL and Qin JS (2013) *Technical Code for Construction Process Analyzing and Monitoring of Building Engineering. Ministry of Housing and Urban-Rural Development of the People's Republic of China, JGJ/T 302-2013 (in Chinese)*. China.

Ministry of Housing and Urban-Rural Development of PRC (2014) *Technical Code for Monitoring of Building And Bridge Structures GB 50982-2014*. China. Available at: www.ChineseStandard.net (Accessed: 3 September 2019).

Moreu F, Li X, Li S and Zhang D (2018) Technical specifications of structural health monitoring for highway bridges: New chinese structural health monitoring code, *Frontiers in Built Environment*, 4(10): 1–12. doi: 10.3389/fbuil.2018.00010.

Osterreichische and Forschungsgellschaf (2012) *Quality Assurance for Structural Maintenance, Surveillance, Checking and Assessment of Bridges and Tunnels, Monitoring of Bridges and Other Engineering Structures, RVS 13-03-01*. Vienna, Austria (in German). Available at: http://www.fsv.at/shop (Accessed: 16 December 2019).

Pacific Earthquake Engineering Center (2017) *TBI Tall Buildings Initiative Guidelines for Performance-Based Seismic Design of Tall Buildings Version 2.03*, *PEER Report 2017/06*. California, USA.

Petrovic B, Dikmen SU and Parolai S (2018) Real data and numerical simulations-based approaches for estimating the dynamic characteristics of a tunnel formwork building, *Bulletin of Earthquake Engineering*, 16(3): 1633–1656. doi: 10.1007/s10518-017-0250-3.

Rojahn C and Matthiesen RB (1977) Earthquake Response and Instrumentation of Buildings, *Journal of the Technical Councils of ASCE*, 103(1): 1–12.

Rucker W, Hille F and Rohrmann R (2006) *F08b Guideline for Structural Health Monitoring*, *SAMCO Final Report*. Berlin, Germany.

Safak E and Cakti E (2014) Simple Techniques to Analyze Vibration Records from Buildings, in *Proceedings of 7th European Workshop on Structural Health Monitoring, July 8–11*. Nantes, France.

Safak E and Celebi M (1991) Seismic response of Transamerica building. II: System identification, *Journal of Structural Engineering*, 117(8): 2405–2425. doi: 10.1061/(ASCE)0733-9445(1991)117:8(2405).

Shakal AF, Huang M and Ventura CE (1998) The California Strong Motion Instrumentation Program: Objectives,Status and Recent Data, in *Proceedings of Ninth World Conference on Earthquake Engineering, August 2–9*. Tokyo-Kyoto, Japan.

Skolnik D, Lei Y, Yu E and Wallace JW (2006) Identification, Model Updating, and Response Prediction of an Instrumented 15-Story Steel-Frame Building,

Earthquake Spectra, 22(3): 781–802. doi: 10.1193/1.2219487.

Skolnik D, Kaiser WJ and Wallace JW (2008) Instrumentation For Structural Health Monitoring: Measuring Interstory Drift, in *Proceedings of 14th World Conference on Earthquake Engineering (14WCEE), October 12–17*. Beijing, China.

The Council on Tall Buildings and Urban Habitat (2020) *The Skyscraper Center in Turkey*. Available at: http://www.skyscrapercenter.com/country/turkey (Accessed: 2 February 2020).

The MathWorks Inc (2019) MATLAB. Available at: www.mathworks.com/products/ matlab. (Accessed:1 February 2019).

The State Unitary Enterprise of the City of Moscow (2010) *Buildings and Constructions Rules of Inspection and Monitoring of the Technical Condition - GOST R 53778-2010*. Moscow, Russia.

Trifunac MD, Ivanovic SS, Todorovska MI, Novikova EI and Gladkov AA (1999) Experimental evidence for flexibility of a building foundation supported by concrete friction piles, *Soil Dynamics and Earthquake Engineering*, 18(3): 169–187. doi: 10.1016/S0267-7261(98)00046-3.

Trifunac MD and Todorovska MI (2001) Evolution of accelerographs, data processing, strong motion arrays and amplitude and spatial resolution in recording strong earthquake motion, *Soil Dynamics and Earthquake Engineering*, 21(6): 537–555. doi: 10.1016/S0267-7261(01)00013-6.

Turkish Standards Institute (1997) *Design Loads for Buildings,* TS498, Ankara, Turkey.

Turkish Standards Institute (2000) *Requirements for Design and Construction of Reinforced Concrete Structures,* TS500:2000, Ankara, Turkey.

USGS (2020) *NSMP Structural and Geotechnical Arrays*. Available at: https://earthquake.usgs.gov/monitoring/nsmp (Accessed: 13 December 2020).

Ventura CE, Lord J and Simpson RD (2002) Effective Use of Ambient Vibration Measurements for Modal Updating of a 48 Storey Building in Vancouver, Canada. Department of Civil Engineering, University of British Columbia, Vancouver, B.C., Canada.

Wang J, Wu JH, Sun YG, He LZ, Li HW and Qi HZ (2011) *Tian jin shi qiao liang jie gou jian kang jian ce xi tong ji shu gui cheng [SHM system technical specification for bridge of Tianjin]. Tian jin shi cheng xiang jian she he jiao tong wei yuan hui, DB/T29-208-2011 (in Chinese).* Tianjin, China.

Yang Y, Li QS and Yan BW (2017) Specifications and applications of the technical code for monitoring of building and bridge structures in China, *Advances in Mechanical Engineering*, 9(1): 1–10. doi: 10.1177/1687814016684272.

Zhang L, Tamura Y and Yoshida A (2004) Evaluation Techniques of Damping in Buildings, in *CTBUH 2004 Seoul Conference, October 10–13*. Seoul, Korea.

Zhou L, Yan G, Wang L and Ou J (2013) Review of benchmark atudies and guidelines for structural health monitoring, *Advances in Structural Engineering*, 16(7): 1187–1206. doi: 10.1260/1369-4332.16.7.1187.